NTATION PAGE

READ INSTRUCTIONS BEFORE COMPLETING FORM

(2)

UMC Report No. 93-03	2. GOVT ACCESSION NO. / 3. RECIPIENT'S CATALOG NUMBER
4. TITLE (and Subtitle) Validation of A-Posteriori Error Estimators by Numerical Approach	5. TYPE OF REPORT & PERIOD COVERED Final Life of Contract 6. PERFORMING ORG. REPORT NUMBER
7. AUTHOR(s) I. Babuska[1] - T. Strouboulis - C. S. Upadhyay S. K. Gangaraj - K. Copps	8. CONTRACT OR GRANT NUMBER(s) [1]ONR/N00014-90-J-1030 & NSF/CCR-88-20279
9. PERFORMING ORGANIZATION NAME AND ADDRESS Institute for Physical Science and Technology University of Maryland, College Park, MD 20742-2431	10. PROGRAM ELEMENT, PROJECT, TASK AREA & WORK UNIT NUMBERS
11. CONTROLLING OFFICE NAME AND ADDRESS Department of the Navy Office of Naval Research Arlington, VA 22217	12. REPORT DATE June 1993 13. NUMBER OF PAGES 64 + 43 figures
14. MONITORING AGENCY NAME & ADDRESS(if different from Controlling Office)	15. SECURITY CLASS. (of this report) 15a. DECLASSIFICATION/DOWNGRADING SCHEDULE

16. DISTRIBUTION STATEMENT (of this Report)

Approved for public release: distribution unlimited

17. DISTRIBUTION STATEMENT (of the abstract entered in Block 20, if different from Report)

18. SUPPLEMENTARY NOTES

19. KEY WORDS (Continue on reverse side if necessary and identify by block number)

20. ABSTRACT (Continue on reverse side if necessary and identify by block number)

A numerical methodology which determines the quality (or robustness) of a-posteriori error estimators is described. The methodology accounts precisely for the factors which affect the quality of error estimators for finite-element solutions of linear elliptic problems, namely, the local geometry of the grid and the structure of the solution. The methodology can be employed to check the robustness of any estimator for the complex grids which are used in engineering computations.

(2)

DD FORM 1 JAN 73 1473 EDITION OF 1 NOV 65 IS OBSOLETE

S N 0102-LF-014-6601

SECURITY CLASSIFICATION OF THIS PAGE (When Data Entered)

MARYLAND

COLLEGE PARK CAMPUS

VALIDATION OF A-POSTERIORI ERROR ESTIMATORS BY NUMERICAL APPROACH

by

I. Babuška
T. Strouboulis
C. S. Upadhyay
S. K. Gangaraj
K. Copps

Technical Note BN-1151

and

CMC Report No. 93-03
Texas Engineering Experiment Station
The Texas A&M University System

June 1993

INSTITUTE FOR PHYSICAL SCIENCE AND TECHNOLOGY

Validation of A-Posteriori Error Estimators by Numerical Approach

I. Babuška[1]

Institute for Physical Science and Technology and Department of Mathematics,
University of Maryland, College Park, MD 20742, U.S.A.

T. Strouboulis[2], C.S. Upadhyay[2], S.K. Gangaraj[2], K. Copps[2]

Department of Aerospace Engineering, Texas A&M University,
College Station, TX 77843, U.S.A.

June 1993

[1]The work of this author was supported by the U.S. Office of Naval Research under Contract N00014-90-J-1030 and by the National Science Foundation under Grant CCR-88-20279.

[2]The work of these authors was supported by the U.S. Army Research Office under Grant DAAL03-G-028, by the National Science Foundation under Grant MSS-9025110 and by the Texas Advanced Research Program under Grant TARP-71071.

Abstract

A numerical methodology which determines the quality (or robustness) of a-posteriori error estimators is described. The methodology accounts precisely for the factors which affect the quality of error estimators for finite-element solutions of linear elliptic problems, namely, the local geometry of the grid and the structure of the solution. The methodology can be employed to check the robustness of any estimator for the complex grids which are used in engineering computations.

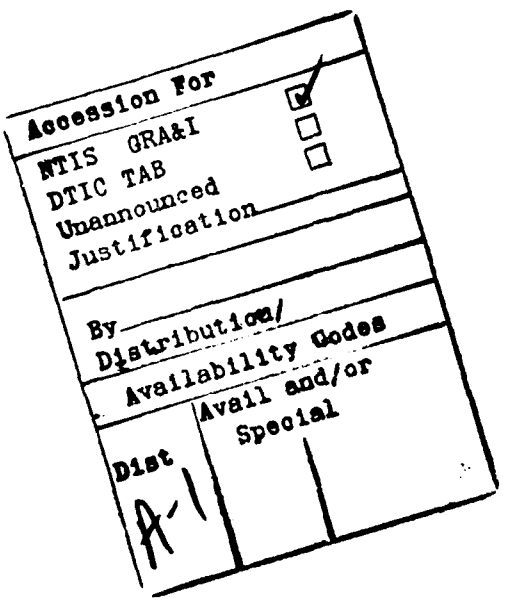

1 Introduction

A-posteriori error estimation has become a key feature of practical finite-element analysis. Because of their practical importance error estimators have been the focus of intensive research; see for example [1-53] and the references in these papers. While some a-posteriori error estimators have been analyzed mathematically (e.g. [1], [6], [9], [13], [14], [15], [16], [17], [23], [38], [39]) many estimators have been derived by purely heuristic reasoning. Usually the estimators are validated numerically on a set of *benchmarks* (example problems) which are selected in an ad-hoc manner. Most benchmark computations fail to isolate the basic factors which influence the performance of estimators and can motivate wrong conclusions. In this paper we present a clearly formulated objective *validation principle* for error estimators which takes into account the major factors influencing the performance of estimators in the case when the element is not at the boundary and the exact solution is smooth (in the neighborhood of the element). The methodology is completely numerical and can be used even when the definition of the estimator is unknown and is given only as a black-box computer program.

In practice, we are interested to have an accurate estimate of the error in a *cell* ω_0^h of the mesh $\mathcal{T}_h$ (we will use the term cell to refer to a small patch of elements; the cell may consist of a few (possibly one) elements). The performance of any error estimator in ω_0^h depends on the local geometry of the mesh in a slightly bigger *patch* ω_s^h which includes ω_0^h in its interior (see Fig. 1) and on the local structure of the solution and no heuristic benchmarks can properly account for these factors. The methodology given below enables us to focus in the cell of interest and to study the robustness of any error estimator (even if it is only available as a black-box subroutine) for the actual geometries of the grids which are used in the engineering computations. The methodology requires the solution of relatively small problems in the regions of interest and is inexpensive. In contrast, benchmarks require global computation (which can be expensive) and do not lead to reliable conclusions.

The quality of an error estimator in the cell ω_0^h is measured by the *effectivity index*

$$\kappa_{\omega_0^h} := \frac{\mathcal{E}_{\omega_0^h}}{|||e_h|||_{\omega_0^h}}, \qquad \mathcal{E}_{\omega_0^h} := \left\{ \sum_{\substack{\tau \in \mathcal{T}_h \\ \tau \cap \omega_0^h \neq \emptyset}} \eta_\tau^2 \right\}^{\frac{1}{2}} \tag{1}$$

where $|||e_h|||_{\omega_0^h}$ is the norm (of interest) of the error over ω_0^h, $\mathcal{E}_{\omega_0^h}$ is an error estimator for this norm which is computed in terms of *element error-indicators* η_τ, τ denotes an element in the mesh $\mathcal{T}_h$. In this paper, we will consider estimators for the energy-norm of the error. The methodology of the paper can also be used to study the quality of estimators for other norms. Let Ω denote the domain of the problem; in [1], [6], [9], [13], [14] it has been shown that the *range* of the *global*

effectivity index, κ_Ω, exists for several estimators based on residuals, namely there exist constants $0 \leq C_L^\Omega \leq C_U^\Omega < +\infty$ such that

$$0 \leq C_L^\Omega \leq \kappa_\Omega \leq C_U^\Omega < \infty \tag{2a}$$

The two-sided inequality (2a) has been proven under very general assumptions about the exact solution (it is only required that the exact solution has finite-energy), reasonable assumptions about the regularity of the data (all practical cases are included) and under mild restrictions on the regularity of the mesh (see the details in [6], [9], [13]). Inequality (2a) can also be written in the form

$$\frac{1}{C_U^\Omega}\,\mathcal{E}_\Omega \leq |||e^h|||_\Omega \leq \frac{1}{C_L^\Omega}\,\mathcal{E}_\Omega \tag{2b}$$

which expresses an *equivalence* between the global norm of the error and the estimator. Practical values for the *equivalency constants* C_L^Ω and C_U^Ω cannot be obtained for a given estimator unless further information is known about the class of solutions of interest and the finite-element meshes employed. A concrete example of how the constants can be estimated in the case of a simple residual estimator was given in [50] and [51]. The values of C_L^Ω and C_U^Ω depend strongly on the geometry of the grid and (relatively weakly) on the smoothness of the solution; the geometry of the grid must be understood in connection with the differential operator (see [50] for the details).

It can also be shown (see [53] and the outline given below) that under reasonable assumptions about the grid we can determine the *asymptotic* range of the effectivity index for any estimator in any small *interior-cell* ω_0^h (a cell which is separated from the boundary by several mesh-layers) of the grid; i.e. there exist constants $0 \leq C_L^{\omega_0^h} \leq C_U^{\omega_0^h} < +\infty$ which depend only on the local geometry of the grid in ω_0^h and *a few mesh-layers around* it (the geometry of the grid in a sufficiently large patch ω_*^h which includes ω_0^h in its interior) such that (as the local mesh-size in ω_0^h and ω_*^h tends to zero)

$$0 \leq C_L^{\omega_0^h} \leq \kappa_{\omega_0^h} \leq C_U^{\omega_0^h} < \infty \tag{3}$$

The constants $C_L^{\omega_0^h}$, $C_U^{\omega_0^h}$ are the best possible constants (i.e. they can be achieved) over an entire class of smooth solutions which occur in the field of application. When the values of the constants $C_L^{\omega_0^h}$, $C_U^{\omega_0^h}$ are known we can also manufacture an *upper*-(resp. *lower*-) estimator version of $\mathcal{E}_{\omega_0^h}$ denoted by $\mathcal{E}'_{\omega_0^h}$ (resp. $\mathcal{E}''_{\omega_0^h}$) defined by

$$\mathcal{E}'_{\omega_0^h} := \frac{1}{C_L^{\omega_0^h}}\,\mathcal{E}_{\omega_0^h}\,, \qquad \mathcal{E}''_{\omega_0^h} := \frac{1}{C_U^{\omega_0^h}}\,\mathcal{E}_{\omega_0^h} \tag{4a}$$

We then have

$$\left.\begin{aligned} 1 \le \kappa'_{\omega_0^h} &:= \frac{\mathcal{E}'_{\omega_0^h}}{|||e^h|||_{\omega_0^h}} \le \frac{C_U^{\omega_0^h}}{C_L^{\omega_0^h}} \\ \frac{C_L^{\omega_0^h}}{C_U^{\omega_0^h}} \le \kappa''_{\omega_0^h} &:= \frac{\mathcal{E}''_{\omega_0^h}}{|||e^h|||_{\omega_0^h}} \le 1 \end{aligned}\right\} \qquad (4b)$$

The lower-estimator version of an estimator may be employed to drive adaptive-refinement algorithms in order to avoid over-refinement while the upper-estimator version may be used to guarantee a safe stopping-criterion.

Let us define the *robustness index* $\mathcal{R}_{\omega_0^h}$ $(0 \le \mathcal{R}_{\omega_0^h} < \infty)$ which expresses the reliability of the estimator:

$$\mathcal{R}_{\omega_0^h} := \max\left\{ \left(|1 - C_U^{\omega_0^h}| + |1 - C_L^{\omega_0^h}| \right) , \left(|1 - \frac{1}{C_U^{\omega_0^h}}| + |1 - \frac{1}{C_L^{\omega_0^h}}| \right) \right\} \qquad (5a)$$

The robustness index expresses the deviation of κ and $\frac{1}{\kappa}$ (see (2a), (2b)) from the *ideal value* $\kappa = 1$. (Hence $\mathcal{R}_{\omega_0^h} = 0$ is the ideal value for the robustness index.) The robustness of an estimator for a given class of meshes $\mathcal{T} = \{\mathcal{T}_h\}$ is given by

$$\mathcal{R}(\mathcal{T}) := \max_{\mathcal{T}_h \in \mathcal{T}} \mathcal{R}_{\mathcal{T}_h} , \qquad \mathcal{R}_{\mathcal{T}_h} := \max_{\omega_0^h \in C(\mathcal{T}_h)} \mathcal{R}_{\omega_0^h} \qquad (5b)$$

Here $C(\mathcal{T}_h)$ is the set of interior cells in the mesh $\mathcal{T}_h$. The robustness index defined in (5b) characterizes the performance of the estimator for elements in the interior of the domain. Because most elements are in the interior of the domain (where the solution is smooth) the validation of the estimators has to be made especially for the case presented in this paper. The validation of the estimators for elements located at the boundary and for unsmooth solutions will be given in subsequent papers.

If an estimator does not display reasonable robustness for the interior-cells, i.e. if $\mathcal{R}(\mathcal{T})$ is too large, the estimator is unreliable and should not be considered any further. The robustness index depends on $\mathcal{T}$, the family of meshes under consideration. (Hence restrictions placed on the mesh-generator could possibly increase the reliability of an estimator.)

The robustness index is an *objective quantitative* characterization of the reliability of an estimator. Hence, analogously as the effectivity index, the robustness index of an estimator should be reported.

Following this Introduction we present the definition of the model problems (linear elasticity and heat-conduction), we describe two types of error estimators, we present the methodology for the computation of the robustness index and we outline its theoretical justification. Finally, we give examples which demonstrate how the robustness index of error estimators for complex finite-element meshes can be computed and how it is possible to increase the reliability of an estimator by proper selection of its various parameters.

2 The model problems

We shall consider the vector-valued boundary-value problem

$$\left.\begin{aligned} L_i(\mathbf{u}) := -\sum_{j=1}^{2} D_j\big(\sigma_{ij}(\mathbf{u})\big) = f_i \qquad & \text{in } \Omega \\ u_i = 0 \qquad & \text{on } \Gamma_D \\ \sum_{j=1}^{2} \sigma_{ij}(\mathbf{u}) n_j = \bar{t}_i \qquad & \text{on } \Gamma_N \end{aligned}\right\} \tag{6}$$

where $i = 1, 2$.

Here $\Omega \subset \mathbf{R}^2$ is a bounded domain with boundary $\partial\Omega = \Gamma_D \cup \Gamma_N$;

$\mathbf{n} := (n_1, n_2)$ is the outward pointing unit-normal on Γ_N;

f_i, $i = 1,2$ are the components of the load-vector (*body-force*);

$\bar{t}_i$, $i = 1,2$ are the components of the normal-flux vector (*traction*) applied on Γ_N;

$\Gamma_D \neq \emptyset$, $\Gamma_D \cap \Gamma_N = \emptyset$; $\mathbf{u} = (u_1, u_2)$ is the solution-vector (*displacement*);

$$\epsilon_{ij}(\mathbf{u}) := \frac{1}{2}(D_j u_i + D_i u_j)\,, \qquad i,j = 1,2 \tag{7a}$$

$$\sigma_{ij}(\mathbf{u}) := \sum_{k,\ell=1}^{2} a_{ijk\ell}\,\epsilon_{k\ell}(\mathbf{u})\,, \qquad i,j = 1,2 \tag{7b}$$

are the components of the flux (*strain, stress*);

$a_{ijk\ell}$, $i,j,k,\ell = 1,2$, are the material-coefficients (*elastic constants*) which satisfy

$$a_{ijk\ell} = a_{jik\ell} = a_{k\ell ij}\,, \qquad i,j,k,\ell = 1,2 \tag{8a}$$

$$\sum_{i,j,k,\ell=1}^{2} a_{ijk\ell}\,\epsilon_{ij}\,\epsilon_{k\ell} \geq c \sum_{i,j=1}^{2} \epsilon_{ij}\,\epsilon_{ij}\,, \quad c>0\,, \qquad \forall\ \epsilon_{ij}=\epsilon_{ji} \tag{8b}$$

(Conditions (8a), (8b) are satisfied for linear elasticity; in the case of isotropic plane elasticity we have $a_{ijk\ell}=\mu(\delta_{ij}\delta_{k\ell}+\delta_{i\ell}\delta_{kj})+\lambda\delta_{ik}\delta_{j\ell}$ where δ_{ij} is Kronecker's delta and $\lambda\,,\mu$ are Lamé's constants.)

We also introduce the scalar elliptic boundary-value problem (*heat-conduction in orthotropic medium*), namely

$$\left.\begin{aligned} L'(u) &:= -\sum_{k,\ell=1}^{2} D_k\left(K_{k\ell}D_\ell u\right) = f \qquad \text{in } \Omega \\ u &= 0 \qquad\qquad\qquad\qquad\quad \text{on } \Gamma_D \\ \sum_{k=1}^{2} q_k(u)n_k &= \bar{t} \qquad\qquad\qquad\quad \text{on } \Gamma_N \end{aligned}\right\} \tag{9}$$

Here $q_k(u) := \sum_{\ell=1}^{2} K_{k\ell}D_\ell u\,,\ k=1,2$ are the components of the flux-vector (*heat-flux*) and $K_{k\ell}$, $k,\ell=1,2$, are the entries of the *thermal-conductivity* matrix which satisfy

$$K_{k\ell}=K_{\ell k}\,, \quad k,\ell=1,2 \tag{10a}$$

$$0<K_{\min}(\xi_1^2+\xi_2^2) \leq \sum_{k,\ell=1}^{2} K_{k\ell}\xi_k\xi_\ell \leq K_{\max}(\xi_1^2+\xi_2^2)\,, \qquad \xi\in\mathbf{R}^2 \tag{10b}$$

Here $K_{\min}, K_{\max}$ denote the principal values of the thermal-conductivity matrix.

Let us now cast the model problem in variational form. Let us denote

$$\mathbf{H}^1 := \left\{(v_1,v_2):\ v_i\in H^1(\Omega)\right\}$$

$$\mathbf{H}^1_{\Gamma_D} := \left\{(v_1,v_2):\ v_i\in H^1(\Omega),\ v_i=0 \text{ on } \Gamma_D\right\}$$

$$\|\mathbf{v}\|_{1,\Omega} := \left(\sum_{i=1}^{2}\|v_i\|^2_{1,\Omega}\right)^{\frac{1}{2}},\ |\mathbf{v}|_{1,\Omega} := \left(\sum_{i=1}^{2}|v_i|^2_{1,\Omega}\right)^{\frac{1}{2}}$$

with $\|v_i\|_{1,\Omega}$ ($|v_i|_{1,\Omega}$) being the usual $H^1(\Omega)$ Sobolev norm (seminorm). The variational form of the boundary-value problem (6) is now posed as:

Find $\mathbf{u} \in \mathbf{H}^1_{\Gamma_D}$ such that

$$\mathcal{B}_\Omega(\mathbf{u},\mathbf{v}) = \int_\Omega \sum_{i=1}^{2} f_i v_i + \int_{\Gamma_N} \sum_{i=1}^{2} \bar{t}_i v_i \qquad \forall\, \mathbf{v} \in \mathbf{H}^1_{\Gamma_D} \tag{11}$$

where the bilinear form $\mathcal{B}_\Omega : \mathbf{H}^1_{\Gamma_D} \times \mathbf{H}^1_{\Gamma_D} \to \mathbf{R}$ is defined by

$$\mathcal{B}_\Omega(\mathbf{u},\mathbf{v}) := \int_\Omega \sum_{i,j,k,\ell=1}^{2} a_{ijk\ell} D_\ell u_j D_k v_i \,. \tag{12}$$

The energy-norm over any subdomain $S \subseteq \Omega$ is defined by

$$|||\mathbf{v}|||_S := \sqrt{\mathcal{B}_S(\mathbf{v},\mathbf{v})} \tag{13}$$

where $\mathcal{B}_S(\mathbf{u},\mathbf{v})$ has the obvious meaning.

In the case of the scalar elliptic problem given by (9) the bilinear form is given by $\mathcal{B}'_\Omega(u,v) := \int_\Omega \sum_{k,\ell=1}^{2} K_{k\ell} D_\ell u D_k v$. The weak-solution of (9) satisfies:

Find $u \in H^1_{\Gamma_D} := \left\{ v \in H^1(\Omega) \;:\; v = 0 \;\text{ on }\; \Gamma_D \right\}$ such that

$$\mathcal{B}'_\Omega(u,v) = \int_\Omega fv + \int_{\Gamma_N} \bar{t}v \qquad \forall\; v \in H^1_{\Gamma_D} \tag{14}$$

The energy-norm in any subdomain $S \subseteq \Omega$ is defined by $|||v|||_S := \sqrt{\mathcal{B}'_S(v,v)}$.

Let $\mathcal{T} = \{\mathcal{T}_h\}$ be a family of meshes of triangles or quadrilaterals with straight edges. It is assumed that the family is regular (i.e.: for the triangles the minimal angle of all the triangles is bounded below by a positive constant, the same for all the meshes; for the quadrilaterals see conditions (37.40) in Ciarlet [58]). The meshes are not assumed to be quasiuniform. Let us introduce the finite-element spaces

$$\mathbf{S}^p_h := \left\{ \mathbf{u} \in \mathbf{H}^1 \;:\; u_i \circ \mathbf{Q}^{(k)} \in \mathcal{P}_p(\hat{\tau}), \quad i = 1,2, \quad k = 1,\ldots,M(\mathcal{T}_h) \right\} \tag{15}$$

where $\mathbf{Q}^{(k)}$ is the mapping function for the kth finite-element which maps either a standard triangular element (using an affine transformation) or a standard quadrilateral element (using a bilinear transformation) onto the kth finite element, $\hat{\tau}$

denotes a standard element, $M(\mathcal{T}_h)$ is the number of elements in the mesh $\mathcal{T}_h$, $\mathcal{P}_p(\hat{\tau})$ denotes the set of polynomials of degree p over $\hat{\tau}$. We let

$$\mathbf{S}^p_{h,\Gamma_D} := \mathbf{S}^p_h \cap \mathbf{H}^1_{\Gamma_D} .$$

The finite element solution $\mathbf{u}^h$ (for the elasticity problem) satisfies:

Find $\mathbf{u}^h \in \mathbf{S}^p_{h,\Gamma_D}$ such that

$$B_\Omega(\mathbf{u}^h, \mathbf{v}^h) = \int_\Omega \sum_{i=1}^{2} f_i v_i^h + \int_{\Gamma_N} \sum_{i=1}^{2} g_i v_i^h \qquad \forall\, \mathbf{v}^h \in \mathbf{S}^p_{h,\Gamma_D} \tag{16}$$

The error is $\mathbf{e}^h := \mathbf{u} - \mathbf{u}^h$.

Remark 2.1. We addressed only (for simplicity) the model problems for which the differential operator $\mathbf{L}$ (or L') is homogeneous with constant coefficients. The theory and the procedure holds for the general case, for non-homogeneous operators with non-constant (but smooth) coefficients.

In the following we give two representative classes of estimators for the energy-norm of the error and we employ the model methodology to check the robustness of various versions of estimators from these classes. Below we define the estimators for the elasticity problem (the estimators for the scalar model problem (9) may be obtained by analogy; see also [53]).

3 Element-residual error estimators

3.1 Implicit element-residual estimator

We introduce notations needed for the description of the estimators (see also [8], [14]). For each closed triangle (quadrilateral) $\tau \in \mathcal{T}_h$, we denote by $E(\tau)$ and $N(\tau)$ the set of its edges and vertices, respectively. We define the local *bubble-spaces* of polynomials (see [8], [11], [12], [14], [21], [22], [23])

$$\mathbf{H}_\tau := \left\{ \mathbf{w} \;:\; w_i \in \mathcal{P}_{p+1}\,, \quad w_i(X) = 0 \qquad \forall\, X \in N(\tau)\,, \quad i = 1,2 \right\} ,$$

over each element $\tau \in \mathcal{T}_h$.

We define the *interior-residual* in element τ as

$$\mathbf{r}_\tau := -\mathbf{L}(\mathbf{u}^h) + \mathbf{f} \tag{17}$$

where $\mathbf{L}(\mathbf{u}^h) := \left(L_1(\mathbf{u}^h), L_2(\mathbf{u}^h)\right)$, $\mathbf{f} := (f_1, f_2)$,

and the *jump* or *edge-residual* associated with the edge ϵ

$$\mathbf{J}_\epsilon := \left[\sigma(\mathbf{u}^h|_{\tau_{\text{out}}}) - \sigma(\mathbf{u}^h|_{\tau_{\text{in}}})\right]\mathbf{n} \tag{18}$$

where $\mathbf{n}$ is the unit-normal for the edge ϵ and τ_{in} and τ_{out} are defined as in Fig. 2. The *residual-functional* for element τ is

$$\mathcal{F}_\tau(\mathbf{v}) := \int_\tau \mathbf{v}\cdot\mathbf{r}_\tau + \frac{1}{2}\sum_{\epsilon\in\mathcal{E}(\tau)}\int_\epsilon \mathbf{v}\cdot\mathbf{J}_\epsilon\,, \qquad \mathbf{v}\in\mathbf{H}^1(\tau) \tag{19}$$

We now define the element-residual estimator for the model problem (6) (we give the estimators only for elements in the interior of the domain).

The element error indicators for the implicit element-residual estimators for elements of any degree p are:

$$\eta_\tau := |||\mathbf{e}_\tau|||_\tau \tag{20}$$

where

$$\mathbf{e}_\tau\in\mathbf{H}_\tau\,: \quad \mathcal{B}_\tau(\mathbf{e}_\tau,\mathbf{v}_\tau) = \mathcal{F}_\tau(\mathbf{v}_\tau)\,, \qquad \forall\ \mathbf{v}_\tau\in\mathbf{H}_\tau \tag{21}$$

3.2 Equilibrium of the residuals

The residual data for the local problems (21) are *equilibrated* if the following *consistency conditions* (*equilibrium equations*) are satisfied,

$$\left.\begin{aligned} \int_\tau \mathbf{r}_\tau + \frac{1}{2}\sum_{\epsilon\in\mathcal{E}(\tau)}\int_\epsilon \mathbf{J}_\epsilon &= 0\,\mathbf{i}_1 + 0\,\mathbf{i}_2 \\ \int_\tau \mathbf{x}\times\mathbf{r}_\tau + \frac{1}{2}\sum_{\epsilon\in\mathcal{E}(\tau)}\int_\epsilon \mathbf{x}\times\mathbf{J}_\epsilon &= 0\,\mathbf{i}_3 \end{aligned}\right\} \tag{22}$$

Here $\mathbf{i}_1$, $\mathbf{i}_2$ denote the unit-vectors along the global coordinate directions in $\mathbf{R}^2$ and $\mathbf{i}_3$ the out-of-plane unit-vector. The element equilibrium equations (22) will hold if

$$\left.\begin{aligned} \sum_{i=1}^{nv}\left\{\mathcal{F}_\tau(\mathbf{i}_1 N_i)\,\mathbf{i}_1 + \mathcal{F}_\tau(\mathbf{i}_2 N_i)\,\mathbf{i}_2\right\} &= 0\,\mathbf{i}_1 + 0\,\mathbf{i}_2 \\ \sum_{i=1}^{nv}\mathbf{x}_i\times\left\{\mathcal{F}_\tau(\mathbf{i}_1 N_i)\,\mathbf{i}_1 + \mathcal{F}_\tau(\mathbf{i}_2 N_i)\,\mathbf{i}_2\right\} &= 0\,\mathbf{i}_3 \end{aligned}\right\} \tag{23}$$

It is assumed that the set of functions $\{N_i\}_{i=1}^{nv}$ satisfies $\sum_{i=1}^{nv} N_i|_\tau = 1\,,\ \forall\,\tau \in \mathcal{T}_h\,.$

The equilibrium conditions for element τ will be satisfied automatically if

$$\mathcal{F}_\tau(\mathrm{i}_\ell N_i) = 0\,, \qquad \ell = 1,2, \qquad i = 1,\ldots,nv \tag{24}$$

These conditions, however, are not expected to hold for general meshes and solutions; below we discuss ways of *correcting* the definition of $\mathcal{F}_\tau$ to satisfy conditions (24).

Remark 3.1. A possible choice for the functions $\{N_i\}_{i=1}^{nv}$ is a set of Lagrangian basis functions of degree $q \leq p$ (p is the polynomial degree of the finite-element space) defined over $\mathcal{T}_h$. In the discussion below we let $q = 1$, $N_i|_\tau$ is the linear (for triangles) or bilinear (for quadrilaterals) element-shape-function which corresponds to the i-th vertex and nv is the number of vertices for element τ ($nv = 3$ for triangles, $nv = 4$ for quadrilaterals).

3.2.1 Ladeveze's flux-splitting technique

The definition of $\mathcal{F}_\tau$ in (19) may to be modified in order to satisfy (24) by letting

$$\mathcal{F}_\tau^{\mathrm{mQ}}(\mathbf{v}) := \mathcal{F}_\tau(\mathbf{v}) + \int_{\partial\tau} \mathbf{v}\cdot\boldsymbol{\theta}_\tau\,, \qquad \mathbf{v} \in \mathbf{H}^1(\tau) \tag{25}$$

Here, $\boldsymbol{\theta}_\tau \in \left(L^2(\partial\tau)\right)^2$ is the *correction* of the edge-residuals for the element τ. We let

$$\boldsymbol{\theta}_\tau|_\epsilon = \zeta_\tau^\epsilon \left(\theta_\epsilon^1\psi_1^\epsilon + \theta_\epsilon^2\psi_2^\epsilon\right)\,, \qquad \epsilon \in E(\tau) \tag{26}$$

where,

$$\zeta_\tau^\epsilon = \begin{cases} +1, & \text{if } \tau = \tau_{\mathrm{in}}, \\ -1, & \text{if } \tau = \tau_{\mathrm{out}}, \end{cases}$$

where it is assumed that the edge normal $\mathbf{n}$ has been assigned to the edge ϵ in an arbitrary but unique way and τ_{in} and τ_{out} are defined as shown in Fig. 2. Here, the linear functions ψ_k^ϵ are defined as,

$$\psi_k^\epsilon := \frac{2}{|\epsilon|}\left(2\lambda_k^\epsilon - \lambda_{k+1}^\epsilon\right)\,, \qquad k = 1,2 \tag{27}$$

where λ_k^ϵ, $k = 1,2$ are the linear shape-functions defined over the edge ϵ and the subscript $k+1$ is taken modulo-2. Using this definition of $\boldsymbol{\theta}_\tau|_\epsilon$ we can decouple the problem of determination of $\boldsymbol{\theta}_\tau|_\epsilon$ for the whole domain into small local problems

involving only patches of elements connected to node X, as shown in Fig. 3a. We have

$$\theta_\epsilon^k := \int_\epsilon \theta_\tau|_\epsilon \, \lambda_k^\epsilon \,, \qquad k = 1,2 \,, \qquad \epsilon \in E(\tau) \tag{28}$$

Thus, for each patch around a node X we obtain a linear system (see [24], [8], [32], [59] and [60] for the details)

$$\int_{\partial \tau_k^X} (\mathbf{i}_\ell \cdot \theta_{\tau_k^X}) \, \phi_X = -\mathcal{F}_\tau(\mathbf{i}_\ell \phi_X) \,, \qquad \ell = 1,2 \qquad k = 1, \ldots, N_X \tag{29}$$

where ϕ_X denotes the elementwise affine basis function (for meshes of triangles) which corresponds to the vertex X, τ_k^X denotes the k-th element connected to the vertex X, N_X is the number of elements (or edges) connected to the vertex X.

The procedure outlined above has been developed by Ladeveze [59]. The linear system (29) has a one parameter family of solutions. Specific choices of solutions are suggested in [8], [25], [32], [60] and [61]; in the numerical implementations we employed these choices. Below we give the definition of the edgewise-linear correction θ_τ (q-degree ($q \geq 1$) polynomial representation of the correction θ_τ over each edge is also possible) which results by using the equilibration procedures in [8], [25], [32], [60] and [61]. Let us consider the interior-vertex X and let us also denote ϵ_i, $i = 1, \ldots, N_X$ the edges connected to X. We will determine the coefficients $\theta_\epsilon^{\nu(\epsilon,X)}$ which is associated with the edge ϵ and the vertex X and is employed in (26). Here the index $\nu(\epsilon, X)$ identifies the local enumeration of node X, as used in (26) for the unknowns associated with the edge; see Fig. 3b.

a. Bank and Weiser's equilibration:

A solution of (29) can be obtained by letting

$$\left.\begin{aligned} &\mathbf{i}_\ell \cdot \theta_{\epsilon_1}^{\nu(\epsilon_1,X)} = -\mathcal{F}_{\tau_1^X}(\mathbf{i}_\ell \phi_X) \,, \qquad \ell = 1,2 \\ &\mathbf{i}_\ell \cdot \theta_{\epsilon_i}^{\nu(\epsilon_i,X)} = \mathbf{i}_\ell \cdot \theta_{\epsilon_{i-1}}^{\nu(\epsilon_{i-1},X)} - \mathcal{F}_{\tau_i^X}(\mathbf{i}_\ell \phi_X) \,, \qquad \ell = 1,2; \quad i = 2, \ldots, N \end{aligned}\right\} \tag{30}$$

This choice of solution has been suggested in [8].

b. Ladeveze's equilibration:

Here the coefficients $\theta_{\epsilon_i}^{\nu(\epsilon_i,X)} = \sum_{\ell=1}^{2} (\mathbf{i}_\ell \cdot \theta_{\epsilon_i}^{\nu(\epsilon_i,X)}) \mathbf{i}_\ell$, $i = 1, \ldots, N$ are selected such that

$$I_\ell^X(\theta) := \sum_{i=1}^{N} \left[w_i \, (\mathbf{i}_\ell \cdot \theta_{\epsilon_i}^{\nu(\epsilon_i,X)}) \right]^2 \tag{31}$$

is minimized for $\ell = 1$ and $\ell = 2$ separately, where w_i is the weight associated with each edge ϵ_i. In [25] and [32] the weights w_i have been taken as 1. For this choice of weights, the solution of (24) is given explicitly as,

$$\left.\begin{aligned}
&\mathbf{i}_\ell \cdot \boldsymbol{\theta}^{\nu(\epsilon_N,X)}_{\epsilon_N} = \frac{1}{N}\sum_{i=1}^{N}(N-i+1)\mathcal{F}_{\tau_i X}(\mathbf{i}_\ell \phi_X)\ ,\ \ell = 1,2 \\
&\mathbf{i}_\ell \cdot \boldsymbol{\theta}^{\nu(\epsilon_1,X)}_{\epsilon_1} = \mathbf{i}_\ell \cdot \boldsymbol{\theta}^{\nu(\epsilon_N,X)}_{\epsilon_N} - \mathcal{F}_{\tau_1 X}(\mathbf{i}_\ell \phi_X)\,,\ \ell = 1,2 \\
&\mathbf{i}_\ell \cdot \boldsymbol{\theta}^{\nu(\epsilon_i,X)}_{\epsilon_i} = \mathbf{i}_\ell \cdot \boldsymbol{\theta}^{\nu(\epsilon_{i-1},X)}_{\epsilon_{i-1}} - \mathcal{F}_{\tau_i X}(\mathbf{i}_\ell \phi_X)\ ,\ \ell = 1,2;\ i = 2,3,\ldots,(N-1)
\end{aligned}\right\} \quad (32)$$

If we take the weights $w_i := |\epsilon_i|^{-1}$, as suggested in [60] and [61], we can obtain a different $\boldsymbol{\theta}_\tau$ satisfying (29).

Remark 3.2. From eq. (29) we can see that the functional $\mathcal{F}^{\mathrm{RQ}}_\tau$ with any of the above choices of the correction $\boldsymbol{\theta}_\tau$ as the above will satisfy (24) and therefore the equilibrium conditions (22).

3.2.2 Ohtsubo-Kitamura flux-splitting

In [29-31] a different procedure for determining equilibrated force-fields for an element τ is described. In this procedure each element can be equilibrated separately from its neighbors i.e. the equilibrations are done at the element-level. The technique has as follows:

Let us define the residual-functional

$$\mathcal{F}'_\tau(\mathbf{v}) = \int_\tau \mathbf{r}_\tau \cdot \mathbf{v} + \sum_{\epsilon \in E(\tau)} \int_\epsilon \alpha^\tau_\epsilon \mathbf{J}_\epsilon \cdot \mathbf{v}\,, \qquad \forall\, \mathbf{v} \in H^1(\tau) \quad (33)$$

Here α^τ_ϵ is the *geometric splitting-factor* for the *initial allocation* of the jump $\mathbf{J}_\epsilon$ defined by

$$\alpha^{\tau_{\mathrm{in}}}_\epsilon := \frac{d^{\tau_{\mathrm{in}}}_\epsilon}{d^{\tau_{\mathrm{in}}}_\epsilon + d^{\tau_{\mathrm{out}}}_\epsilon}\,, \quad \alpha^{\tau_{\mathrm{out}}}_\epsilon := \frac{d^{\tau_{\mathrm{out}}}_\epsilon}{d^{\tau_{\mathrm{in}}}_\epsilon + d^{\tau_{\mathrm{out}}}_\epsilon}$$

where $d^{\tau_{\mathrm{in}}}_\epsilon$, $d^{\tau_{\mathrm{out}}}_\epsilon$ is the distance of the centroid of the element τ_{in}, τ_{out}, respectively, from the common edge ϵ (the choice of the splitting-factors is motivated from the one-dimensional case where a unique flux-splitting exists; see [25], [26] and page 296 in [62]). Following [29-31] we will assume that the finite-element solution has been computed using bilinear quadrilaterals (or linear triangles) and the local

element-residual problem is discretized using 8-node serendipity quadrilateral (6-node Lagrangian triangle). Then the discrete nodal-forces for the local problem are

$$\mathbf{g}_i = \sum_{e \in E(\tau)} \int_e \alpha_e^\tau \mathbf{J}_e \widetilde{N}_i \tag{34}$$

where $\widetilde{N}_i$, $i = 1, \ldots, nv'$ ($nv' = 8$ for quadrilaterals, $nv' = 6$ for triangles) are the Lagrangian shape-functions used in the discretization of the local residual-problem.

The consistency conditions for the discrete element-residual problem in element τ are

$$\left.\begin{aligned} \int_\tau \mathbf{r}_\tau + \sum_{i=1}^{nv'} \bar{\mathbf{g}}_i &= 0\,\mathbf{i}_1 + 0\,\mathbf{i}_2 \\ \int_\tau \mathbf{x} \times \mathbf{r}_\tau + \sum_{i=1}^{nv'} \mathbf{x}_i \times \bar{\mathbf{g}}_i &= 0\,\mathbf{i}_3 \end{aligned}\right\} \tag{35}$$

Here $\bar{\mathbf{g}}_i$ $i = 1, \ldots, nv'$ are the *consistent nodal-forces* which satisfy (35). In general the loads $\mathbf{g}_i$ given by (34) (from the initial flux-splitting) do not satisfy the consistency conditions (35). We seek *corrective-loads* $\Delta\mathbf{g}_i$ such that

$$\bar{\mathbf{g}}_i = \mathbf{g}_i + \Delta\mathbf{g}_i \tag{36}$$

Following [31] we will select $\{\Delta\mathbf{g}_i\}_{i=1}^{nv'}$ such that it satisfies (35) and has minimal Euclidean-norm in $\mathbf{R}^{nv'}$ (this choice is motivated by the idea that the correction should be as small as possible; see [31]).

4 Error estimators based on smoothening techniques

Error estimators based on *recovery methods* are given in [33-44]. Here we focus on the *superconvergent patch-recovery* technique [40-44]. The element error-indicators for elements of any degree p are

$$\eta_\tau := ||\sigma^* - \sigma(\mathbf{u}^h)||_{L^2(\tau), a^{-1}} \tag{37}$$

where

$$||\sigma||^2_{L^2(\tau), a^{-1}} := \int_\tau \sigma_{ij}\, a^{-1}_{ijk\ell}\, \sigma_{k\ell} \tag{38}$$

where $a^{-1}_{ijk\ell}$ are the entries of the compliance tensor, σ^* is the recovered flux.

Let $\omega_X := \bigcup_{X \in N(\tau')} \tau'$ denote the patch of elements connected to vertex X. For each patch ω_X we recover the *patch-projection* $\tilde{\sigma}^X$ by solving the following least-squares problem:

$$\inf_{\substack{\sigma^X_{ij} \in \mathcal{P}_p(\omega_X) \\ i,j=1,2}} ||\sigma(\mathbf{u}^h) - \sigma^X||_{L^2(\omega_X),a^{-1},\{\mathbf{y}_\ell\}_{\ell=1}^{nsp}} = ||\sigma(\mathbf{u}^h) - \tilde{\sigma}^X||_{L^2(\omega_X),a^{-1},\{\mathbf{y}_\ell\}_{\ell=1}^{nsp}} \quad (39)$$

where $\{\mathbf{y}_\ell\}_{\ell=1}^{nsp}$ denotes a set of *sampling points* in ω_X and

$$||\sigma||^2_{L^2(\omega_X),a^{-1},\{\mathbf{y}_\ell\}_{\ell=1}^{nsp}} := \sum_{m=1}^{nsp} \left[\sum_{i,j,k,\ell=1}^{2} \sigma_{ij}(\mathbf{y}_m)\ a^{-1}_{ijk\ell}\ \sigma_{k\ell}(\mathbf{y}_m) \right] \quad (40)$$

σ^* is obtained by averaging the patch-projections $\tilde{\sigma}^X$ over the elements (see [40], [41]).

Note that the class of estimators given in [40-41], [43-44] use only the approximate solution $\mathbf{u}^h$ to estimate the error. It is possible to modify the definition of the estimators to include the information given by the data and the differential equation. In [42] a modified patch-projection $\tilde{\sigma}^X$ was defined to take into account the additional information, namely

$$F(\tilde{\sigma}^X) = \inf_{\substack{\sigma^X_{ij} \in \mathcal{P}_p(\omega_X) \\ i,j=1,2}} F(\sigma^X) \quad (41)$$

where

$$F(\sigma) := ||\sigma(\mathbf{u}^h) - \sigma||^2_{L^2(\omega_X),a^{-1},\{\mathbf{y}_\ell\}_{\ell=1}^{nsp}} + \sum_{i=1}^{2} ||f_i + \sum_{j=1}^{2} D_j(\sigma_{ij})||^2_{L^2(\omega_X),\{\mathbf{y}_\ell\}_{\ell=1}^{nsp}} \quad (42)$$

and

$$||v||^2_{L^2(\omega_X),\{\mathbf{y}_\ell\}_{\ell=1}^{nsp}} := \sum_{m=1}^{nsp} \Big(v(\mathbf{y}_m)\Big)^2, \qquad v \in C^0(\omega_X) \quad (43)$$

In the majority of the practical problems the body-force vanishes identically ($f_i = 0,\ i = 1,2$). To take this information into account we define the space of "harmonic" polynomial fluxes:

$$\mathbf{S}^\sigma_p(\omega_X) := \left\{ \sigma\ :\ \sigma_{ij} \in \mathcal{P}_p(\omega_X)\,,\ i,j = 1,2 \ \text{ and } \ \sum_{j=1}^{2} D_j(\sigma_{ij}) = 0\,,\ i = 1,2 \right\} \quad (44)$$

We may now modify the minimization problem in (39) by seeking the minimum over $\mathbf{S}_p^o(\omega_X)$; σ^X in this case will be called "harmonic" patch-projection.

Remark 4.1. Although the intention is to use superconvergence points, the estimator performs very well (as will be seen later) also if the sampling points are not superconvergence points (which for general meshes do not exist). In general, the performance of the estimator depends on the selection of the sampling points. The sampling points in each element are obtained by mapping the points defined in the standard-element for each element-type (see Fig. 4; the performance of the estimators for the various choices of sampling points will be addressed below) and may be selected, more or less, arbitrarily but must be invariant with respect to cyclic permutations of the vertices of the elements (the error estimator must be independent from the enumeration of the grid).

5 Theoretical setting of the methodology

The theoretical justification of the numerical methodology for checking error estimators is outlined below (see [53] for the complete presentation). The mathematical framework is outlined for special types of grids which are *locally-periodic* in the regions of interest (here we assume triangular grids; the theoretical setting for meshes of quadrilaterals with straight-edges follows similar steps). These grids are made locally by the periodic repetition of a *super-patch* as shown in Fig. 5b. The theory has asymptotic character (it holds for sufficiently small size of the super-patch) and can be also used to study the local asymptotic properties of general grids like the ones shown in Figs. 1 and 6. These are typical meshes produced by automatic mesh generators and include various patches of different geometrical structure (The grid of triangles shown in Fig. 6 was constructed using a commercial mesh-generator; the grid of quadrilaterals shown in Fig. 1 was obtained by *converting* the mesh of triangles shown in Fig. 6 into a mesh of quadrilaterals. Note that the grids are refined in the interior because they were originally constructed to include an interior material interface. We adopted these grids because they are rich in patterns and we considered model problems in *homogeneous* continua.). Here, for simplicity, we will address only the case where u satisfies Poisson's equation ($-\Delta u = f$; $K_{k\ell} = \delta_{k\ell}$ in (9)) and is approximated by piecewise-linear finite-elements, ($p = 1$). Nevertheless, the results could be easily generalized to the general setting of elasticity in orthotropic medium (see eqs. (6)-(8)), to meshes of quadrilaterals and to higher-order elements.

It will be shown that the robustness index of the shaded cell shown in Fig. 5c depends practically (in the range of engineering accuracy) on the mesh in its neighborhood (the grid-geometry in the patch included within the thick-line perigram in Fig. 5c) and not on the further extension of the mesh into the periodic super-patch. Let us now specify more precisely the class of meshes employed by the

mathematical analysis. Let $0 < H_{Z_0} < H_{\Omega_0} < H^0$, $\mathbf{x}^0 = (x_1^0, x_2^0) \in \Omega$,

$$S(\mathbf{x}^0, H) := \left\{ \mathbf{x} = (x_1, x_2) \ : \ |x_i - x_i^0| < H, \ \ i = 1,2 \right\} \tag{45}$$

and assume that H^0 is sufficiently small that $\bar{S}(\mathbf{x}^0, H^0) \subset \Omega$. By $\bar{S}(\mathbf{x}^0, H)$ we denote the domain of $S(\mathbf{x}^0, H)$ with its boundary. We have

$$Z_0 := S(\mathbf{x}^0, H_{Z_0}) \subseteq \Omega_0 := S(\mathbf{x}^0, H_{\Omega_0}) .$$

Further, let $(i,j) \in \gamma$ be a set of multi-indices, $\mathbf{x}^{(i,j)} = (x_1^{(i,j)}, x_2^{(i,j)}) \in \Omega$ and

$$c(\mathbf{x}^{(i,j)}, h) := S(\mathbf{x}^{(i,j)}, h) \subset S(\mathbf{x}^0, H^0) , \qquad (i,j) \in \gamma \tag{46}$$

be the set of the h-super-patches (briefly super-patches) which cover $S(\mathbf{x}^0, H^0)$ such that

$$\bigcup_{(i,j) \in \gamma} \bar{c}(\mathbf{x}^{(i,j)}, h) = \bar{S}(\mathbf{x}^0, H^0) \tag{47a}$$

$$c(\mathbf{x}^{(i_1,j_1)}, h) \bigcap c(\mathbf{x}^{(i_2,j_2)}, h) = \emptyset \ \text{ for } \ (i_1, j_1) \neq (i_2, j_2) \ . \tag{47b}$$

We will assume that $S(\mathbf{x}^0, H_{Z_0})$ (and $S(\mathbf{x}^0, H_{\Omega_0})$) can be partitioned into the set of super-patches

$$\bar{S}(\mathbf{x}^0, H_{Z_0}) = \bigcup_{\bar{c}(\mathbf{x}^{(i,j)}, h) \cap S(\mathbf{x}^0, H_{Z_0}) \neq \emptyset} \bar{c}(\mathbf{x}^{(i,j)}, h) \ .$$

(An example of a general domain Ω with the subdomains Z_0, Ω_0 and $S(\mathbf{x}^0, H^0)$ is given in Fig. 5a)

Denoting by

$$\tilde{c} := \left\{ (x_1, x_2) : \ \ | \, x_1 \, | < 1, \ \ | \, x_2 \, | < 1 \right\} \tag{48}$$

the *unit-* (*master-*) super-patch $\tilde{c}$, the h-cell is an h-scaled and translated master super-patch.

Let further $\tilde{\mathcal{T}}$ be a triangular mesh on the master-super-patch (the master-mesh) and $\tilde{\mathcal{T}}_h^{(i,j)}$ be the mesh on $c(\mathbf{x}^{(i,j)}, h)$ which is the scaled and translated image of $\tilde{\mathcal{T}}$. Let us now consider the family of regular triangular meshes $\mathcal{T}_h = \mathcal{T}(\Omega, h)$ on Ω with elements τ and their restrictions $\mathcal{T}_h(\mathbf{x}^0, H^0)$ on $S(\mathbf{x}^0, H^0)$. We will denote by $\mathcal{T}_h^{(i,j)}$ the restriction of $\mathcal{T}_h(\mathbf{x}^0, H^0)$ on $c(\mathbf{x}^{(i,j)}, h)$. We assume that the meshes

under consideration are such that $\mathcal{T}_h^{(i,j)} = \tilde{\mathcal{T}}_h^{(i,j)}$ and are translation-invariant in $S(\mathbf{x}^0, H^0)$. An example of such a mesh is shown in Fig. 5b where the master mesh is shown in Fig. 5c. We note that we are dealing with a one-parameter family of meshes $\mathcal{T}(\Omega, h)$. The parameter $2h$ has the meaning of the length of the side of the super-patch in $S(\mathbf{x}^0, H^0)$. In $\Omega - S(\mathbf{x}^0, H^0)$ it has, in general, nothing common with the size of the elements used.

Given a function u and the multi-index $\alpha := (\alpha_1, \alpha_2)$ with $|\alpha| := \alpha_1 + \alpha_2$ we denote

$$D^\alpha u := \frac{\partial^{|\alpha|} u}{\partial x_1^{\alpha_1}\, \partial x_2^{\alpha_2}} \tag{49a}$$

$$(\mathcal{D}^k u)(\mathbf{x}) := \left[\left(\sum_{|\alpha|=k} |D^\alpha u|^2\right)(\mathbf{x})\right]^{\frac{1}{2}}, \quad k \geq 0, \text{ integer} \tag{49b}$$

We will make the following assumptions about the exact solution u:

Assumption I

On $\bar{S}(\mathbf{x}^0, H_{\Omega_0})$

$$|D^\alpha u| \leq K < \infty, \quad 0 \leq |\alpha| \leq 3 \tag{50}$$

Remark 5.1. Assumption I states that the solution is smooth in the neighborhood of the subdomain of interest (the subdomain must be sufficiently far from singular points, boundaries and material-interfaces).

Assumption II

$$R^2 = \sum_{|\alpha|=2} \left[(D^\alpha u)(\mathbf{x}^0)\right]^2 > 0 \tag{51}$$

We will assume that H^0 is sufficiently small depending on K and R.

Remark 5.2. Assumption II implies that the principal part of the error is related to the (nonzero) second-derivative of the exact solution.

Assumption III

On $S(\mathbf{x}^0, H_{Z_0})$, $\quad H_{Z_0} < H_{\Omega_0} < H^0$

$$||e_h||_{S(\mathbf{x}^0, H_{Z_0})} \leq C h^\beta H_{Z_0} \tag{52}$$

with $\beta \geq \frac{16}{9}$ and where C is independent of $T(\Omega, h)$, H_{Z_0}, but it depends on K and R. Here $||\cdot||$ denotes the usual L^2-norm.

Remark 5.3. We do not assume that u is smooth in Ω outside of $S(\mathbf{x}^0, H_{\Omega_0})$. For example, Ω can have a boundary with corners (as in Fig. 5a) and hence u can be unsmooth in the neighborhood of these corners. Nevertheless assumption III makes an implicit requirement on the (refinement of the) mesh in the neighborhood of these corners (so that there is no significant influence (pollution) of the errors in the neighborhood of the corner on the errors in $S(\mathbf{x}^0, H_{Z_0})$; for further discussion about pollution see [55]).

In the following we give the major theorems which justify the methodology of the paper (for a complete presentation with proofs see [53]).

Let Q be a quadratic Taylor-expansion of u about $\mathbf{x}^0$ defined on $S(\mathbf{x}^0, H_{\Omega_0})$ and let Q_h^{INT} be its linear interpolant on the mesh $\mathcal{T}_h(\mathbf{x}^0, H_{\Omega_0})$. We define the *interpolation error*

$$\rho := Q - Q_h^{\text{INT}} \tag{53}$$

which is a periodic function on $S(\mathbf{x}^0, H_{\Omega_0})$ with period $2h$ (see [53]). Let

$$H^1_{\text{PBR}}\left(c(\mathbf{x}^{(i,j)}, h)\right) := \left\{u \in H^1\left(c(\mathbf{x}^{(i,j)}, h)\right) : u \text{ satisfies (54b)}\right\} \tag{54a}$$

where

$$\left.\begin{aligned} u(x_1^{(i,j)} + h, x_2) &= u(x_1^{(i,j)} - h, x_2), \qquad |x_2 - x_2^{(i,j)}| < h \\ u(x_1, x_2^{(i,j)} + h) &= u(x_1, x_2^{(i,j)} - h), \qquad |x_1 - x_1^{(i,j)}| < h \end{aligned}\right\} \tag{54b}$$

is the *periodicity-condition* in $c(\mathbf{x}^{(i,j)}, h)$ and

$$S^1_{h,\text{PBR}}\left(c(\mathbf{x}^{(i,j)}, h)\right) := \left\{u \in H^1_{\text{PBR}}\left(c(\mathbf{x}^{(i,j)}, h)\right) : \; u|_\tau \in \mathcal{P}_1, \; \tau \in \mathcal{T}_h^{(i,j)}\right\} \tag{55}$$

We introduce the *periodic finite-element problem*:

Find $z_h^\rho \in S^1_{h,\text{PBR}}\left(c(\mathbf{x}^{(i,j)}, h)\right)$ such that

$$\mathcal{B}'_{c(\mathbf{x}^{(i,j)},h)}(z_h^\rho, v_h) = \mathcal{B}'_{c(\mathbf{x}^{(i,j)},h)}(\rho, v_h) \qquad \forall\, v_h \in S^1_{h,\text{PBR}}\left(c(\mathbf{x}^{(i,j)}, h)\right) \tag{56}$$

and

$$\int_{c(\mathbf{x}^{(i,j)},h)} (\rho - z_h^\rho) = 0 \tag{57}$$

The function z_h^ρ will be called the *periodic finite element approximation* of the interpolation-error ρ. Let us remark that by scaling and translating the mesh we can solve the finite element problem in the master super-patch using the master mesh. We will denote by $\tilde{z}_h^\rho$ the *periodic extension* of z_h^ρ on $S(\mathbf{x}^0, H_{\Omega_0})$. Let us now define the error in the periodic finite-element approximation of the interpolation-error

$$\psi := \rho - \tilde{z}_h^\rho \tag{58}$$

The main theorem of the paper states that e^h (the error in the finite-element approximation) has the same asymptotic behavior as ψ (the error in the periodic finite-element approximation of the interpolation-error in the quadratic Taylor-expansion of the solution about $\mathbf{x}^0$) in the neighborhood of $\mathbf{x}^0$.

Theorem 1. Let $H_{Z_0} < H_{\Omega_0} < H^0$, and let assumptions I-III hold and

$$C_1 H_{Z_0}^\alpha \leq h \leq C_2 H_{Z_0}^\alpha, \qquad \alpha = \frac{9}{5} \ . \tag{59}$$

Then if $\beta = \dfrac{16}{9}$ in assumption III

$$|||e^h|||_{S(\mathbf{x}^0, H_{Z_0})} = |||\psi|||_{S(\mathbf{x}^0, H_{Z_0})}\left(1 + C|||\psi|||^{\bar{\gamma}}_{S(\mathbf{x}^0, H_{Z_0})}\right) \tag{60}$$

where C is independent of h and H_{Ω_0}, $\bar{\gamma} = \dfrac{1}{14}$.

Let $\xi^h := Q_h^{\text{INT}} + \tilde{z}_h^\rho$ denote the finite-element approximation in the uniform-patch $S(\mathbf{x}^0, H_{Z_0})$ of u constructed from the interpolant and the periodic finite-element approximation of the interpolation error (note that ξ^h can be constructed from the interpolant Q_h^{INT} and by solving a small discrete problem to obtain z_h^ρ in one super-patch). It can then be shown that $u^h \approx \xi^h$ in $S(\mathbf{x}^0, H_{Z_0})$.

Theorem 2. Let the assumptions of Theorem 1 hold then

$$|||u^h - \xi^h|||_{S(\mathbf{x}^0, H_{Z_0})} = |||u^h - Q_h^{\text{INT}} - \tilde{z}_h^\rho|||_{S(\mathbf{x}^0, H_{Z_0})} \leq C h^{\frac{1}{9}} |||\psi|||_{S(\mathbf{x}^0, H_{Z_0})} \tag{61}$$

where C is independent of H and h

In (17)-(44) we introduced various specific *element error-indicators* η_τ which depend on the finite element solution u^h and the data-function f. The error-estimate in Z_0 is

$$\mathcal{E}_{Z_0} = \mathcal{E}_{Z_0}(u^h, f) \;:=\; \Big\{ \sum_{\substack{\tau \in \mathcal{T}_h \\ \tau \cap Z_0 \neq \emptyset}} \Big(\eta_\tau(u^h, f)\Big)^2 \Big\}^{\frac{1}{2}} \quad .$$

$\mathcal{E}_{Z_0}$ utilizes the finite element solution u^h on $\tau \in \mathcal{T}_h$, $\tau \subset Z_0$, and on the neighborhood of Z_0. Let us denote by Z_0^h a slightly larger subdomain which includes the element in Z_0 and their neighbors (the estimator in Z_0 depends on the finite-element solution u^h in Z_0^h and the function f (see (9))).

We will impose on the estimators the requirements of *scale-invariance* and *stability*.

Definition 1: Let $X_1 = cx_1$, $X_2 = cx_2$ and

$$\left.\begin{aligned} Z_0^c &:= \Big\{ (X_1, X_2) \;:\; (x_1, x_2) \in Z_0 \Big\}, \qquad U_h^c(X_1, X_2) := u^h(x_1, x_2)\,, \\ \mathcal{T}_h^c &:= \Big\{ (X_1, X_2) \;:\; (x_1, x_2) \in \mathcal{T}_h \Big\}, \qquad F^c(X_1, X_2) := c^{-2} f(x_1, x_2)\,. \end{aligned}\right\} \tag{62a}$$

Then the estimator is *scale-invariant* if for any $c \in (0, \infty)$

$$\mathcal{E}_{Z_0^c}(U_h^c, F^c) = \mathcal{E}_{Z_0}(u^h, f) \tag{62b}$$

Remark 5.4. The energy-norm is invariant with respect to the scaling of the coordinates and hence the estimators should also be invariant. On the other hand because the differential operator is of second-order the scaling appears in $F(X_1, X_2)$. It is obvious that every error estimator should be scale-invariant.

Definition 2: The estimator $\mathcal{E}_{Z_0}$ is *stable* if for any Z_0, any v^h, $\varphi^h \in S_h^1(Z_0^h)$ and $s, g \in L^2(Z_0)$ and $0 < \alpha \leq 1$

$$\Big| \mathcal{E}_{Z_0}^2(v^h + \varphi^h, s + g) - \mathcal{E}_{Z_0}^2(v^h, s) \Big| \leq C \Big[\alpha \mathcal{E}_{Z_0}^2(v^h, s) + (1 + \alpha^{-1}) \mathcal{E}_{Z_0}^2(\varphi^h, g) \Big] \tag{63}$$

where C is independent of h and the class of admissible meshes under consideration.

Remark 5.5. The stability of the error estimator describes the requirement that small changes in the finite-element solution u^h and the data f should result in small changes in the value of the estimator. It can be shown that all estimators mentioned above are scale-invariant and stable.

The following theorem states that whenever an estimator is stable we can employ the results from the error-estimation in the periodic super-patch to study the quality of the estimator in the actual finite-element mesh.

Theorem 3. Let the assumptions of theorem 1 hold and the estimator be scale-invariant and stable. Further assume that for the estimators

$$\kappa(c(\mathbf{x}^0,h),\xi^h,L'Q)=\frac{\mathcal{E}_{c(\mathbf{x}^0,h)}(\xi^h,L'Q)}{|||\psi|||_{c(\mathbf{x}^0,h)}}\geq\alpha>0 \tag{64}$$

(Here we use the notation $L'Q:=-\Delta Q$; $L'Q$ is a constant function. Recall that we address here only the case $p=1$ and Q is a polynomial of degree 2). Then

$$\kappa^2(S(\mathbf{x}^0,H_{Z_0}),u^h,f)=\kappa^2(S(\mathbf{x}^0,H_{Z_0}),\xi^h,L'Q)(1+Ch^{\frac{1}{3}}) \tag{65}$$

Theorem 3 states that the effectivity index $\kappa(S(\mathbf{x}^0,H_{Z_0}),u^h,f)$ is asymptotically (as $h\rightarrow 0$) the same as the effectivity index $\kappa(S(\mathbf{x}^0,H_{Z_0}),\xi^h,L'Q)$ and it is easy to see that

$$\kappa(S(\mathbf{x}^0,H_{Z_0}),\xi^h,L'Q)=\kappa(c(\mathbf{x}^0,h),\xi^h,L'Q) \tag{66}$$

Hence we can compute the effectivity index by solving a small discrete problem in one super-patch only and because of invariancy with respect to scalings we can study only the master mesh on the master super-patch. Note that the asympotical rate, as stated in the theorem 3, is very low. Let us underline that the aim of the theorem was to show the asymptotic behavior and not to obtain the optimal asymptotic rate. We have numerically shown (see [53]) that the effectivity index computed from the cell analysis is not too sensitive to the surrounding meshes and that the term $Ch^{\frac{1}{3}}$ in (65) can be neglected.

The fact that we have used square super-patches is not essential (for example it is possible to employ regular hexagons or parallelograms as super-patches). For the proofs it is only essential that the mesh is locally translation-invariant. Let us mention that if the solution u is harmonic ($\Delta u=0$) we can analyze the effectivity index of the estimator only for harmonic polynomials. Let us also underline that the assumption that u satisfies Poisson's equation and the elements are linear, was made only for simplicity. The theorems hold for general elliptic operators with non-constant coefficients which are allowed to vary smoothly throughout the domain, and for higher-order elements. Although the theorems were formulated for the energy-norm they can also be restated for other norms under proper assumptions.

6 The methodology for checking the estimators

We now describe the numerical methodology which is employed in the calculation of the robustness index for a given estimator. The robustness index depends on the following factors (see also [50-53]):

a. The geometry of the grid:

The main factor which affects any error estimator is the *geometry of the grid* namely the connectivity or topology of the grid and the geometry (*distortion*) of the elements. The element geometry has to be considered in connection with the differential operator for the boundary-value problem. For example the orthotropic heat-conduction operator can be transformed by an affine transformation to Laplace's operator on a distorted mesh which has different minimal and maximal angles.

b. The class of solutions:

In this paper we study the robustness of error estimators for linear elliptic equations and *interior mesh-subdomains*. It is well-known that the solutions of elliptic boundary-value problems are analytic in the interior of the domain if the coefficients of the operator and the right-hand side are analytic; for this reason we will consider the class of smooth solutions. Of particular interest is the subclass of smooth functions which satisfies the homogeneous differential equation (we will refer to such solutions as "harmonic"; if the solution satisfies Laplace's equation it is truly harmonic). The asymptotic properties of error estimators for the class of smooth solutions can be studied by considering the class of polynomials of degree $(p+1)$.

We now give an outline of the numerical procedure which determines the robustness index $\mathcal{R}$ for any error estimators.

Let us assume that we would like to determine the robustness of an estimator for a mesh $\mathcal{T}_h$ from a given class of meshes (the class may be defined as the class of meshes produced by a commercial mesh-generator or an adaptive code). Let $\{\omega_X\}_{X=1}^{nv}$ the cells of elements connected to the vertices of the mesh. Let ω_X an *interior-cell* (it is separated by several layers of elements from the boundary, singular-points and material-interfaces). Let

$$\omega_0^h := \omega_X$$

and for $s \geq 1$, integer, define recursively

$$\omega_s^h := \bigcup_{\substack{X \in \mathcal{N}(\tau') \\ \tau' \subseteq \omega_{s-1}^h}} \omega_X$$

From the analysis (given in [53] for locally-periodic meshes) and numerical experience (for more general meshes) we know that the effectivity index for any estimator in the cell ω_0^h depends practically on the geometry of the mesh in the patch ω_s^h for only a small s (s = 1 - 4) (more precisely increasing s will change the robustness index only minimally). Given a mesh $\mathcal{T}_h$ (resp. class of meshes $\mathcal{T}$) constructed by

a mesh generator, there are patches ω_s^h of various types (topologies). We can now analyze all these patches separately and compute $\mathcal{R}_{\mathcal{T}_h}$ (resp. $\mathcal{R}(\mathcal{T})$) as defined in (5b). For example, in Fig. 9 (resp. Fig. 10) we indicate the mesh-cells ω_0^h shaded and the patch ω_3^h (resp. ω_4^h) with its perigram shown by thick line, for various interior-cell/patch combinations from the grid shown in Fig. 6 (resp. Fig. 1). We can determine the robustness of any error-estimator in ω_0^h as follows:

1. Completion of the mesh-cell to a periodic super-patch.

We translate and scale the subdomain ω_s^h so that its image $\tilde{\omega}_s^h \subseteq \tilde{c} = [-1,1] \times [-1,1]$ (see Fig. 7b). Then we employ a mesh-generator to complete the mesh in $\tilde{\omega}_s^h$ into a *periodic-mesh* $\tilde{\mathcal{T}}$ in the super-patch $\tilde{c}$ (see Fig. 7c).

2. Periodic boundary-value problem:

For given exact solution $\mathbf{u}$ with components being homogeneous polynomials of degree $(p+1)$ denoted by $\hat{P}_{p+1}$ ($\mathbf{u} \in (\hat{\mathcal{P}}_{p+1})^2$ or exact "harmonic" solution $\mathbf{u} \in (\hat{P}_{p+1})^2$ such that $L_i(\mathbf{u}) = 0\,, \quad i = 1,2$), material properties and *mesh-pattern* (the local geometry of the grid in the cell ω_0^h and the patch ω_s^h) determine

a) The finite element solution $\mathbf{u}^h$,

b) The exact error $\mathbf{e}^h$,

by solving the following *periodic boundary-value problem*:

Find $\mathbf{z}^h \in \mathbf{H}^h_{per}(\tilde{c})$ such that

$$\mathcal{B}_{\Omega_{per}}(\mathbf{z}^h, \mathbf{v}^h) = \mathcal{B}_{\Omega_{per}}(\mathbf{u} - \mathbf{u}_I^h, \mathbf{v}^h) \qquad \forall\ \mathbf{v}^h \in \mathbf{H}^h_{per}(\Omega_{per}) \tag{67}$$

where

$$\mathbf{H}^h_{per}(\tilde{c}) = \Big\{ \mathbf{w}^h \in \mathbf{H}^1(\tilde{c}) : \mathbf{w}^h(-1, x_2) = \mathbf{w}^h(1, x_2),\ \ \mathbf{w}^h(x_1, -1) = \mathbf{w}^h(x_1, 1)$$

$$\text{and} \quad \mathbf{w}^h|_\tau \in (\mathcal{P}_p)^2\,,\ \ \tau \in \tilde{\mathcal{T}} \Big\}\,,$$

$\mathbf{u}_I^h$ denotes a continuous piecewise p-degree interpolant of the exact solution $\mathbf{u}$. We select the solution $\mathbf{z}^h$ of (66) which satisfies

$$\int_{\tilde{c}} \mathbf{z}^h = \int_{\tilde{c}} (\mathbf{u} - \mathbf{u}_I^h) \tag{68}$$

and we define

$$\mathbf{u}^h = \mathbf{u}_I^h + \mathbf{z}^h \quad ; \qquad \mathbf{e}^h = (\mathbf{u} - \mathbf{u}_I^h) - \mathbf{z}^h\,. \tag{69}$$

Thus from (69) we obtain the finite-element solution $\mathbf{u}^h$ and the exact error $\mathbf{e}^h$ and for a given estimator we compute the effectivity index

$$\kappa_{\omega_0^h} = \kappa_{\omega_0^h} \text{ (material coeff., grid-material orientation, pattern, solution coeff.)}$$

Remark 6.1. We note that the effectivity index κ is independent of the normalization of the coefficients in $(\hat{\mathcal{P}}_{p+1})^2$.

3. Numerical optimization

We let

$$C_U^{\omega_0^h} = \max_{\text{material coeff.}} \max_{\text{solution coeff.}} \kappa_{\omega_0^h} , \qquad C_L^{\omega_0^h} = \min_{\text{material coeff.}} \min_{\text{solution coeff.}} \kappa_{\omega_0^h} \tag{70}$$

The bounds $C_U^{\omega_0^h}$, $C_L^{\omega_0^h}$ for a given class of solutions and materials, a given pattern and for a given grid-material orientation can now be computed using numerical optimization. We compute the robustness of the estimator in $\omega_0^h \subseteq \omega_s^h$ from

$$\left.\begin{aligned} \mathcal{R}_{\omega_0^h} &:= \max_{s=1,2,3,\ldots} \mathcal{R}^s_{\omega_0^h} , \\ \mathcal{R}^s_{\omega_0^h} &:= \max\left\{ \left(|1 - C_U^{\omega_0^h}| + |1 - C_L^{\omega_0^h}| \right) , \quad \left(|1 - \frac{1}{C_U^{\omega_0^h}}| + |1 - \frac{1}{C_L^{\omega_0^h}}| \right) \right\} \end{aligned}\right\} \tag{71}$$

We can then compute the robustness of the estimator for the mesh $\mathcal{T}_h$ by computing

$$\mathcal{R}_{\mathcal{T}_h} := \max_{\substack{\omega_0^h = \omega_x \\ x \in \mathcal{N}_{int}(\mathcal{T}_h)}} \mathcal{R}_{\omega_0^h} \tag{72}$$

Here $\mathcal{N}_{int}(\mathcal{T}_h)$ denotes the *interior vertices* of the mesh (the vertices must be separated by two (or more) layers of elements from the boundary of the domain and from material-interfaces).

Let us underline the reason for the optimization. In general we know *only* that the solution satisfies the differential equation, e.g. it is harmonic (when $f = 0$). Hence we wish that the effectivity index is small for the entire considered class. From the results of the theoretical study (see [53]) we can restrict the class of functions to harmonic polynomials of degree $(p + 1)$ only. Establishing the bounds for the classes of meshes and solutions of interest is essential for judging the robustness of an estimator.

Remark 6.2. Note that the methodology assumed that the local mesh-size h is sufficiently small so that the exact solution u can be replaced by its local Taylor expansion of degree $(p+1)$ (the validity of the methodology is asymptotic).

However numerical studies show that the robustness index governs the performance of estimators in the range of the practical engineering computations which often employ relatively coarse grids.

7 Numerical studies of robustness of various error-estimators

We present examples of the application of the methodology described earlier to study the robustness of several error estimators, namely:

1. Implicit element residual (Est. 1) (Eqs. (17)-(21)) [8], [11], [13], [14].
2. Implicit element residual with equilibration (Est. 2) (Eqs. (17)-(36)) [8], [17], [25], [29], [59], [60], [61].
3. Implicit element residual based on complementary energy principle (Est. 3) (defined below) [25], [26], [27], [28], [32], [60], [61].
4. Estimators based on smoothening or *Z-Z estimators* (Est. 4) (Eqs. (37)-(44)) [40], [41], [42], [43], [44].

Note that in [53] we also studied the performance of several other estimators (explicit element-residual, subdomain residual etc.).

We now proceed to the discussion of the numerical studies.

7.1 The robustness index for polynomial solutions

Here we address three questions:

1) How many layers of elements should be taken around the cell ω_0^h, for the values of $C_U^{\omega_0^h}$, $C_L^{\omega_0^h}$, $\mathcal{R}_{\omega_0^h}$ to be practically independent of the surrounding mesh in the periodic super-patch $\tilde{c}$?

2) How much do $C_U^{\omega_0^h}$, $C_L^{\omega_0^h}$ and $\mathcal{R}_{\omega_0^h}$ computed from a periodic super-patch which includes ω_s^h ($s = 3$ for meshes of triangles and $s = 4$ for meshes of quadrilaterals) differ from the same quantities computed from the entire original mesh?

3) What is the robustness index for the various estimators?

We will consider the interior-patterns (cell/patch combinations) shown in Figs. 10 and 9 which occur in the meshes shown in Figs. 1 and 6, respectively.

For the scalar elliptic problem we chose the exact solution to be either a *general (homogeneous) polynomial* of degree $(p+1)$

$$Q^G(x_1,x_2) = \sum_{i,j} a_{ij}\, x_1^i x_2^j\,, \qquad i+j=p+1\,, \qquad i,j \geq 0 \tag{73}$$

or a *harmonic polynomial* by imposing the constraint $\sum_{k,\ell=1}^{2} D_k(K_{k\ell} D_\ell Q^H) = 0$; for example for $K_{k\ell} = \delta_{k\ell}$ we have

$$Q^H(x_1,x_2) = a_1(x_1^2 - x_2^2) + a_2\, x_1 x_2\,, \qquad \text{for } \; p+1=2 \tag{74a}$$

and

$$Q^H(x_1,x_2) = a_1(x_1^3 - 3x_1x_2^2) + a_2(3x_1^2x_2 - x_2^3)\,, \qquad \text{for } \; p+1=3 \tag{74b}$$

In the case of the vector-valued model problem (linear elasticity) we employed homogeneous "harmonic" polynomial solutions of degree $(p+1)$

$$\mathbf{Q}^H \in (\hat{\mathcal{P}}_{p+1})^2 \;:\; \sum_{j=1}^{2} D_j(\sigma_{ij}(\mathbf{Q}^H)) = 0\,, \quad i = 1,2 \tag{75}$$

We determined the robustness index of the error estimators for the cells ω_0^h using the approach of the paper. In Table 1 we give the values of $C_L^{\omega_0^h}$, $C_U^{\omega_0^h}$, $\mathcal{R}_{\omega_0^h}$ for Est. 1 for the scalar elliptic problem with $p=1$, for the pattern 1 (shown in Fig. 9a), when $s = 1, 2, 3, 4, 5$ layers of elements around ω_0^h are taken in the patch ω_s^h (see Fig. 8). In Tables 2 and 3 we give the values of $C_L^{\omega_0^h}$, $C_U^{\omega_0^h}$, and $\mathcal{R}^s_{\omega_0^h}$ ($s=3$ for the meshes of triangles and $s=4$ for the meshes of quadrilaterals) for the Est. 1, Est. 2, and Est. 4 for the scalar elliptic problem with $p=1$ and 2 respectively. These are compared with the values of the effectivity indices $\bar{C}_L^{\omega_0^h}$, $\bar{C}_U^{\omega_0^h}$ and $\bar{\mathcal{R}}$ ($\bar{\mathcal{R}}$ is obtained by substituting $\bar{C}_L^{\omega_0^h}$, $\bar{C}_U^{\omega_0^h}$ into (5a)) obtained from the finite-element solution of a Dirichlet boundary-value problem in the grids shown in Figs. 1, 6 (the *big* mesh) with data consistent with the homogeneous polynomial solutions which give the extremal values $C_L^{\omega_0^h}$, $C_U^{\omega_0^h}$ of the effectivity index $\kappa_{\omega_0^h}$ in the periodic super-patch calculations. The periodic super-patches employed for the various patterns were constructed using a mesh-generator, as shown in Fig. 7. In Table 4 a similar comparison is made for isotropic elasticity (Poisson's ratio $\nu = 0.3$) using meshes of triangles.

From the reported data we can make the following conclusions related to the questions formulated above:

1) For linear elements the values of $C_L^{\omega_0^h}$, $C_U^{\omega_0^h}$, $\mathcal{R}_{\omega_0^h}$ in the cell ω_0^h do not practically change when the patch ω_s^h has $s \geq 3$ layers of elements around the cell ω_0^h. For higher order elements, a smaller s can be taken, i.e. s = 1-2 (thus for our numerical experiments, we considered patches with $s = 3$ for the meshes of triangles and $s = 4$ for the meshes of quadrilaterals).

2) For a given exact solution which is a homogeneous polynomial (harmonic or general) of degree $(p+1)$ the values of $C_L^{\omega_0^h}$, $C_U^{\omega_0^h}$, obtained from a periodic super-patch are very close to the values $\bar{C}_L^{\omega_0^h}$, $\bar{C}_U^{\omega_0^h}$ obtained from the approximate solution of a boundary-value problem (with data compatible with the polynomial solutions which correspond to the extrema of the effectivity index in the periodic super-patch) obtained using the big mesh. Note that we did not exactly answer question 2 because we did not perform the optimization in the big mesh; however the numerical experience from [53] indicates that $\bar{C}_L^{\omega_0^h}$, $\bar{C}_U^{\omega_0^h}$ are very close to the extremal values of the effectivity index when the optimization is performed in the big mesh.

3a) The element-residual without equilibration (Est. 1) is not robust for the general meshes (like the meshes shown in Fig. 1 and Fig. 6) and should not be used.

3b) The equilibration of the flux increases the robustness of the element-residual estimators.

3c) The Z-Z estimator appears to be the most robust.

7.2 The robustness index for general solutions

In 7.1 above, we assumed that the exact solution is a (homogeneous) polynomial of degree $(p+1)$. The following question arises:

Are the conclusions based on the assumption that the solution is a polynomial valid for general solutions?

We now give an example which shows that the results on the robustness of estimators obtained using polynomials of degree $(p+1)$ give a good indication of the local performance of the estimators for any general solution (the theoretical justification for patchwise uniform meshes is given in theorem 3). Let us consider the general solution

$$u(x_1,x_2) = (r_1(x_1,x_2))^{\frac{2}{3}} \sin\Big(\frac{2}{3}\theta_1(x_1,x_2)\Big) + \Big(r_2(x_1,x_2)\Big)^{\frac{1}{2}} \sin\Big(\frac{1}{2}\theta_2(x_1,x_2)\Big)$$

where

$$r_1(x_1,x_2) = \left[(x_1-\frac{1}{2})^2+(x_2-3)^2\right]^{\frac{1}{2}}, \qquad \theta_1(x_1,x_2) = \tan^{-1}\left(\frac{x_2-3}{x_1-\frac{1}{2}}\right),$$

$$r_2(x_1,x_2) = \left[(x_1-3)^2+(x_2-\frac{1}{2})^2\right]^{\frac{1}{2}}, \qquad \theta_2(x_1,x_2) = \tan^{-1}\left(\frac{x_2-\frac{1}{2}}{x_1-3}\right),$$

we let $\Omega = (0,1)\times(0,1)$ and let $\mathcal{T}_h$ be the grid shown in Fig. 6. We solved the Neumann boundary-value problem in Ω using $\mathcal{T}_h$ (the big mesh) and data consistent with the exact solution given above and we computed the effectivity index for Est. 1, Est. 2 and Est. 4 for five of the patterns shown in Fig. 9. We also computed the effectivity index in the cells ω_0^h by:

a) Solving the Neumann problem in Ω using the grid $\mathcal{T}_h$ with data corresponding to the local Taylor-expansion (up to quadratic degree) about the central node X of the cell $\omega_0^h \equiv \omega_X$.

b) By using the local Taylor-expansion (about the central node of the patch) as exact solution to pose the periodic boundary-value problem (66) over the periodic super-patches for the patterns shown in Figs. 9a-9e (patterns 1-5).

The effectivity indices for the cells calculated from the approximate solution (which was obtained using the three different ways stated above) are given in Table 5.

We observe that the effectivity indices obtained using the approximate solution (computed from the big mesh $\mathcal{T}_h$) of the Neumann boundary-value problem formulated using data obtained either from the general solution or from its local Taylor series expansion are essentially identical. The results obtained using the local Taylor series expansion and the periodic boundary-value problem (67) are also very close to the values obtained from the other two types of problems; still better agreement could be obtained by increasing the number of layers s in ω_s^h (here we have used $s = 3$ layers).

7.3 The influence of various parameters on the robustness of the estimators

The definitions of Est. 2, Est. 3 and Est. 4 include the choice of some *free parameters*, namely:

1) The choice of the correction of the edge residuals for Est. 2 and Est. 3.

2) The number and location of the sampling points involved in the definition of Est. 4.

3) The discrete space of polynomials used in the patch-projections or the solution of the element-residual problem (we may use the bubble-space or the complete space of polynomials of degree $(p+1)$ or some intermediate space).

Here we show that the approach can be used for the study of the dependence of the robustness index on the parameters involved in the definition of the estimators or to find the most robust version of an estimator for the grids of interest. We also note that the methodology can be used to design robust versions of estimators by considering additional parameters (like for example the location of the sampling points) as variables and by performing the optimization for the finite number of cell/patch-patterns which occur in the grids of interest.

To show the influence of the various parameters we will consider, in the numerical studies given below, a set of *distorted* meshes in the periodic super-patches shown in Figs. 11, 12. (These meshes were selected to include non-standard mesh-topologies and elements with large maximum angle and aspect ratios.)

A. Z-Z estimators

The robustness of Z-Z estimators depends on the choice of the sampling points. The following choices are studied for the quadrilaterals with $p = 1$:

(i) One sampling point at the center of the element (*Type 1*) as shown in Fig. 4d.

(ii) Four sampling points along the axes of the master-element (*Type 2*) as shown in Fig. 4e. These sampling points correspond to the one-dimensional Gauss-Legendre integration points of order two along the coordinate-axes of the master-element.

(iii) Four sampling points (*Type 3*) at the integration-points of the (2×2) Gauss-Legendre product-rule (shown in Fig. 4f).

We studied the performance of the above estimators for the periodic-grids shown in Fig. 11; here the cell ω_0^h coincides with the periodic super-patch. In Table 6 we give the values of $C_L^{\omega_0^h}$, $C_U^{\omega_0^h}$ and $\mathcal{R}_{\omega_0^h}$ for these cells when the solution is a general polynomial of degree 2. We observe that the Z-Z estimator of *Type 3* which uses sampling points at the integration points of the 2×2 Gauss product-rule shows the best robustness for these meshes.

For the triangles we studied the following choices of sampling points shown in Fig. 4a, b, c.

(i) One sampling-point located at the centroid of the triangle (Fig. 4a); this point will be used only for linear elements.

(ii) Three sampling-points located at the midsides of the edges of the triangle (Fig. 4b).

(iii) Seven sampling points which include the points in (i) and (ii) and the midpoints of the segments which connect the centroid with the vertices of the triangle (Fig. 4c).

We computed the upper- and lower-bound of the effectivity-index and the robustness index for the periodic meshes shown in Figs. 12; the periodic meshes have given aspect-ratio, *1/a* (see Fig. 12a) and include some elements with very large maximum angle. For this example we took aspect-ratio of 1/2 for the periodic meshes shown in Figs. 12a-12d, and aspect-ratio of 1/8 for the periodic meshes shown in Figs. 12e, 12f. In Tables 7, 8 we give the results for $p = 1$ and $p = 2$, respectively, obtained by solving Laplace's equation. In Table 9 we give the results for $p = 1$ for isotropic linear elasticity. It should be noted that the *Z-Z* estimator is exact for the mesh shown in Fig. 12e (for linear elements). We observe that for the meshes shown in Fig. 12:

(i) For Laplace's equation and $p = 1$ the choice of sampling points shown in Fig. 4b (3 sampling points) shows the best robustness.

(ii) For Laplace's equation and $p = 2$ the choice of sampling points shown in Fig. 4c is the most robust.

(iii) For isotropic elasticity and $p = 1$ the choice of sampling points shown in Fig. 4a gives the most robust *Z-Z* estimator.

To take into account the nature of the exact solution (when for example it is harmonic) we may consider another version of the *Z-Z* estimator which employs harmonic polynomials in the patch-projections. To check if harmonic patch-projections will improve the robustness of the *Z-Z* estimator for grids of general quadrilaterals we employed the *Z-Z* estimator with one-sampling point per element and the periodic cells shown in Fig. 11. The results for the values of $C_L^{\omega_0^h}$, $C_U^{\omega_0^h}$, $\mathcal{R}_{\omega_0^h}$ for the *Z-Z* estimator (for the Laplacian) with the general or the harmonic patch-projection are given in Table 10. From these results we conclude that the *Z-Z* estimator is less robust when the harmonic patch-projection is employed.

B. Element residual estimators with various types of equilibration

The robustness of the residual estimators depends on the definition of the residual-functional. Here we considered two types of equilibration methods, namely, Ladeveze's and Ohtsubo-Kitamura's techniques. Ladeveze's method splits the interelement fluxes by minimizing the functional given in (31) subject to the constraints (29), as discussed earlier. We considered three choices of the weight w_i in the definition of (31). These are:

(i) $w_i = 1$ (see for example [25], [32]) (equilibration of *Type A*);

(ii) $w_i = |\epsilon_i|^{-1}$ (see [60], [61]) (equilibration of *Type B*);

(iii) $w_i = |\epsilon_i'|^{-1}$, where ϵ_i' denote the length of side ϵ_i in the *transformed plane* in which the operator is the Laplacian (equilibration of *Type C*).

We computed the robustness of the element-residual estimator with Ladeveze's equilibration of *Type A, B, C* for the periodic meshes shown in Figs. 11, 12a-12e. It should be noted that the estimator is exact for linear elements and the mesh shown in Fig. 12f, while for quadratic elements it is exact for the mesh in Fig. 12e. The results are given in Tables 11-17. Table 11 gives the results for bilinear quadrilaterals for Est. 2 with equilibrations of *Type A* and *C* and for the periodic meshes shown in Fig. 11. Tables 12-15 give the results for the meshes of triangular elements shown in Fig. 12. In particular Tables 12, 13 give the results of the optimization for Est. 2 (*Type A* and *B*) for linear and quadratic elements, respectively (note that we selected aspect-ratio 1/2 for the meshes shown in Figs. 12a-12d and aspect-ratio of 1/8 for the meshes shown in Figs. 12e, 12f). Table 14, 15 give the results of the optimization for the model problem (9) (orthotropic heat-conduction) with $1 \leq K_{\max}/K_{\min} \leq 10$ (the ratio $K_{\max}/K_{\min}$ was included as a parameter in the optimization) and various orientations of the principal axes of orthotropy with respect to the periodic meshes shown in Fig. 12c, Fig. 12e respectively (here we selected aspect-ratio 1/1). Table 16 gives the results for the robustness of Est. 2 (*Types A* and *B*) for the model problem of isotropic elasticity (with Poisson's ratio $\nu = 0.3$). It should be noted that for the elasticity problem we used aspect-ratio of 1/2 for the meshes shown in Figs. 12a-12d and aspect-ratio of 1/8 for the mesh shown in Fig. 12e. We observe that:

(i) For the meshes of quadrilaterals, where we employed Est. 2 (with equilibration of *Type A* and *C*), the robustness depends on the mesh-topology; both types have reasonable robustness.

(ii) For the meshes of triangles Est. 2 with equilibration of *Type B* has the best robustness for the Laplacian.

(iii) From the results for the case of orthotropic heat-conduction we cannot make a general statement about which type of equilibration is the best. All three types seem to give reasonably robust element-residual estimator.

(iv) For the case of isotropic elasticity the equilibration of *Type B* produces the most robust estimator.

We also implemented element-residual estimators with Ohtsubo-Kitamura flux-splitting for the isotropic elasticity problem. The element-residual problem is defined as in (21) with the right-hand side defined (with or without equilibration) as

described in 3.2.2. The discrete space employed in the solution of the local problem was defined as:

(i) The discrete space which corresponds to the 8-node serendipity element (*complete serendipity space*).

(ii) The discrete space spanned by the shape-functions of the mid-side nodes in the 8-node serendipity element (*bubble serendipity space*).

In Table 17 we give the values of $C_L^{\omega_0^h}$, $C_U^{\omega_0^h}$, $\mathcal{R}_{\omega_0^h}$ for the element-residual estimators with Ohtsubo-Kitamura's flux-splitting (isotropic elasticity with $\nu = 0.3$). In columns 2-4 we give the results when the initial flux-splitting (eq. (33)) is employed (without equilibration) together with the serendipity bubble-space. In columns 5-7 (resp. 8-10) we give the results when the equilibration is employed together with the complete (resp. bubble) serendipity space. We observe the following:

(i) When the complete serendipity space is employed (together with equilibration) the estimator lacks robustness.

(ii) When the bubble serendipity space is used together with equilibration a robust estimator is obtained.

C. Estimators based on the complementary energy principle

Error estimators based on the complementary energy principle (e.g. [25], [26], [27], [28], [60], [61]) are often preferred by engineers because they provide guaranteed upper-bounds of the error. Here we use the methodology of the paper to check the robustness of a-posteriori error estimators based on the complementary-energy principle for the orthotropic heat-conduction and elasticity problems and the class of periodic grids shown in Figs. 11, 12. The error estimators are defined as follows:

a. Orthotropic heat-conduction:

$$\eta_\tau := |||\hat{e}|||_\tau \tag{76}$$

where

$$\hat{e} \in \mathcal{P}_{p+1} : \qquad B'_\tau(\hat{e}_\tau, v_\tau) = \mathcal{F}_\tau^{\mathbf{aq}}(v_\tau) \qquad \forall\ v_\tau \in \mathcal{P}_{p+1} \tag{77}$$

b. Elasticity

$$\eta_\tau := ||\hat{\sigma} - \sigma(\mathbf{u}_h)||_{L^2(\tau),\mathbf{a}^{-1}} \tag{78}$$

where $\hat{\sigma} \in \mathbf{JM}_1$ such that

$$\left.\begin{aligned} -\nabla\cdot\hat{\sigma} &= \mathbf{f} \qquad \text{in } \tau \\ \hat{\sigma}\mathbf{n}\,|_{\epsilon} &= \frac{1}{2}\mathbf{J}_{\epsilon} + \theta_{\tau}\,|_{\epsilon}\,, \qquad \forall\ \epsilon \in E(\tau) \end{aligned}\right\} \tag{79}$$

Here $\mathbf{JM}_1$ denotes the stress-space for the *Johnson-Mercier composite equilibrium triangular element* (see [63]). (We employed the explicit solution of (79) given in [60].)

For the problem of orthotropic heat-conduction we computed the robustness of Est. 3 using Ladeveze's flux-splitting with *Type A* and *Type B* equilibrations; the results are given in Table 18. For the elasticity problem we repeated the computations for the above types of equilibration and for the periodic meshes shown in Fig. 12a, b, c; the results are given in Table 19. It should be noted that we employed aspect-ratio of 1/2 for the meshes in Fig. 12a-12d and aspect-ratio of 1/8 for the mesh shown in Fig. 12e. We observe that:

a) For both cases (scalar and vector-valued problem) the estimator with equilibration of *Type B* shows superior robustness than the estimator with equilibration of *Type A*.

b) The error estimators based on the complementary energy principle are less robust (by far) than the corresponding element-residual estimators.

8 Summary of conclusions

1. The validation of the performance of the estimators based on the robustness index allows objective comparisons between the various error estimators.

2. A numerical methodology for computing the robustness index is given.

3. The methodology takes directly into account the factors which affect the performance of estimators namely the geometry of the grid, the differential operator and the nature of the solution. The methodology has theoretical basis and can be used to study the robustness of error estimators for the complex grids which are used in engineering computations.

4. The methodology allows us to check the quality of any new estimator even if it is only available as a black-box computer subroutine.

5. It is possible to use the methodology to maximize the robustness of a given estimator for a class of meshes of interest.

6. The methodology addresses the robustness index for the estimators for elements in the interior of the domain and smooth solutions. The case of unsmooth solutions and elements at the boundary will be addressed in a forthcoming paper.

7. The *Z-Z* estimator seems to be the most robust. For the bilinear quadrilateral elements the sampling points defined in Fig. 4f are recommended. For the linear (resp. quadratic) triangular elements the choice shown in Fig. 4b (resp. 4a) is the best for Laplace's equation, while for linear triangles and elasticity the choice 4a is the most robust. Thus, for linear elements the choice 4a or 4b could be recommended.

8. The element residual estimators should be used only with equilibration. Ladeveze's equilibration of *Type B* is recommended.

9. The Ohtsubo-Kitamura flux-splitting technique gives a robust estimator only when a bubble space is employed in the element-residual problem.

10. The estimators based on the complementary energy-principle have poor robustness and are *not* recommended.

We remark that the conclusions made above are related to the use of general meshes. Use of families of particular meshes could influence the conclusions.

References

1. I. BABUŠKA and W.C. RHEINBOLDT, "Error estimates for adaptive finite element computations", *SIAM J. Numer. Anal.*, **15**, 736-754, 1978.

2. I. BABUŠKA and W.C. RHEINBOLDT, "A-posteriori error estimates for the finite element method", *Internat. J. Numer. Methods Engrg.*, **12**, 1597-1615, 1978.

3. I. BABUŠKA and W.C. RHEINBOLDT, "Adaptive approaches and reliability estimations in finite element analysis", *Comput. Methods Appl. Engrg.* **17/18**, 519-540, 1979.

4. I. BABUŠKA and W.C. RHEINBOLDT, "Reliable error estimation and mesh adaptation for the finite element method", in: *Computational Methods in Nonlinear Mechanics*, edited by J.T. ODEN, North Holland, Amsterdam, 1980, pp. 67-108.

5. I. BABUŠKA and W.C. RHEINBOLDT, "A posteriori error analysis of finite element solutions for one-dimensional problems", *SIAM J. Numer. Anal.* **18** (3), 565-589, 1981.

6. I. BABUŠKA and A. MILLER, "A-posteriori error estimates and adaptive techniques for the finite element method", *Technical Note BN-968*, Institute for Physical Science and Technology, University of Maryland, College Park, 1981.

7. D.W. KELLY, J.P. DE S.R. GAGO, O.C. ZIENKIEWICZ, and I. BABUŠKA, "A posteriori error analysis and adaptive processes in the finite element method: Part I-Error analysis", *Internat. J. Numer. Methods Engrg.* **19**, 1593-1619, 1983.

8. R.E. BANK and A. WEISER, "Some a posteriori error estimators for elliptic partial differential equations", *Math. Comp.* **44**, 283-301, 1985.

9. I. BABUŠKA and A. MILLER, "A feedback finite element method with a posteriori error estimation: Part I. The finite element method and some basic properties of the a posteriori error estimator", *Comput. Methods Appl. Mech. Engrg.* **61**, 1-40, 1987.

10. I. BABUŠKA and D. YU, "Asymptotically exact a posteriori error estimator for biquadratic elements", *Finite Elements in Analysis and Design* **3**, 341-354, 1987.

11. J.T. ODEN, L. DEMKOWICZ, W. RACHOWICZ and T.A. WESTERMANN, "Toward a universal h-p adaptive finite element strategy: Part 2, A posteriori error estimates", *Comput. Methods Appl. Mech. Engrg.* **77**, 113-180, 1989.

12. T.A. WESTERMANN, "A Posteriori Estimation of Errors in hp Finite Element Methods for Linear Elliptic Boundary Value Problems", *M.Sc. Thesis*, The University of Texas at Austin, Austin, Texas 1989.

13. R. VERFÜRTH, "A posteriori error estimators for the Stokes equation", *Numer. Math.* **55**, 309-325, 1989.

14. R. VERFÜRTH, "A posteriori error estimation and adaptive mesh refinement techniques", preprint, 1992.

15. J. BARANGER and H. EL-AMRI, "Estimateurs a posteriori d' erreur pour le calcul adaptatif d' ecoulements quasi-newtoniens", *RAIRO Math. Model. Numer. Anal.* **25** (1), 31-48, 1991.

16. M. AINSWORTH and A. CRAIG, "A posteriori error estimators in the finite element method", *Numer. Math.* **60**, 429-463, 1992.

17. M. AINSWORTH and J.T. ODEN, "A unified approach to a-posteriori error estimation using element residual methods", *Numer. Math.*, in press.

18. R. DURÁN and R. RODRIGUEZ, "On the asymptotic exactness of Bank-Weiser's estimator", *Numer. Math.* **62**, 297-303, 1992.

19. P.L. BAEHMANN, M.S. SHEPHARD and J.E. FLAHERTY, "A posteriori error estimation for triangular and tetrahedral quadratic elements using interior residuals", *Internat. J. Numer. Methods Engrg.* **34**, 979-996, 1992.

20. M. AINSWORTH and J.T. ODEN, "A procedure for a posteriori error estimation for h-p finite element methods", *Comput. Methods Appl. Mech. Engrg.* **101**, 73-96, 1992.

21. T. STROUBOULIS and K.A. HAQUE, "Recent experiences with error estimation and adaptivity, Part I: Review of error estimators for scalar elliptic problems", *Comput. Methods Appl. Mech. Engrg.* **97**, 399-436, 1992.

22. T. STROUBOULIS and K.A. HAQUE, "Recent experiences with error estimation and adaptivity, Part II: Error estimation for h-adaptive approximations on grids of triangles and quadrilaterals," *Comput. Methods Appl. Mech. Engrg.* **100**, 359-430, 1992.

23. R.E. BANK and B.D. WELFERT, "A posteriori error estimates for the Stokes equations: A comparison", Comput. Methods Appl. Mech. Engrg. 82, 323-340, 1990.

24. R.E. BANK and R.K. SMITH, "A posteriori error estimates based on hierarchical bases", preprint, 1992.

25. P. LADEVEZE and D. LEGUILLON, "Error estimate procedure in the finite element method and applications", *SIAM J. Numer. Anal.* **20** (3), 485-509, 1983.

26. D.W. KELLY, "The self-equilibration of residuals and complementary a posteriori error estimates in the finite element method", *Internat. J. Numer. Methods Engrg.* **20**, 1491-1506, 1984.

27. D.W. KELLY, R.J. MILLS, J.A. REIZES and A.D. MILLER, "A posteriori estimates of the solution error caused by discretization in the finite element, finite difference and boundary element methods", *Internat. J. Numer. Methods Engrg.* **24**, 1921-1939, 1987.

28. D.W. KELLY and J.D. ISLES, "A procedure for a posteriori error analysis for the finite element method which contains a boundary measure", *Computers & Structures* **31** (1), 63-71, 1989.

29. H. OHTSUBO and M. KITAMURA, "Element by element a posteriori error estimation and improvement of stress solutions for two-dimensional elastic problems", *Internat. J. Numer. Methods Engrg.* **29**, 223-244, 1990.

30. H. OHTSUBO and M. KITAMURA, "Numerical investigation of elementwise a-posteriori error estimation in two and three dimensional elastic problems", *Internat. J. Numer. Methods Engrg.* **34**, 969-977, 1992.

31. H. OHTSUBO and M. KITAMURA, "Element by element a posteriori error estimation of the finite element analysis for three-dimensional elastic problems", *Internat. J. Numer. Methods Engrg.* **33**, 1755-1769, 1992.

32. P. LADEVEZE, P. MARIN, J.P. PELLE and G.L. GASTINE, "Accuracy and optimal meshes in finite element computation for nearly compressible materials", *Comput. Methods Appl. Mech. Engrg.* **94**, 303-315, 1992.

33. O.C. ZIENKIEWICZ and J.Z. ZHU, "A simple error estimator and the adaptive procedure for practical engineering analysis", *Internat. J. Numer. Methods Engrg.* **24**, 337-357, 1987.

34. E. RANK and O.C. ZIENKIEWICZ, "A simple error estimator in the finite element method", *Comm. Appl. Numer. Methods* **3**, 243-249, 1987.

35. M. AINSWORTH, J.Z. ZHU, A.W. CRAIG and O.C. ZIENKIEWICZ, "Analysis of the Zienkiewicz-Zhu a posteriori error estimator in the finite element method", *Internat. J. Numer. Methods Engrg.* **28**, 2161-2174, 1989.

36. M.S. SHEPHARD, Q. NIU and P.L. BAEHMANN, "Some results using stress projectors for error indication" in: J.E. FLAHERTY, P.J. PASLOW, M.S. SHEPHARD, J.D. VASILAKIS, eds., *Adaptive Methods for Partial Differential Equations* SIAM, Philadelphia, 1989, pp. 83-99.

37. I. BABUŠKA and R. RODRIGUEZ, "The problem of the selection of an a-posteriori error indicator based on smoothening techniques", *Internat. J. Numer. Methods Engrg.* **36**, 539-567, 1993.

38. R. DURÁN, M.A. MUSCHIETTI and R. RODRIGUEZ, "On the asymptotic exactness of the error estimators for linear triangular elements", *Numer. Math.* **59**, 107-127, 1991.

39. R. DURÁN, M.A. MUSCHIETTI and R. RODRIGUEZ, "Asymptotically exact error estimators for rectangular finite elements", *SIAM J. Numer. Anal.* **29** (1), 78-88, 1992.

40. O.C. ZIENKIEWICZ and J.Z. ZHU, "The superconvergent patch recovery and a posteriori error estimates. Part 1: The recovery technique", *Internat. J. Numer. Methods Engrg.* **33**, 1331-1364, 1992.

41. O.C. ZIENKIEWICZ and J.Z. ZHU, "The superconvergent patch recovery and a posteriori error estimates. Part 2: Error estimates and adaptivity", *Internat. J. Numer. Methods Engrg.* **33**, 1365-1382, 1992.

42. N.E. WIBERG and F. ABDULWAHAB, "A posteriori error estimation based on superconvergent derivatives and equilibrium", *Publ 92:1*, Department of Structural Mechanics, Chalmers University of Technology, 1992.

43. O.C. ZIENKIEWICZ and J.Z. ZHU, "The superconvergent patch recovery (SPR) and adaptive finite element refinement", *Comput. Methods Appl. Mech. Engrg.*, **101**, 207-224, 1992.

44. O.C. ZIENKIEWICZ, J.Z ZHU and J. WU, "Superconvergent patch recovery techniques. Some further tests", *Comm. Numer. Methods Engrg.* **9**, 251-258, 1993.

45. B.A. SZABO, "Mesh design for the p-version of the finite element method", *Comput. Methods Appl. Mech. Engrg.* **55**, 181-197, 1986.

46. A.R. DIAZ, N. KIKUCHI and J.E. TAYLOR, "A method of grid optimization for finite element methods", *Comput. Methods Appl. Mech. Engrg.* **41**, 29-45, 1983.

47. L. DEMKOWICZ, P. DEVLOO and J.T. ODEN, "On an h-type mesh-refinement strategy based on minimization of interpolation error", *Comput. Methods Appl. Mech. Engrg.* **53**, 67-89, 1985.

48. K. ERIKSSON and C. JOHNSON, "An adaptive finite element method for linear elliptic problems", *Math. Comp.* **50**, 361-383, 1988.

49. C. JOHNSON and P. HANSBO, "Adaptive finite element methods in computational mechanics", *Comput. Methods Appl. Mech. Engrg.* **101**, 143-181, 1992.

50. I. BABUŠKA, R. DURÁN and R. RODRIGUEZ, "Analysis of the efficiency of an a-posteriori error estimator for linear triangular finite elements", *SIAM J. Numer. Anal.* **29** (4), 947-964, 1992.

51. I. BABUŠKA, L. PLANK and R. RODRIGUEZ, "Quality assessment of the a-posteriori error estimation in finite elements", *Finite Elements in Analysis and Design* **11**, 285-306, 1992.

52. I. BABUŠKA, L. PLANK and R. RODRIGUEZ, "Basic problems of a-posteriori error estimation", *Comput. Methods Appl. Mech. Engrg.* **101**, 97-112, 1992.

53. I. BABUŠKA, T. STROUBOULIS and C.S. UPADHYAY, "A model study of the quality of a-posteriori estimators for linear elliptic problems, Part Ia: Error estimation in the interior of patchwise uniform grids of triangles", Technical Note BN-1147, Institute for Physical Science and Technology, University of Maryland, College Park, 1993.

54. L.B. WAHLBIN, "Local behavior in finite element methods", in: P.G. CIARLET and J.L. LIONS, eds., *Handbook of Numerical Analysis*, Vol. II, North-Holland, Amsterdam, 1991, pp. 357-522.

55. I. BABUŠKA, T. STROUBOULIS, A. MATHUR and C.S. UPADHYAY, "Pollution error in the h-version of the finite-element method and a-posteriori error estimation", in preparation.

56. J. ROBINSON, E.A.W. MAUNDER and A.C.A. RAMSAY, "Some studies of simple error estimators, Part I - The Philosophy", *Finite Element News*, Issue No. 4, 38-42, 1992.

57. J. ROBINSON, E.A.W. MAUNDER and A.C.A. RAMSAY, "Some studies of simple error estimators, Part II, Problem I - Convergence characteristics of the error estimators", *Finite Element News*, Issue No. 5, 36-41, 1992.

58. P.G. CIARLET, "Basic error estimates for elliptic problems", in: P.G. CIARLET and J.L. LIONS, eds., *Handbook of Numerical Analysis*, Vol. II, North-Holland, Amsterdam, 1991, pp. 17-351.

59. P. LADEVEZE, "Comparaison de modeles de milieux continus", These, Universite P. et M. Curie, Paris, 1975.

60. P. ROUGEOT, "Sur le Controle de la Qualite des Maillages Elements Finis", These de Doctorate de l'Universite, Paris 6, Cachan, France.

61. P. LADEVEZE, J.P. PELLE and P. ROUGEOT, "Error estimation and mesh optimization for classical finite elements", Engineering Computations **9**, 69-80, 1991.

62. B.A. SZABO and I. BABUŠKA, "Finite Element Analysis", John Wiley & Sons, Inc., New York, 1991.

63. C. JOHNSON and B. MERCIER, "Some equilibrium finite element methods for two-dimensional elasticity problems", Numer. Math. **30**, 103-116, 1978.

Laplace's Equation, Linear Triangles			
Element residual without equilibration (Est. 1)			
No. of layers, s	Periodic Problem		
	$C_L^{\omega_0^h}$	$C_U^{\omega_0^h}$	$\mathcal{R}^s_{\omega_0^h}$
1	1.084	1.312	0.396
2	1.079	1.297	0.376
3	1.080	1.327	0.407
4	1.080	1.317	0.397
5	1.080	1.312	0.392

Table 1. Influence of the size of the patch ω_s^h on the value of the robustness-index $\mathcal{R}_{\omega_0^h}$ obtained from the periodic super-patch. Laplace's equation, quadratic harmonic polynomial solution, linear elements ($p = 1$). Pattern 1 (shown in Fig. 9a) with $s = 1, 2, 3, 4, 5$ layers around the cell ω_0^h (as shown in Fig. 8) is employed in the computation of the robustness for Est. 1.

Laplace's Equation, Linear Triangles						
Pattern	Periodic Problem			Dirichlet BVP		
Element residual without equilibration (Est. 1)						
	$C_L^{\omega_0^h}$	$C_U^{\omega_0^h}$	$\mathcal{R}^s_{\omega_0^h}$	$\bar{C}_L^{\omega_0^h}$	$\bar{C}_U^{\omega_0^h}$	$\bar{\mathcal{R}}$
1	1.080	1.312	0.392	1.080	1.308	0.388
2	1.041	1.418	0.459	1.028	1.413	0.441
3	0.998	1.011	0.013	0.999	1.014	0.015
4	0.996	1.128	0.132	0.983	1.116	0.133
5	0.960	1.701	0.741	0.954	1.701	0.747
Element residual with equilibration (Est. 2) (Ladeveze's equilibration, eq. (32))						
1	0.993	0.999	0.008	0.986	0.999	0.015
2	0.999	1.003	0.004	0.977	0.999	0.025
3	0.989	1.026	0.037	0.991	1.030	0.039
4	0.980	1.016	0.036	0.963	1.010	0.048
5	0.923	1.069	0.148	0.916	1.070	0.157
6	0.913	0.993	0.102	0.917	0.999	0.092
7	0.999	1.001	0.002	0.999	1.001	0.002
ZZ estimator (Est. 4)						
1	1.004	1.012	0.016	1.004	1.005	0.009
2	0.995	1.035	0.040	0.992	1.021	0.029
3	0.989	0.994	0.015	0.993	0.995	0.012
4	0.958	1.005	0.049	0.941	0.999	0.064
5	0.982	1.013	0.031	0.978	1.010	0.032
6	0.926	0.998	0.082	0.930	1.004	0.079
7	0.979	1.005	0.026	0.979	1.005	0.026

Table 2a. Accuracy of the methodology for general meshes: Laplace's equation, quadratic harmonic polynomial solution, linear elements ($p = 1$). The mesh of triangles shown in Fig. 6 and the patterns 1-7 shown in Figs. 9a-9g are employed in the computation of the robustness.

Laplace's Equation, Bilinear Quadrilaterals						
Element residual without equilibration (Est. 1)						
Pattern	Periodic Problem			Dirichlet BVP		
	$C_L^{\omega_0^h}$	$C_U^{\omega_0^h}$	$\mathcal{R}^4_{\omega_0^h}$	$\bar{C}_L^{\omega_0^h}$	$\bar{C}_U^{\omega_0^h}$	$\bar{\mathcal{R}}$
1	1.096	1.323	0.420	1.113	1.298	0.412
2	1.051	1.577	0.628	1.053	1.561	0.616
3	1.114	1.882	0.996	1.131	1.896	1.027
4	1.218	2.240	1.458	1.189	2.261	1.450
5	1.340	2.210	1.550	1.298	2.224	1.524
Element residual with equilibration (Est. 2) (Bank & Weiser equilibration, eq. (30))						
1	0.819	0.978	0.243	0.813	0.979	0.251
2	0.833	0.999	0.201	0.852	1.011	0.185
3	0.776	0.979	0.310	0.784	0.988	0.288
4	0.731	0.953	0.417	0.749	0.976	0.360
5	0.702	0.947	0.480	0.715	0.965	0.435
ZZ estimator (Est. 4)						
1	1.010	1.022	0.032	1.011	1.029	0.040
2	1.008	1.017	0.025	1.008	1.018	0.026
3	0.991	1.033	0.042	0.998	1.033	0.035
4	0.978	1.016	0.038	0.980	1.014	0.034
5	0.938	0.999	0.067	0.940	1.001	0.065

Table 2b. Accuracy of the methodology for general meshes: Laplace's equation, quadratic harmonic polynomial solution, linear elements ($p = 1$). The mesh of quadrilaterals shown in Fig. 1 and the patterns 1-5 shown in Figs. 10a-10e are employed in the computation of the robustness.

Laplace's Equation, Quadratic Triangles						
Element residual with equilibration (Est. 2) (Ladeveze's equilibration, eq. (32))						
Pattern	Periodic Problem			Dirichlet BVP		
	$C_L^{\omega_0^h}$	$C_U^{\omega_0^h}$	$\mathcal{R}^3_{\omega_0^h}$	$\bar{C}_L^{\omega_0^h}$	$\bar{C}_U^{\omega_0^h}$	$\bar{\mathcal{R}}$
1	0.960	1.032	0.073	0.960	1.032	0.073
2	0.982	1.009	0.027	0.978	1.008	0.030
3	1.011	1.021	0.032	1.010	1.021	0.032
4	0.973	1.011	0.039	0.973	1.011	0.039
5	0.718	0.894	0.511	0.718	0.894	0.511
6	0.806	1.035	0.275	0.811	1.035	0.267
7	0.998	1.007	0.009	0.997	1.006	0.009
ZZ estimator (Est. 4)						
Pattern	Periodic Problem			Dirichlet BVP		
	$C_L^{\omega_0^h}$	$C_U^{\omega_0^h}$	$\mathcal{R}^3_{\omega_0^h}$	$\bar{C}_L^{\omega_0^h}$	$\bar{C}_U^{\omega_0^h}$	$\bar{\mathcal{R}}$
1	0.969	0.995	0.037	0.969	0.995	0.037
2	0.919	0.935	0.158	0.915	0.933	0.165
3	1.001	1.060	0.061	1.001	1.060	0.061
4	1.006	1.044	0.050	1.005	1.043	0.048
5	0.875	0.933	0.215	0.875	0.933	0.215
6	0.854	0.923	0.254	0.854	0.923	0.254
7	0.978	0.979	0.044	0.977	0.979	0.045

Table 3. Accuracy of the methodology for general meshes: Laplace's equation, cubic harmonic polynomial solution, quadratic elements ($p = 2$). (a) The mesh of triangles shown in Fig. 6 and the patterns 1-7 shown in Figs. 9a-9g are employed in the computation of the robustness.

Isotropic Elasticity, Linear Triangles						
Element residual with equilibration (Est. 2) (Ladeveze's equilibration, eq. (32))						
Pattern	Periodic Problem			Dirichlet BVP		
	$C_L^{\omega_0^h}$	$C_U^{\omega_0^h}$	$\mathcal{R}^3_{\omega_0^h}$	$\bar{C}_L^{\omega_0^h}$	$\bar{C}_U^{\omega_0^h}$	$\bar{\mathcal{R}}$
1	0.965	1.033	0.068	0.949	1.000	0.054
3	0.959	1.049	0.090	0.951	1.048	0.097
4	0.875	1.037	0.179	0.899	1.005	0.117
5	0.853	1.195	0.342	0.856	1.190	0.334
ZZ estimator (Est. 4)						
Pattern	Periodic Problem			Dirichlet BVP		
	$C_L^{\omega_0^h}$	$C_U^{\omega_0^h}$	$\mathcal{R}^3_{\omega_0^h}$	$\bar{C}_L^{\omega_0^h}$	$\bar{C}_U^{\omega_0^h}$	$\bar{\mathcal{R}}$
1	0.992	1.054	0.062	0.992	1.027	0.035
3	0.943	1.004	0.064	0.955	1.004	0.051
4	0.944	1.002	0.061	0.931	0.997	0.077
5	0.948	1.043	0.096	0.946	1.002	0.059

Table 4. Accuracy of the methodology for general meshes: Isotropic elasticity, quadratic "harmonic" polynomial solution, linear elements ($p = 1$). The mesh of triangles shown in Fig. 6 and the patterns 1, 3, 4, 5 shown in Fig. 9a, c, d, e are employed in the computation of the robustness.

Laplace's Equation, Linear Triangles									
Pattern	Neumann BVP						Periodic Problem		
	General solution			Taylor series			Taylor series		
	κ (Est. 1)	κ (Est. 2)	κ (Est. 3)	κ (Est. 1)	κ (Est. 2)	κ (Est. 3)	κ (Est. 1)	κ (Est. 2)	κ (Est. 3)
1	1.219	0.993	1.006	1.220	0.993	1.006	1.228	0.999	1.013
2	1.293	0.995	1.006	1.293	0.995	1.006	1.298	0.998	1.009
3	1.007	1.015	0.992	1.007	1.015	0.992	1.006	1.014	0.991
4	1.085	1.003	0.990	1.086	1.003	0.991	1.098	1.015	1.003
5	1.316	1.031	0.983	1.317	1.031	0.983	1.316	1.034	0.987

Table 5. Applicability of the methodology for general solutions: Laplace's equation, harmonic solution, linear elements ($p = 1$). Comparison of the values of the effectivity index for the cells computed using three different approximate solutions: The solution of a Neumann boundary-value problem in the domain and mesh shown in Fig. 6 with the data taken from the exact solution (Columns 2, 3, 4); the solution of a Neumann boundary-value problem in the domain and mesh shown in Fig. 6 with the data taken from the quadratic Taylor-series expansion about the central-node of the mesh-cell ω_0^h for which the effectivity index is computed (Columns 5, 6, 7); the solution of a periodic boundary-value problem in super-patches which include the patches shown in Figs. 9a-9e with the data taken from the quadratic Taylor-series expansion about the central node of each of the mesh-cells (Columns 8, 9, 10).

Poisson's Equation, Bilinear Quadrilaterals Z-Z Estimators				
Periodic Mesh 1				
Type	$\frac{K_{max}}{K_{min}}$	C_L	C_U	$\mathcal{R}$
1	1	0.940	1.035	0.098
2	1	0.959	1.008	0.051
3	1	0.992	1.026	0.034
1	100	0.810	1.044	0.277
2	100	0.843	1.004	0.190
3	100	0.893	1.015	0.135

Table 6a. Influence of various parameters on the robustness of estimators: Z-Z estimators, Poisson's equation, general quadratic polynomial solution, bilinear quadrilaterals ($p = 1$). Comparison of the robustness of the various versions of the Z-Z-estimator. The robustness results are given for the periodic mesh shown in Fig. 11a.

Poisson's Equation, Bilinear Quadrilaterals Z-Z Estimators				
Periodic Mesh 2				
Type	$\frac{K_{max}}{K_{min}}$	C_L	C_U	$\mathcal{R}$
1	1	0.945	1.015	0.073
2	1	0.962	1.008	0.047
3	1	0.995	1.009	0.014
1	100	0.860	1.343	0.483
2	100	0.891	1.329	0.438
3	100	0.946	1.185	0.239

Table 6b. Influence of various parameters on the robustness of estimators: Z-Z estimators, Poisson's equation, general quadratic polynomial solution, bilinear quadrilaterals ($p = 1$). Comparison of the robustness of the various versions of the Z-Z-estimator. The robustness results are given for the periodic mesh shown in Fig. 11b.

Poisson's Equation, Bilinear Quadrilaterals *Z-Z* Estimators				
Periodic Mesh 3				
Type	$\frac{K_{max}}{K_{min}}$	C_L	C_U	$\mathcal{R}$
1	1	0.995	1.026	0.031
2	1	1.001	1.009	0.010
3	1	0.999	1.004	0.005
1	100	0.956	1.015	0.061
2	100	0.955	1.011	0.058
3	100	0.989	1.023	0.034

Table 6c. Influence of various parameters on the robustness of estimators: *Z-Z* estimators, Poisson's equation, general quadratic polynomial solution, bilinear quadrilaterals ($p = 1$). Comparison of the robustness of the various versions of the *Z-Z*-estimator. The robustness results are given for the periodic mesh shown in Fig. 11c.

Poisson's Equation, Bilinear Quadrilaterals Z-Z Estimators				
Periodic Mesh 4				
Type	$\frac{K_{max}}{K_{min}}$	C_L	C_U	$\mathcal{R}$
1	1	0.991	1.006	0.015
2	1	0.993	1.005	0.012
3	1	0.994	1.005	0.011
1	100	0.849	1.021	0.198
2	100	0.848	1.008	0.187
3	100	0.847	1.009	0.190

Table 6d. Influence of various parameters on the robustness of estimators: Z-Z estimators, Poisson's equation, general quadratic polynomial solution, bilinear quadrilaterals ($p = 1$). Comparison of the robustness of the various versions of the Z-Z-estimator. The robustness results are given for the periodic mesh shown in Fig. 11d.

Laplace's Equation, Linear Triangles									
Periodic Mesh	ZZ estimator (*Type 1*)			ZZ estimator (*Type 2*)			ZZ estimator (*Type 3*)		
	C_L	C_U	$\mathcal{R}$	C_L	C_U	$\mathcal{R}$	C_L	C_U	$\mathcal{R}$
1	0.963	1.005	0.043	0.955	1.003	0.050	0.957	1.005	0.050
2	0.998	1.011	0.013	0.992	0.995	0.013	0.984	1.005	0.021
3	0.832	1.075	0.272	0.832	0.977	0.225	0.833	0.966	0.236
4	0.833	1.093	0.286	0.766	1.000	0.305	0.744	0.994	0.350
5	1.000	1.000	0.000	1.000	1.000	0.000	1.002	1.005	0.007

Table 7. Influence of various parameters on the robustness of estimators: Z-Z-estimators, Laplace's equation, harmonic quadratic polynomial solution, linear triangles. Comparison of the robustness of the various versions of the Z-Z estimator. The robustness results are given for the periodic meshes shown in Fig. 12.

Laplace's Equation, Quadratic Triangles						
Periodic Mesh	ZZ estimator (*Type 2*)			ZZ estimator (*Type 3*)		
	C_L	C_U	$\mathcal{R}$	C_L	C_U	$\mathcal{R}$
1	0.955	1.002	0.049	0.977	1.003	0.027
2	0.893	1.002	0.122	0.964	0.987	0.051
3	0.782	0.990	0.289	0.873	0.972	0.174
4	0.823	1.003	0.218	0.843	1.006	0.192
6	1.001	1.006	0.007	1.013	1.047	0.060

Table 8. Influence of various parameters on the robustness of estimators: Z-Z-estimators, Laplace's equation, harmonic cubic polynomial solution, quadratic triangles ($p = 2$). Comparison of the robustness of the various versions of the Z-Z estimator. The robustness results are given for the periodic meshes shown in Fig. 12.

Isotropic Elasticity, Linear Triangles									
Periodic Mesh	*ZZ* estimator (*Type 1*)			*ZZ* estimator (*Type 2*)			*ZZ* estimator (*Type 3*)		
	C_L	C_U	$\mathcal{R}$	C_L	C_U	$\mathcal{R}$	C_L	C_U	$\mathcal{R}$
1	0.948	1.011	0.066	0.944	1.006	0.065	0.945	1.008	0.066
2	0.980	1.018	0.038	0.969	1.001	0.033	0.959	1.010	0.053
3	0.833	1.111	0.300	0.726	1.044	0.420	0.728	1.039	0.411
4	0.774	1.117	0.397	0.693	1.039	0.481	0.675	1.019	0.500
5	1.000	1.000	0.000	1.000	1.000	0.000	1.000	1.006	0.006

Table 9. Influence of various parameters on the robustness of estimators: *Z-Z*-estimators, isotropic elasticity problem, "harmonic" quadratic polynomial solution, linear triangles ($p = 1$). Comparison of the robustness of the various versions of the *Z-Z* estimator. The robustness results are given for the periodic meshes shown in Fig. 12.

Laplace's Equation, Bilinear Quadrilaterals *Z-Z* Estimators						
Periodic Mesh	Harmonic projection			Original projection		
	C_L	C_U	$\mathcal{R}$	C_L	C_U	$\mathcal{R}$
1	0.998	1.442	0.444	0.999	1.025	0.026
2	0.998	1.551	0.553	0.999	1.015	0.016
3	1.000	1.465	0.465	0.995	1.017	0.022
4	0.999	1.301	0.302	0.999	1.012	0.013

Table 10. Influence of various parameters on the robustness of estimators: *Z-Z* estimators, Laplace's equation, bilinear quadrilaterals. Comparison of the robustness of two versions of the *Z-Z* estimator based on the general or the harmonic patch projection for the periodic *meshes shown* in Fig. 11.

Laplace's Equation, Bilinear Quadrilaterals							
Element residual with equilibration							
Periodic Mesh	$\frac{K_{max}}{K_{min}}$	*Type A* ($w_i = 1$)			*Type C* ($w_i = \lvert\epsilon_i'\rvert^{-1}$)		
		C_L	C_U	$\mathcal{R}$	C_L	C_U	$\mathcal{R}$
1	1	0.9905	1.2390	0.2485	0.9902	1.2444	0.2542
2	1	0.9857	1.2488	0.2631	0.9976	1.2490	0.2514
3	1	0.9794	0.9991	0.0201	0.9918	1.0701	0.0783
4	1	0.9891	1.1267	0.1376	0.9967	1.1974	0.2007
1	100	0.6197	0.9938	0.6074	0.7861	1.9658	1.1797
2	100	0.6210	0.9922	0.6025	0.8715	1.9737	1.1022
3	100	0.4925	0.9930	1.0234	0.8774	0.9706	0.1094
4	100	0.6334	0.9987	0.5775	0.8912	1.2436	0.3524

Table 11. Influence of various parameters on the robustness of estimators: Element-residual error-estimators with various types of equilibration. Laplace's equation, quadratic harmonic polynomial solution, bilinear quadrilaterals ($p = 1$). Comparison of the robustness of estimators Est. 2/*Type A*, Est. 2/*Type C* for the periodic meshes shown in Fig. 11.

Laplace's Equation, Linear Triangles						
Element residual with equilibration						
Periodic Mesh	*Type A* ($w_i = 1$)			*Type B* ($w_i = \|\epsilon_i\|^{-1}$)		
	C_L	C_U	$\mathcal{R}$	C_L	C_U	$\mathcal{R}$
1	0.958	1.002	0.046	0.957	1.020	0.065
2	0.999	1.226	0.227	0.999	1.012	0.013
3	1.079	1.636	0.715	0.998	1.058	0.060
4	0.972	1.266	0.294	0.949	1.062	0.113
5	1.000	2.958	1.958	1.000	1.003	0.003

Table 12. Influence of various parameters on the robustness of estimators: Element-residual error-estimators with various types of equilibration. Laplace's equation, quadratic harmonic polynomial solution, linear triangles ($p = 1$). Comparison of the robustness of estimators Est. 2/*Type A*, Est. 2/*Type B* for the periodic meshes shown in Fig. 12.

Laplace's Equation, Quadratic Triangles						
Element residual with equilibration						
Periodic Mesh	*Type A* ($w_i = 1$)			*Type B* ($w_i = \|\epsilon_i\|^{-1}$)		
	C_L	C_U	$\mathcal{R}$	C_L	C_U	$\mathcal{R}$
1	0.944	1.016	0.075	0.958	0.984	0.060
2	0.991	1.020	0.029	0.991	1.007	0.016
3	1.007	1.262	0.269	0.989	1.003	0.014
4	0.999	1.082	0.083	0.919	0.994	0.094
6	1.000	2.369	1.369	1.000	1.001	0.001

Table 13. Influence of various parameters on the robustness of estimators: Element-residual error-estimators with various types of equilibration. Laplace's equation, cubic harmonic polynomial solution, quadratic triangles ($p = 2$). Comparison of the robustness of estimators Est. 2/*Type A*, Est. 2/*Type B* for the periodic meshes shown in Fig. 12.

Orthotropic Heat-Conduction, Linear Triangles									
Element residual with equilibration									
Grid-Material Orientation θ (deg)	*Type A* ($w_i = 1$)			*Type B* ($w_i = \lvert\epsilon_i^{-1}\rvert$)			*Type C* ($w_i = \lvert\epsilon_1'\rvert^{-1}$)		
	C_L	C_U	$\mathcal{R}$	C_L	C_U	$\mathcal{R}$	C_L	C_U	$\mathcal{R}$
-90	1.004	2.280	1.284	0.962	1.474	0.512	0.877	1.237	0.360
-75	1.023	1.727	0.750	1.002	1.495	0.497	0.941	1.301	0.360
-60	1.041	1.638	0.679	0.995	1.992	0.997	0.995	1.989	0.994
-45	0.994	1.693	0.699	0.994	2.245	1.251	0.995	2.124	1.129
-30	0.972	1.435	0.463	0.994	1.451	0.457	0.993	1.331	0.338
-15	0.972	1.948	0.976	0.960	1.061	0.101	0.894	1.079	0.192
00	1.004	2.280	1.284	0.962	1.474	0.512	0.877	1.237	0.360
15	1.023	1.727	0.750	0.995	1.495	0.500	0.941	1.301	0.360
30	1.041	1.638	0.679	0.995	1.992	0.997	0.995	1.989	0.994
45	0.994	1.693	0.699	0.994	2.245	1.251	0.995	2.124	1.129
60	0.972	1.435	0.463	0.994	1.451	0.457	0.993	1.331	0.338
75	0.972	1.948	0.976	0.960	1.061	0.101	0.894	1.079	0.192
90	1.004	2.280	1.284	0.962	1.474	0.512	0.877	1.237	0.360

Table 14. Influence of various parameters on the robustness of estimators: Element-residual error-estimators with various types of equilibration. Orthotropic heat-conduction problem ($1 \leq K_{\max}/K_{\min} \leq 10$), quadratic "harmonic" polynomial solution, linear triangles ($p = 1$). Comparison of the robustness of estimators Est. 2/*Type A*, Est. 2/*Type B*, Est. 2/*Type C* for the periodic mesh shown in Fig. 12c and various grid-material orientations.

Orthotropic Heat-Conduction, Linear Triangles						
Element residual with equilibration						
Grid-Material Orientation θ (deg)	*Type A* ($w_i = 1$)			*Type C* ($w_i = \lvert\epsilon_i'\rvert^{-1}$)		
	C_L	C_U	$\mathcal{R}$	C_L	C_U	$\mathcal{R}$
-90	1.000	1.419	0.419	1.000	1.010	0.010
-75	1.000	1.156	0.156	0.968	1.002	0.035
-60	0.894	1.000	0.119	0.871	1.013	0.161
-45	0.816	1.000	0.225	0.816	1.030	0.255
-30	0.894	1.000	0.119	0.871	1.000	0.148
-15	1.000	1.156	0.156	0.968	1.002	0.035
00	1.000	1.419	0.419	1.000	1.010	0.010
15	1.000	1.156	0.156	0.968	1.002	0.035
30	0.894	1.000	0.119	0.871	1.000	0.148
45	0.816	1.000	0.225	0.816	1.030	0.255
60	0.894	1.000	0.119	0.871	1.013	0.161
75	1.000	1.156	0.156	0.968	1.002	0.035
90	1.000	1.419	0.419	1.000	1.010	0.010

Table 15. Influence of various parameters on the robustness of estimators: Element-residual error-estimators with various types of equilibration. Orthotropic heat-conduction problem ($1 \leq K_{\max}/K_{\min} \leq 10$), quadratic "harmonic" polynomial solution, linear triangles ($p = 1$). Comparison of the robustness of estimators Est. 2/*Type A*, Est. 2/*Type C* for the periodic mesh shown in Fig. 12f and various grid-material orientations.

Isotropic Elasticity, Linear Triangles						
Element residual with equilibration						
Periodic Mesh	*Type A* ($w_i = 1$)			*Type B* ($w_i = \|\epsilon_i'\|^{-1}$)		
	C_L	C_U	$\mathcal{R}$	C_L	C_U	$\mathcal{R}$
1	0.909	1.052	0.150	0.908	1.075	0.171
2	0.991	1.526	0.535	0.999	1.053	0.054
3	1.053	2.526	1.579	1.007	1.365	0.372
4	0.965	1.510	0.545	0.910	1.374	0.464
5	1.000	5.292	4.292	0.996	1.028	0.032

Table 16. Influence of various parameters on the robustness of estimators: Element-residual error-estimators with various types of equilibration. Isotropic elasticity, quadratic "harmonic" polynomial solution, linear triangles ($p = 1$). Comparison of the robustness of estimators Est. 2/*Type A*, Est. 2/*Type B* for the periodic meshes shown in Fig. 12.

Isotropic Elasticity, Bilinear Quadrilaterals									
Element residual with Ohtsubo and Kitamura flux-splitting									
Periodic Mesh	no equilibration bubble space			with equilibration complete space			with equilibration bubble space		
	C_L	C_U	$\mathcal{R}$	C_L	C_U	$\mathcal{R}$	C_L	C_U	$\mathcal{R}$
1	1.219	1.490	0.708	1.341	1.950	1.291	0.947	1.129	0.183
2	1.157	1.554	0.712	1.320	1.950	1.271	0.944	1.129	0.185
3	1.094	1.949	1.403	1.383	1.594	0.977	0.936	1.159	0.223
4	1.065	1.555	0.620	1.223	1.872	1.095	0.979	1.140	0.161

Table 17. Influence of various parameters on the robustness of estimators: Isotropic elasticity, quadratic "harmonic" polynomial solution, bilinear quadrilaterals ($p = 1$). Element-residual error-estimator without equilibration using the residual functional in (33) (columns 2-4) and with Ohtsubo-Kitamura equilibration (using the complete serendipity space (columns 5-7) and using the serendipity bubble space (columns 8-10)). Comparison of the robustness of the estimators for the periodic meshes shown in Figs. 11a-11f.

Laplace's Equation, Linear Triangles						
Estimators based on complementary energy						
Periodic Mesh	Equilibration of *Type A*			Equilibration of *Type B*		
	C_L	C_U	$\mathcal{R}$	C_L	C_U	$\mathcal{R}$
1	1.520	1.636	1.156	1.520	1.636	1.156
2	1.254	1.966	1.220	1.254	1.772	1.026
3	1.641	2.673	2.314	1.362	1.742	1.104
4	2.007	4.205	4.212	1.792	3.696	3.488
5	1.225	3.825	3.050	1.225	1.735	0.960

Table 18. Influence of various parameters on the robustness of estimatorr· Estimators based on the complementary energy-principle. Laplace's equation, quadratic harmonic polynomial solution, linear triangles ($p = 1$). Comparison of the robustness of estimators Est. 3/*Type A* and Est. 3/*Type B* for the periodic meshes shown in Fig. 12.

Isotropic Elasticity, Linear Triangles						
Estimators based on complementary energy						
Periodic Mesh	Equilibration of *Type A*			Equilibration of *Type B*		
	C_L	C_U	$\mathcal{R}$	C_L	C_U	$\mathcal{R}$
1	1.184	4.113	3.297	1.171	4.046	3.217
2	1.399	8.180	7.579	1.359	5.902	5.261
3	14.399	89.634	102.033	1.541	65.359	64.900

Table 19. Influence of various parameters on the robustness of estimators: Estimators based on the complementary energy-principle. Isotropic elasticity problem, quadratic "harmonic" polynomial solution, linear triangles ($p = 1$). Comparison of the robustness of estimators Est. 3/*Type A* and Est. 3/*Type B* for the periodic meshes shown in Fig. 12a, b, c.

List of Figures

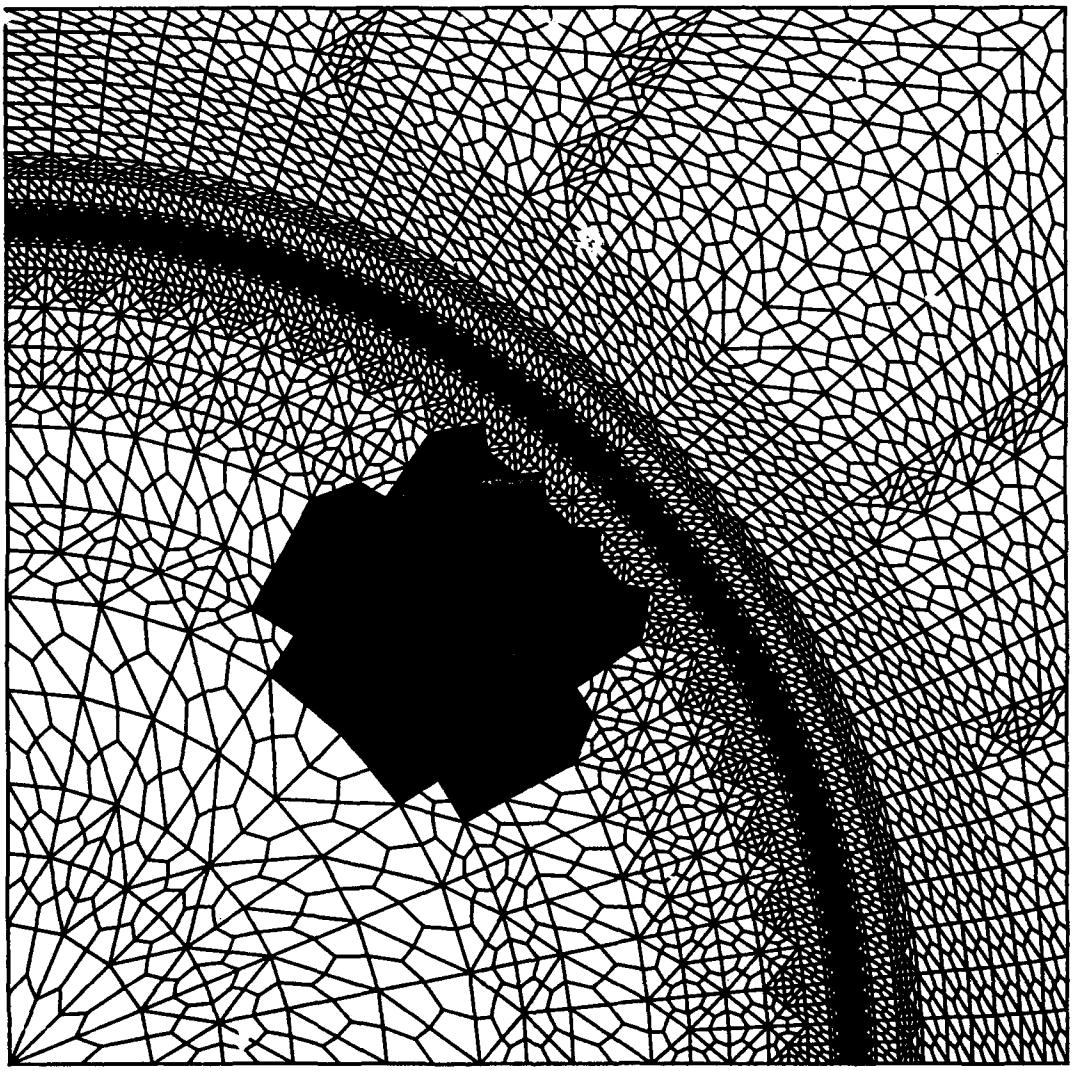

Fig. 1

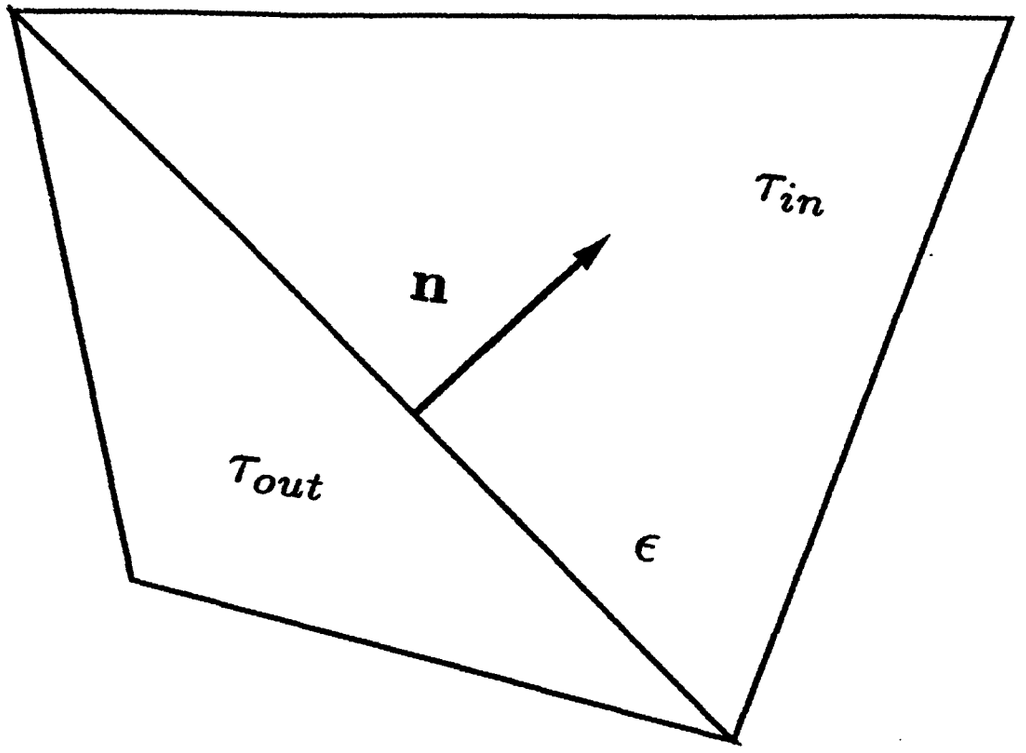

Fig. 2

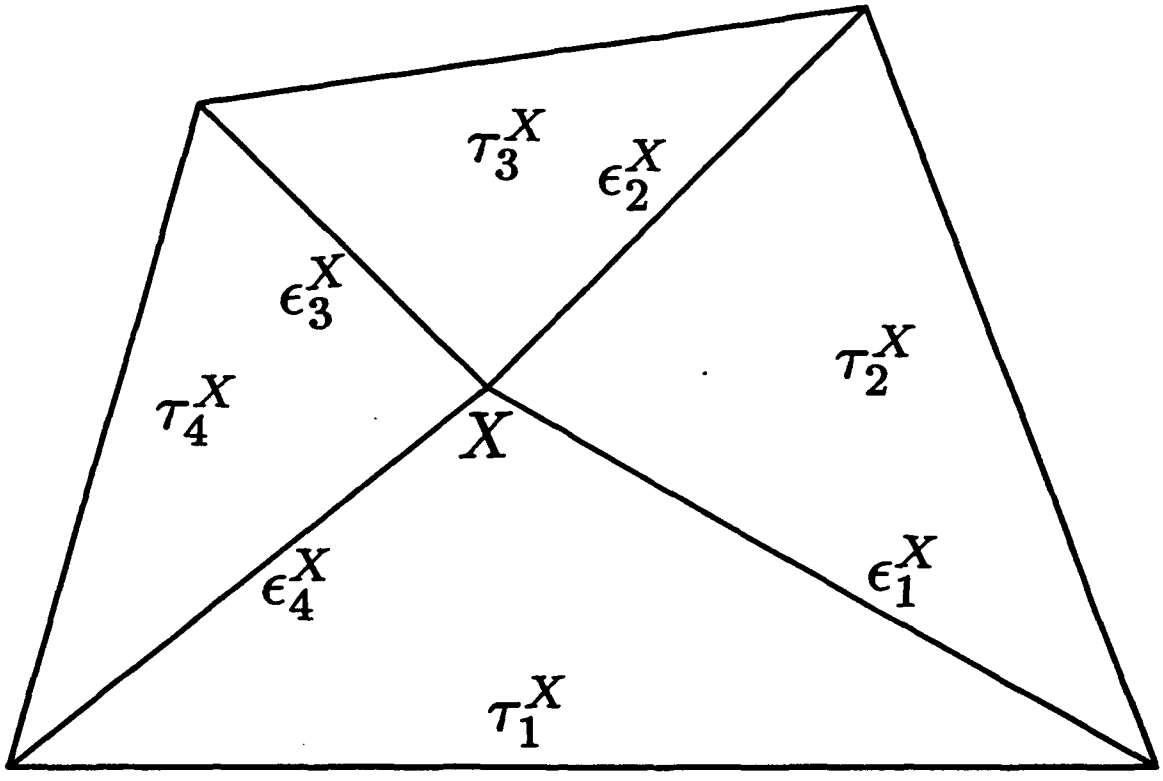
τ_3^X
ϵ_2^X
ϵ_3^X
τ_2^X
τ_4^X
X
ϵ_4^X
ϵ_1^X
τ_1^X

Fig. 3a

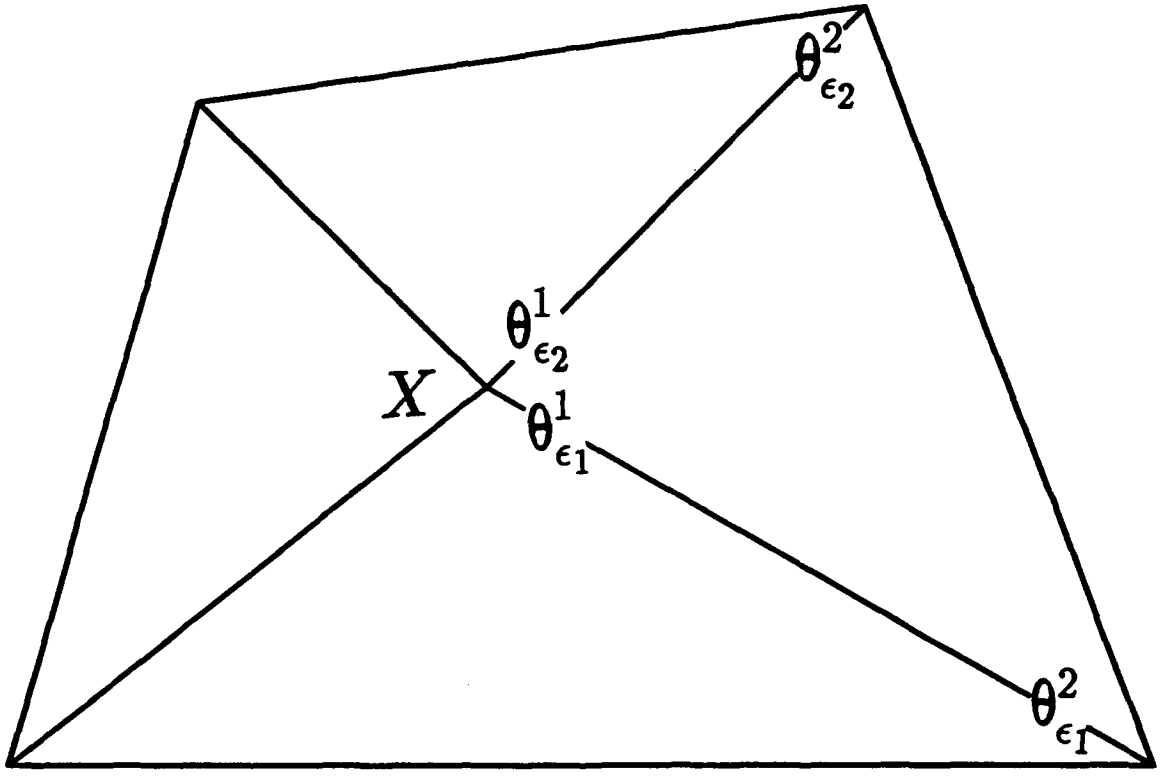
$\theta^2_{\epsilon_2}$
$\theta^1_{\epsilon_2}$
X
$\theta^1_{\epsilon_1}$
$\theta^2_{\epsilon_1}$

Fig. 3b

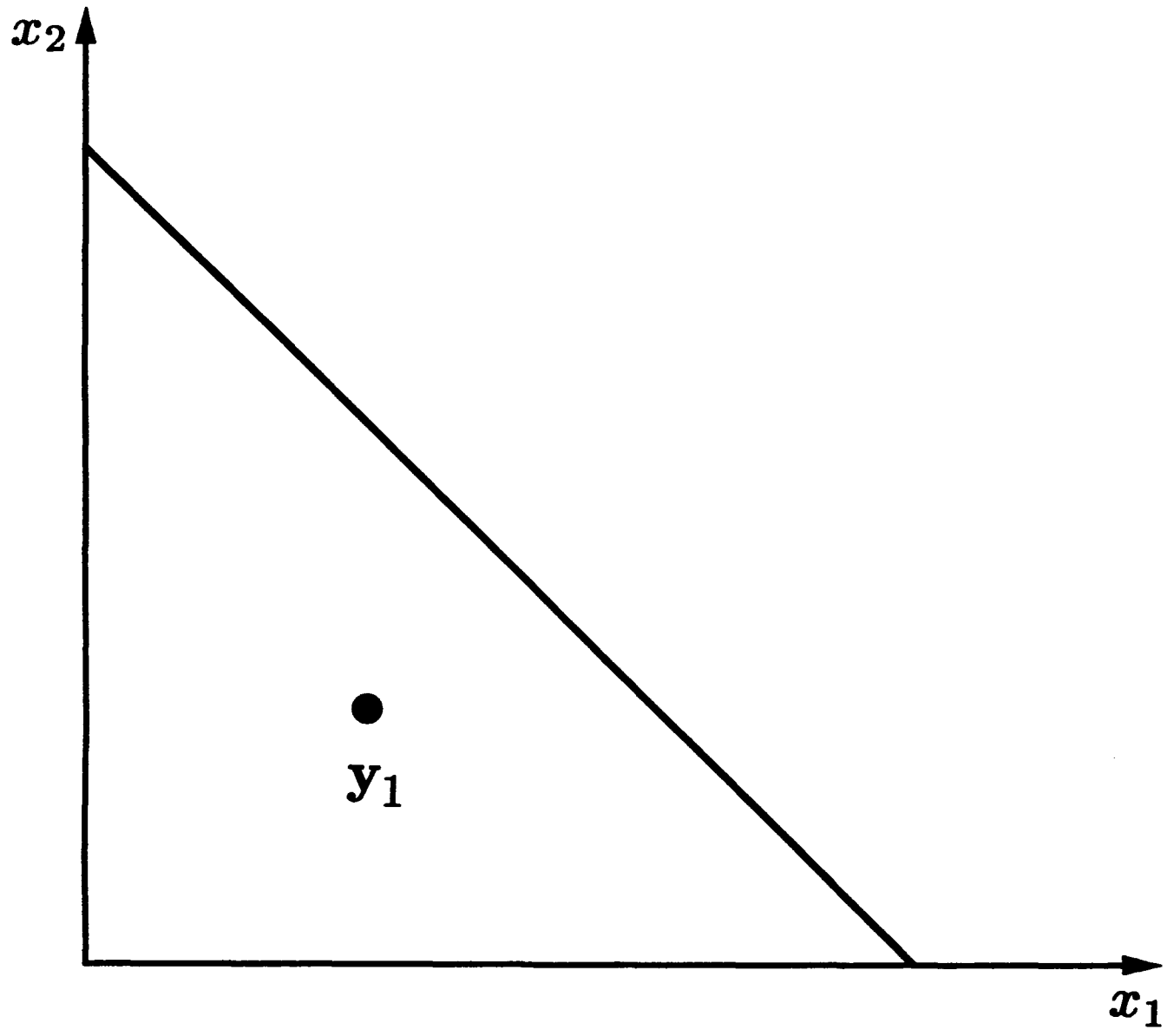

Fig. 4a

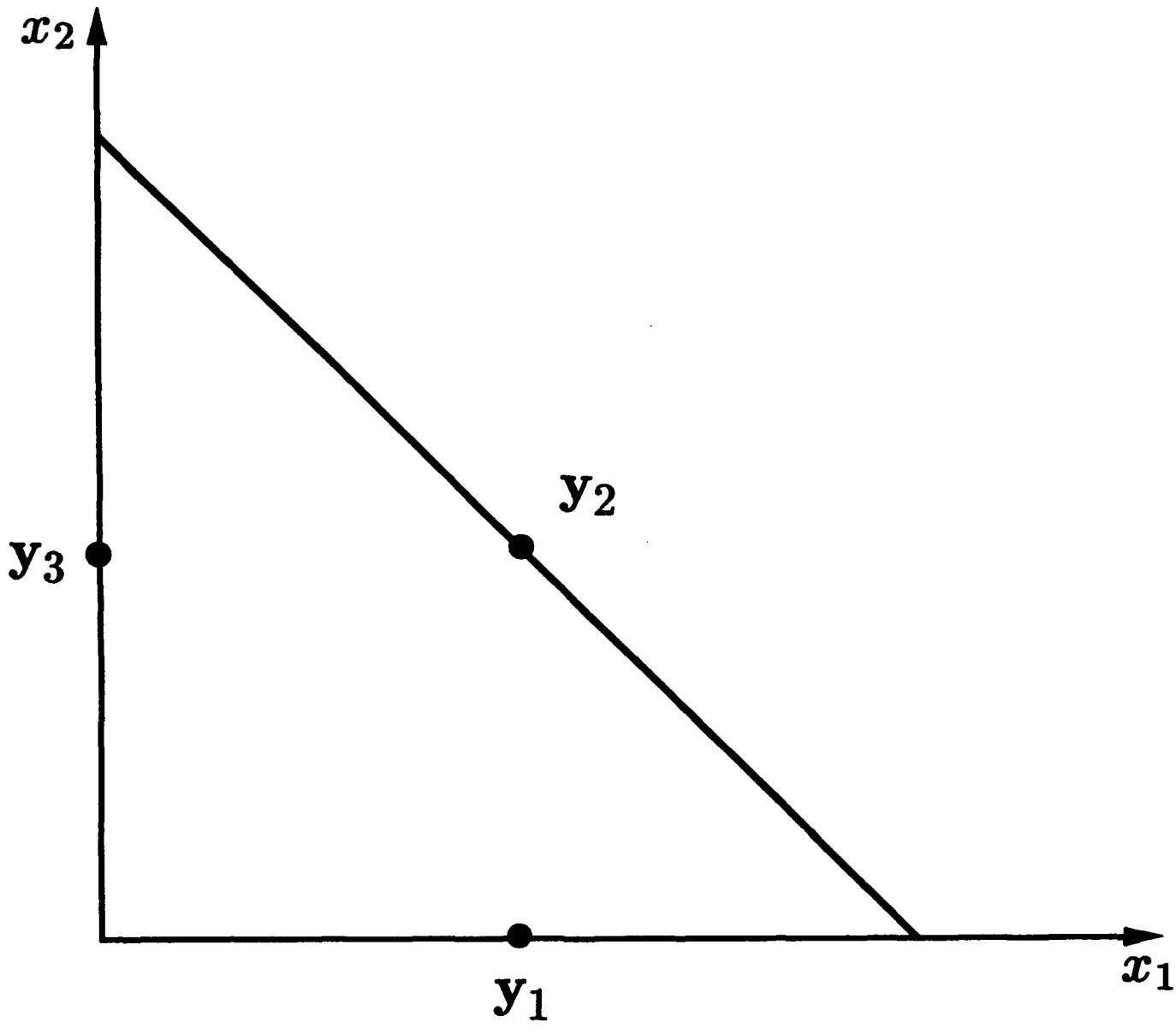

Fig. 4b

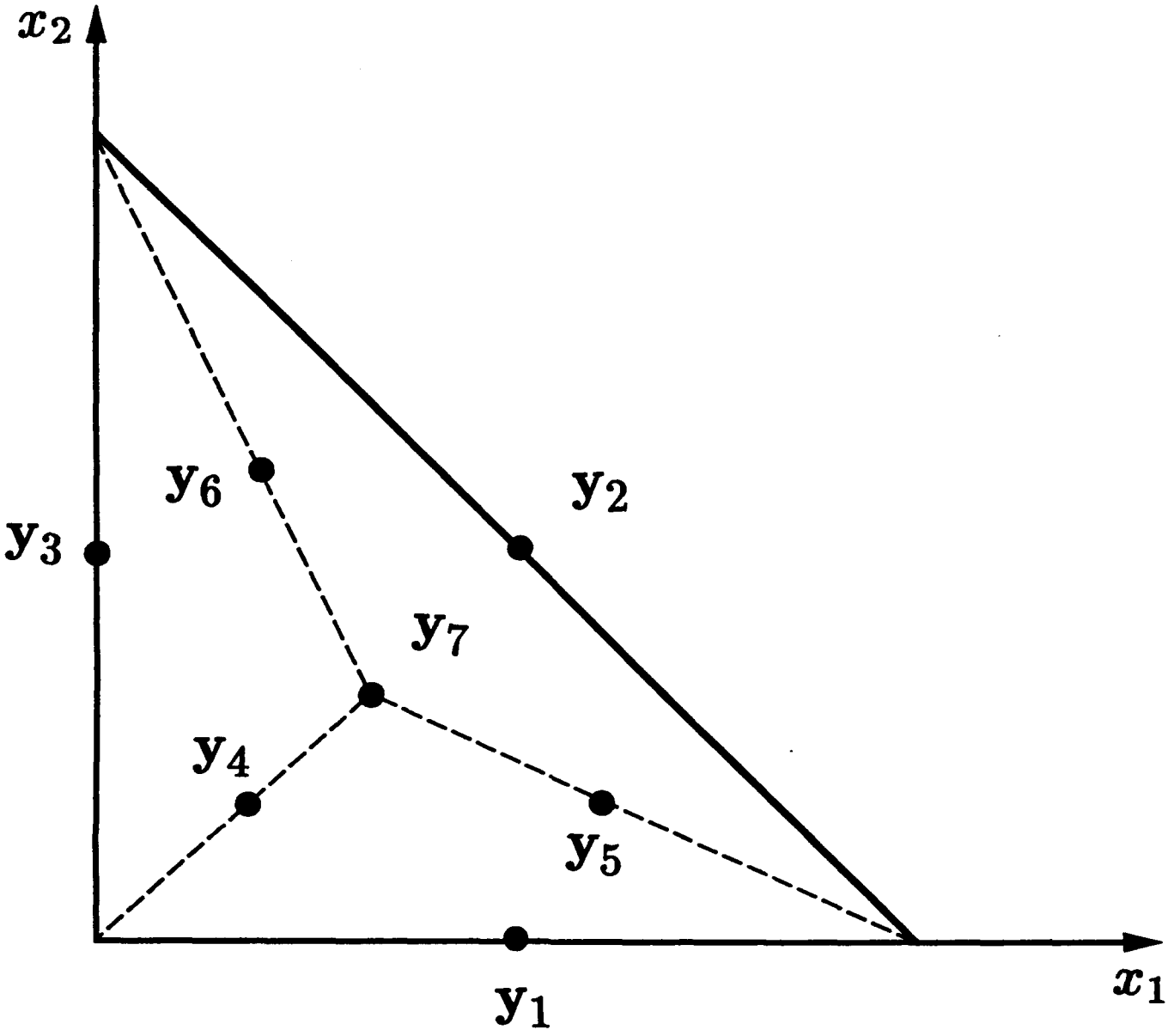

Fig. 4c

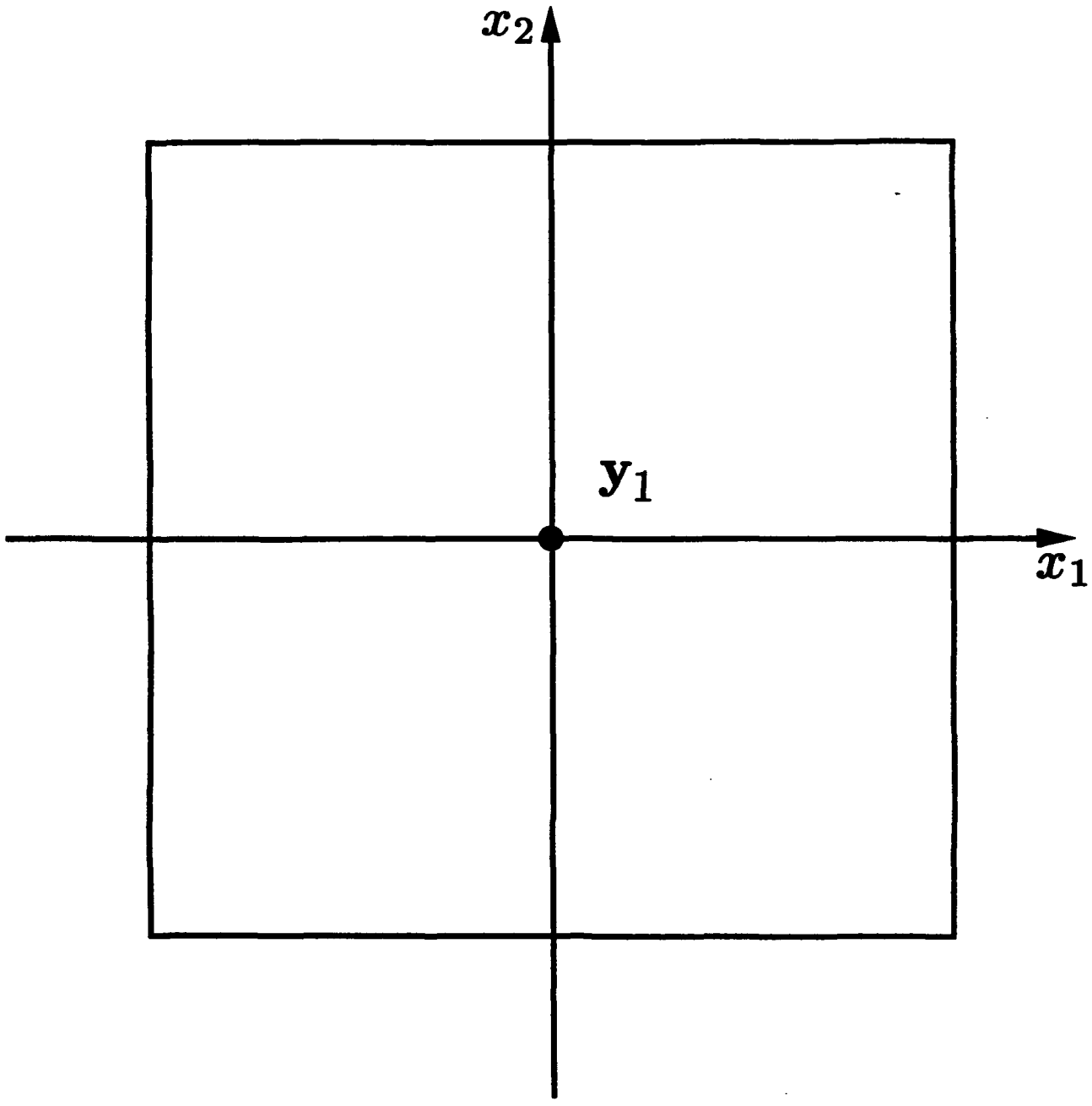

Fig. 4d

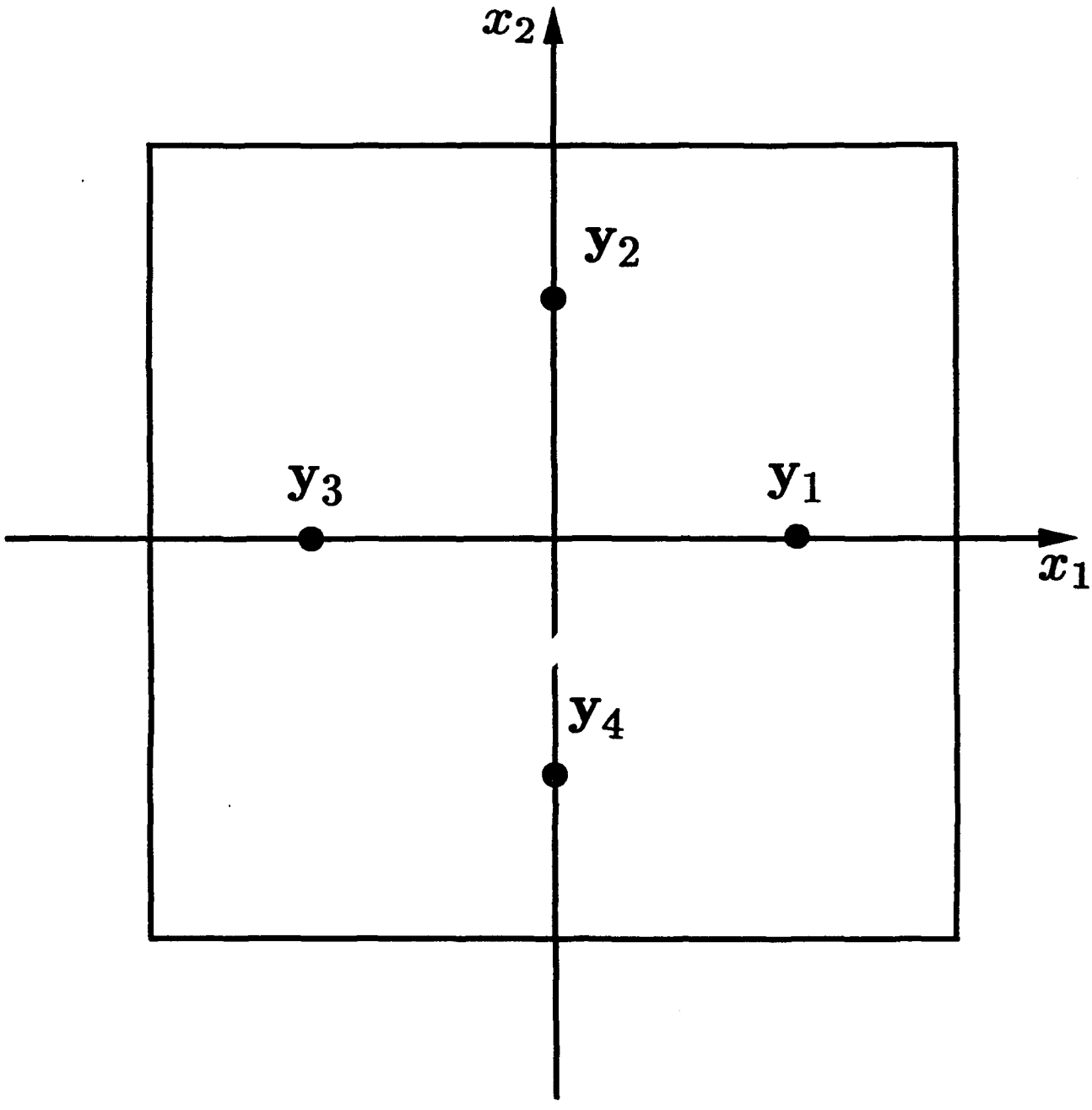

Fig. 4e

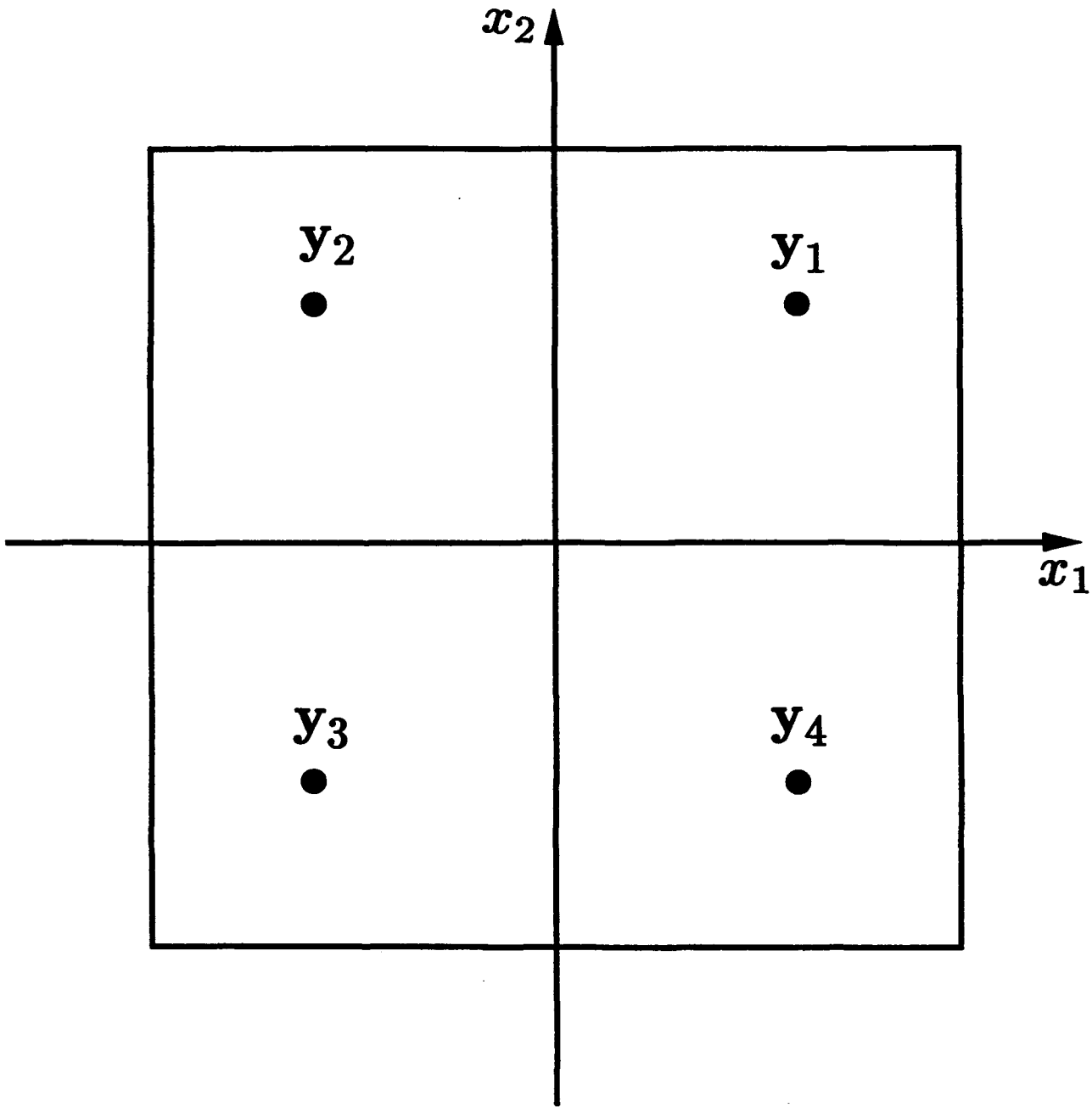

Fig. 4f

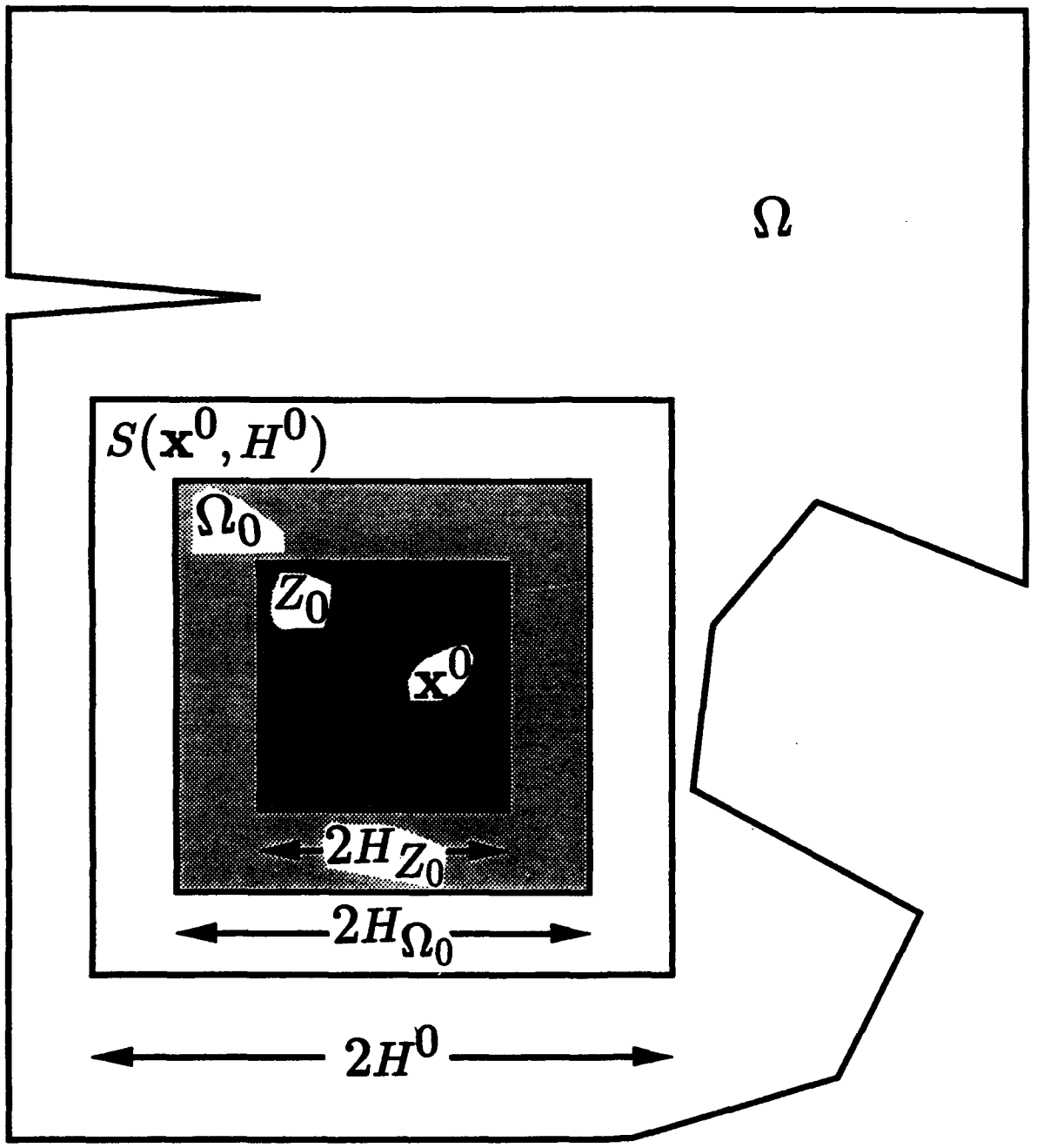

Fig. 5a

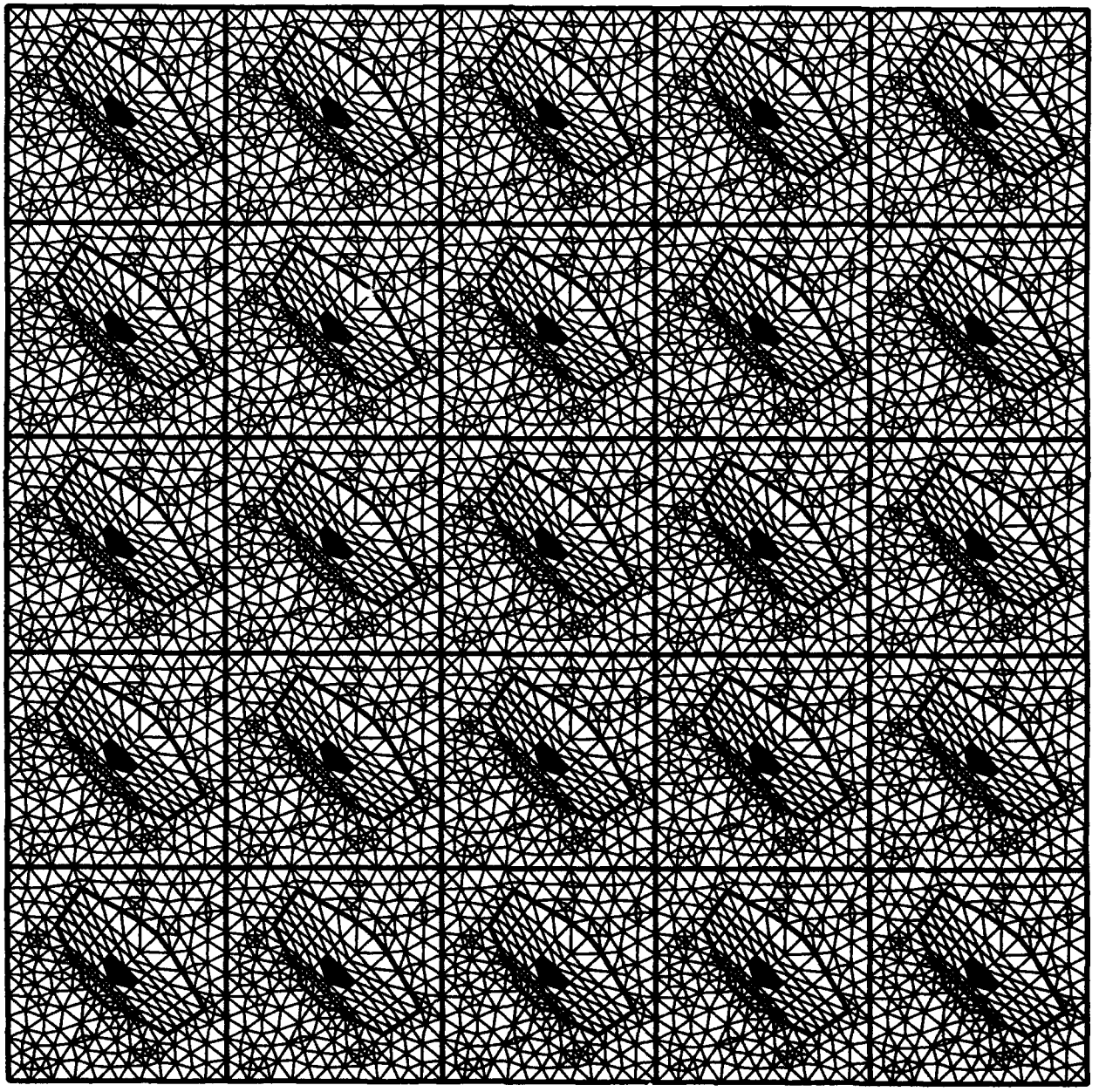

Fig. 5b

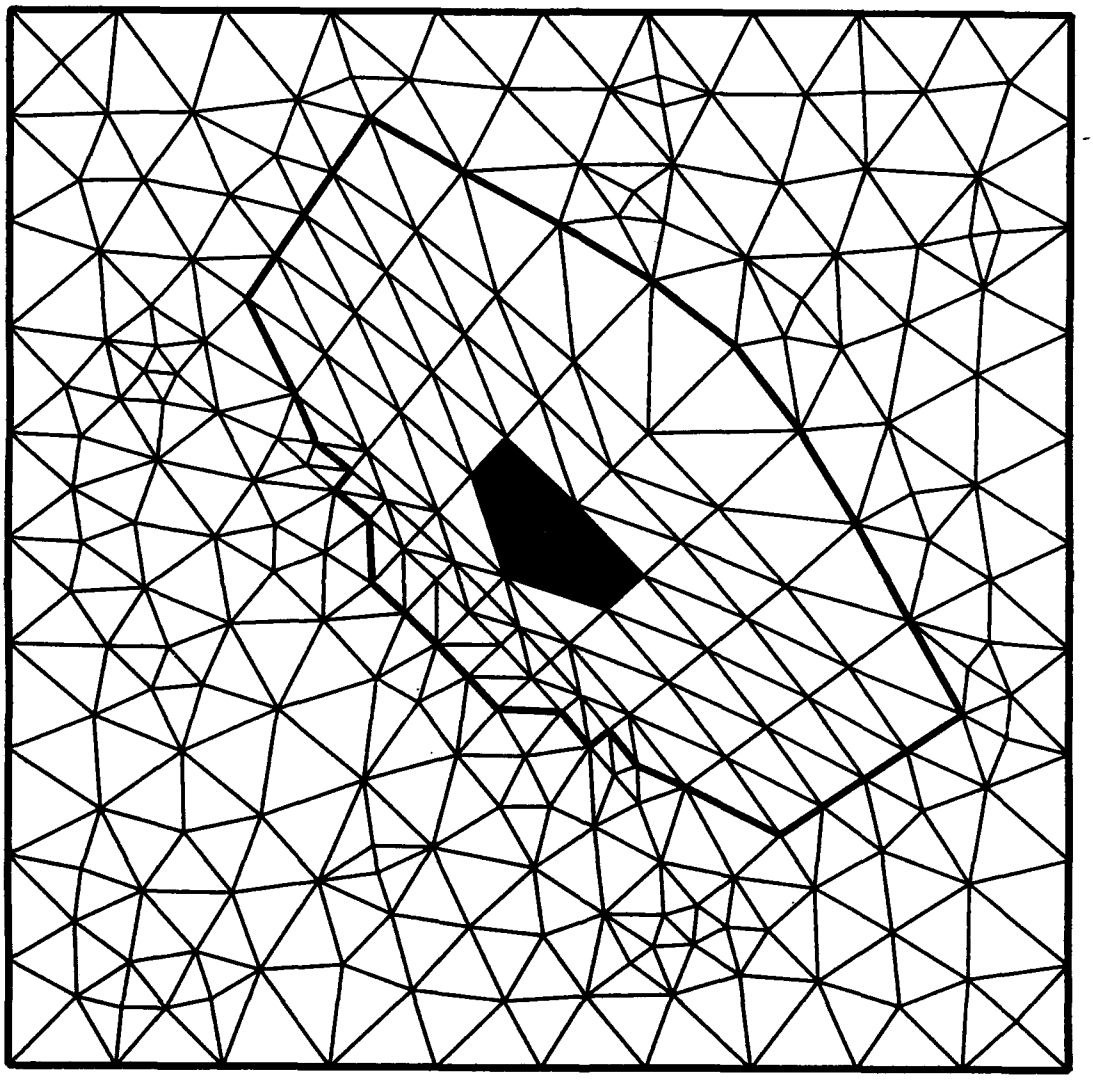

Fig. 5c

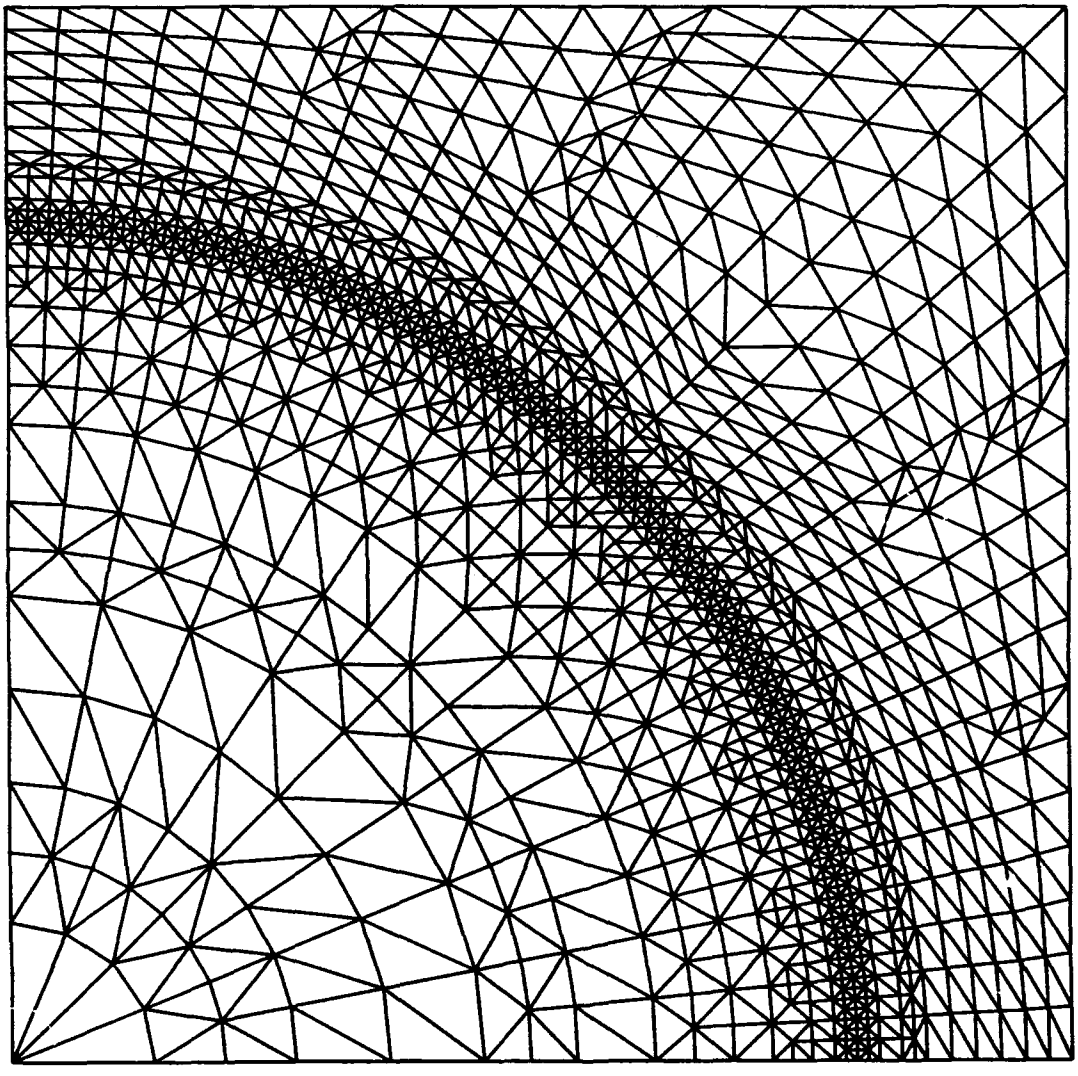

Fig. 6

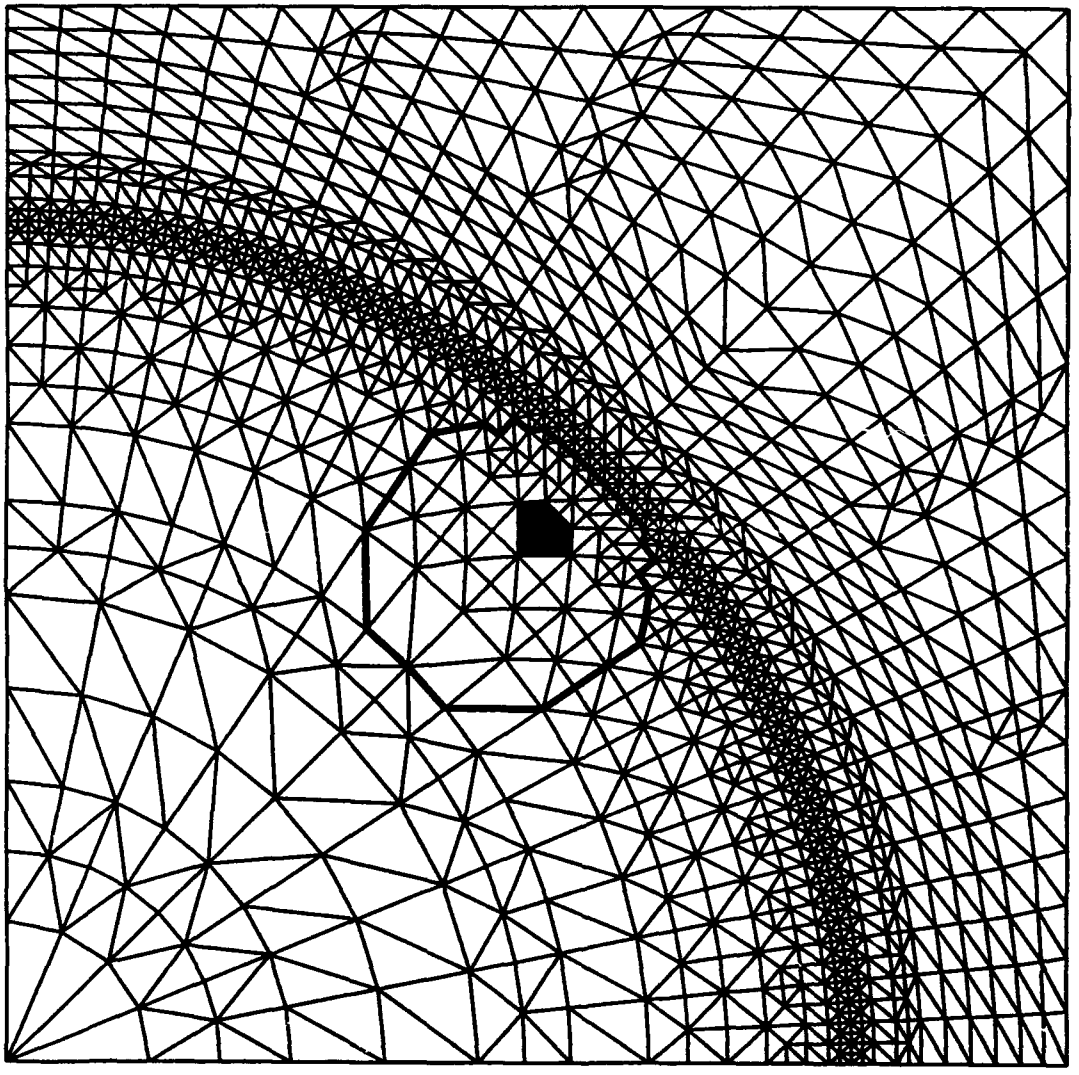

Fig. 7a

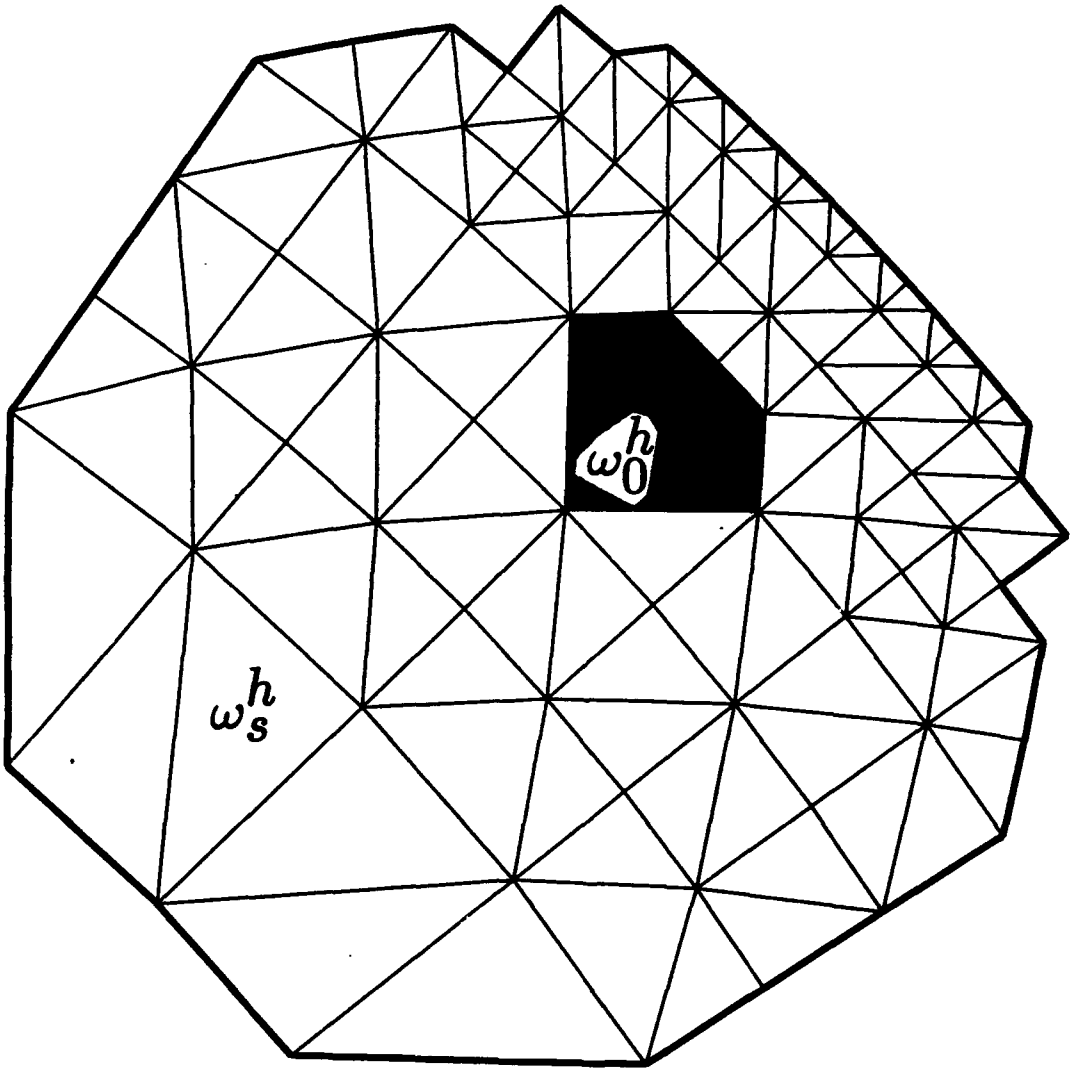

Fig. 7b

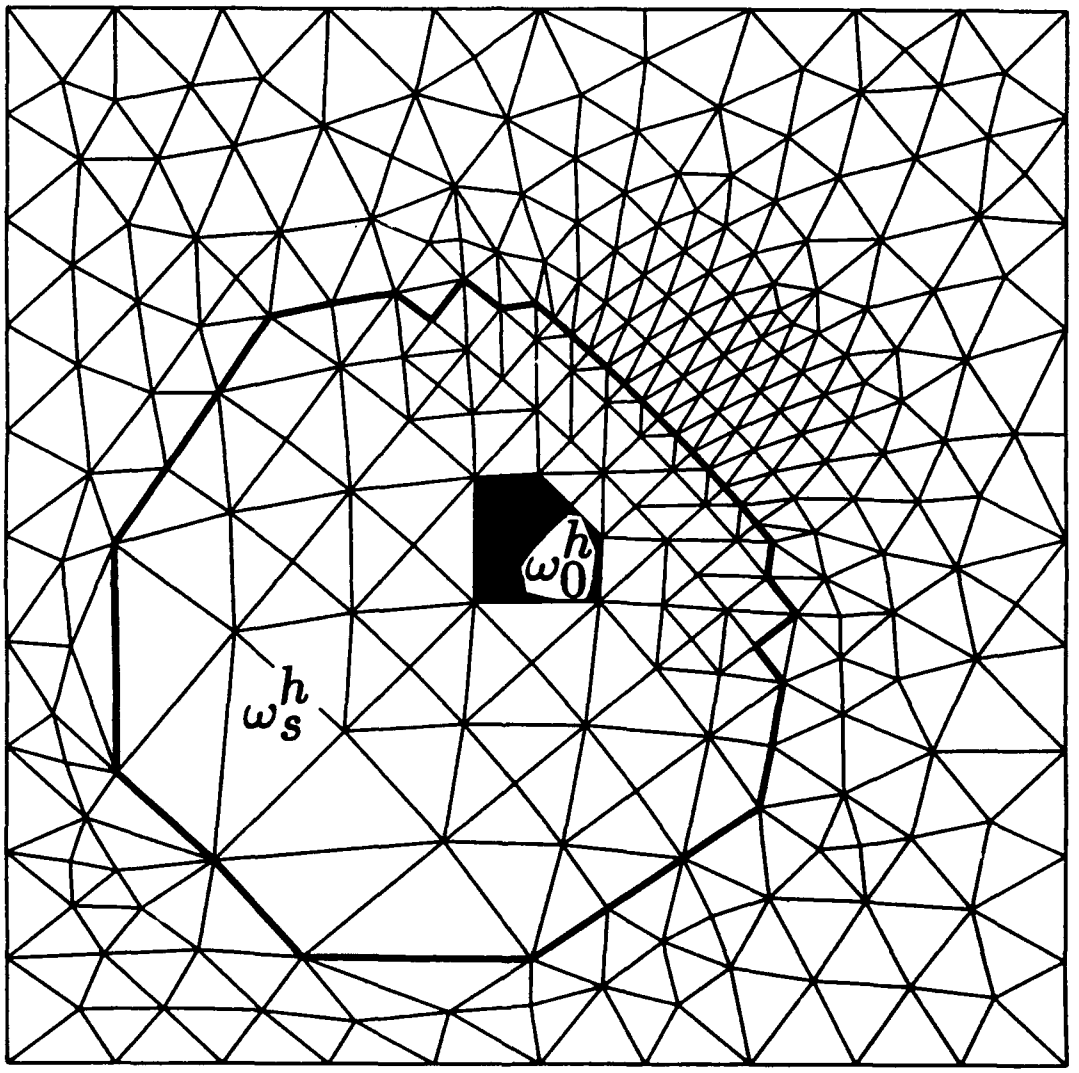

Fig. 7c

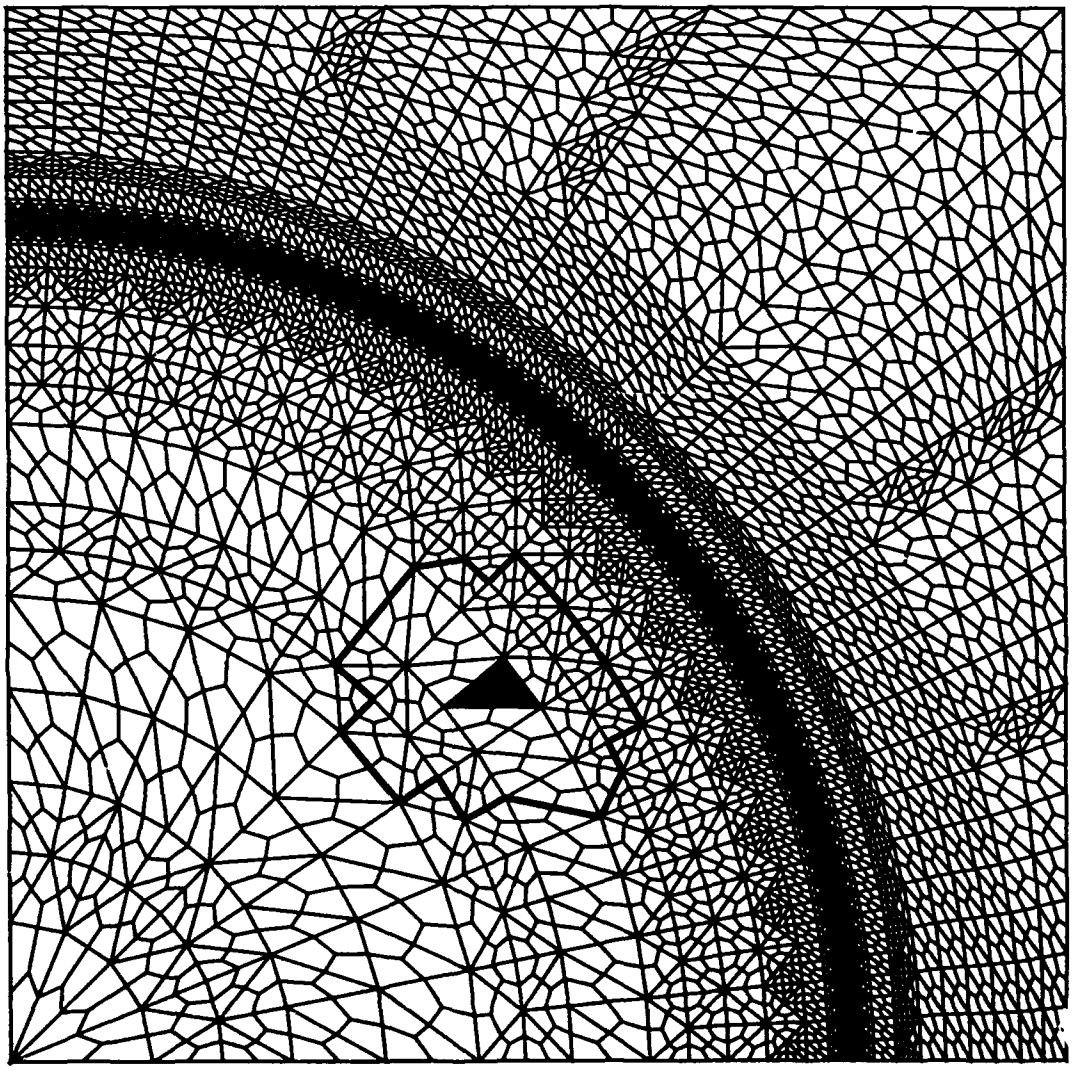

Fig. 7d

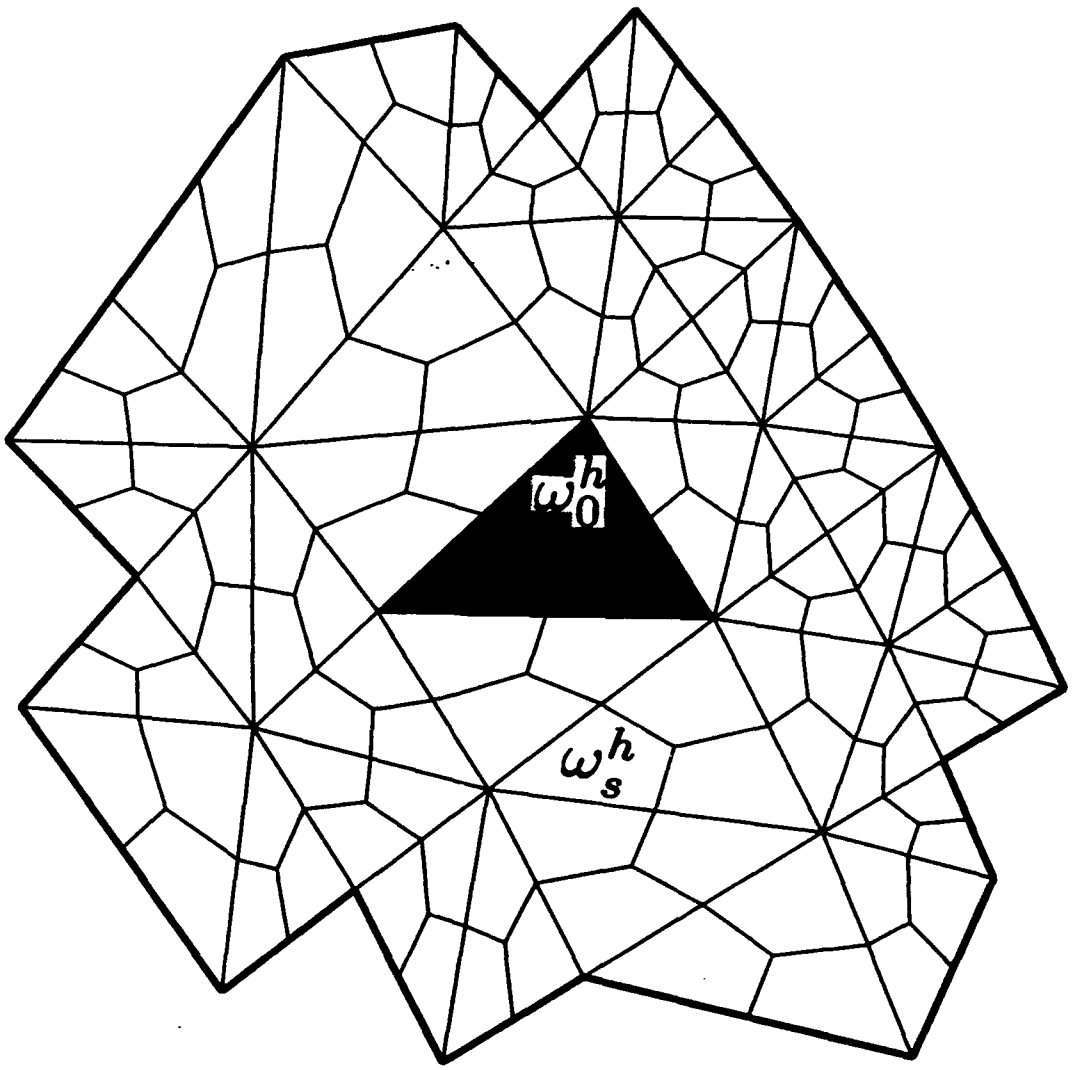

Fig. 7e

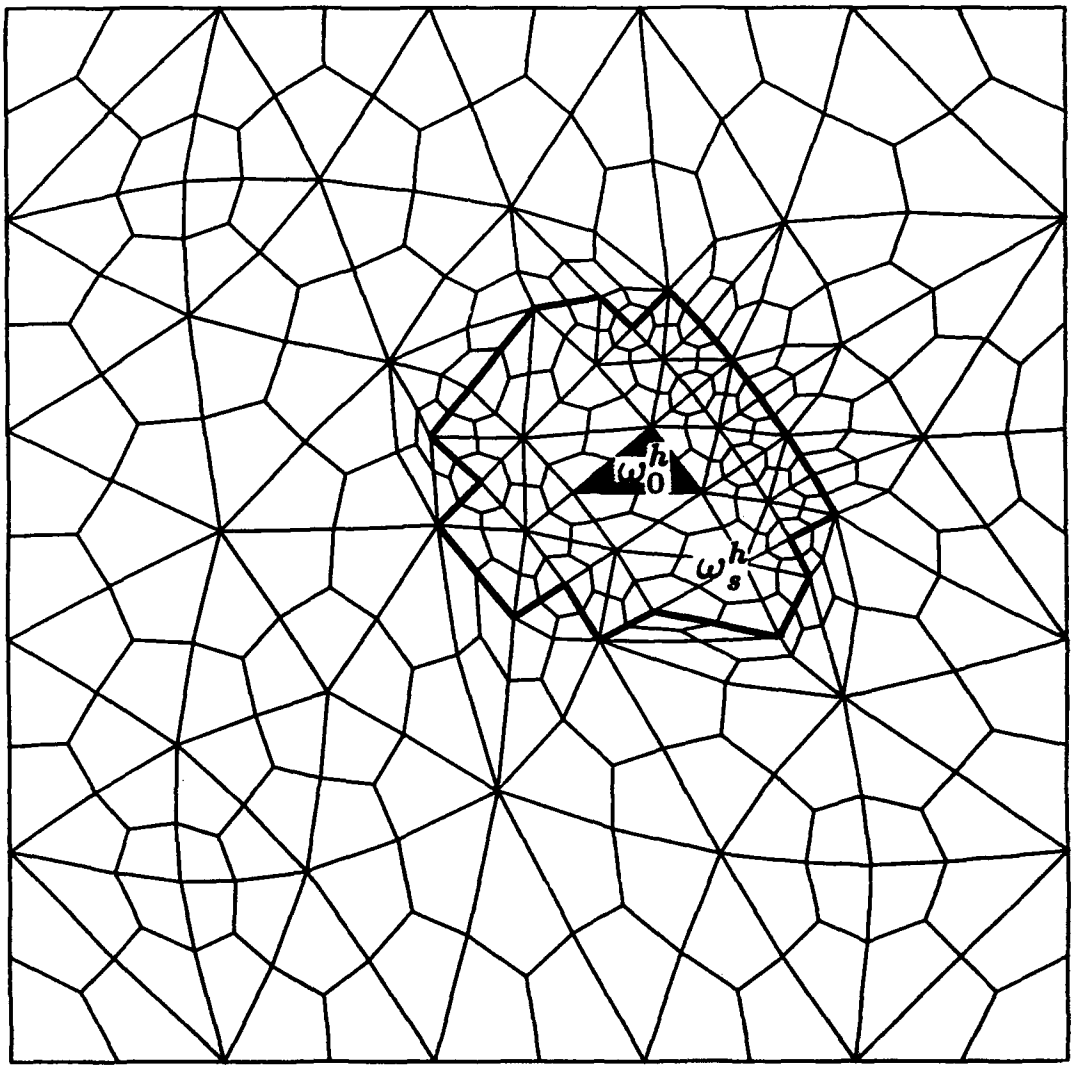

Fig. 7f

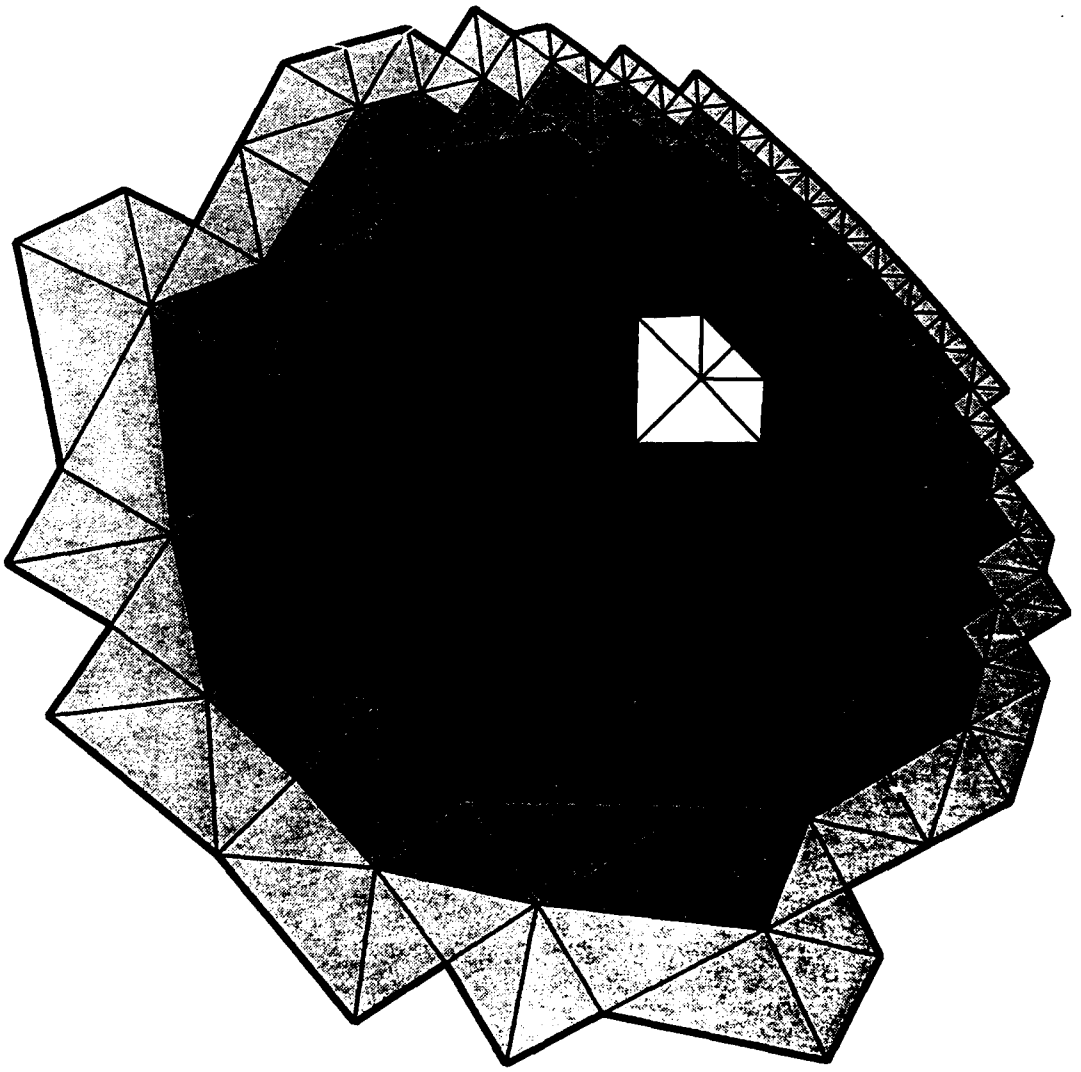

Fig. 8

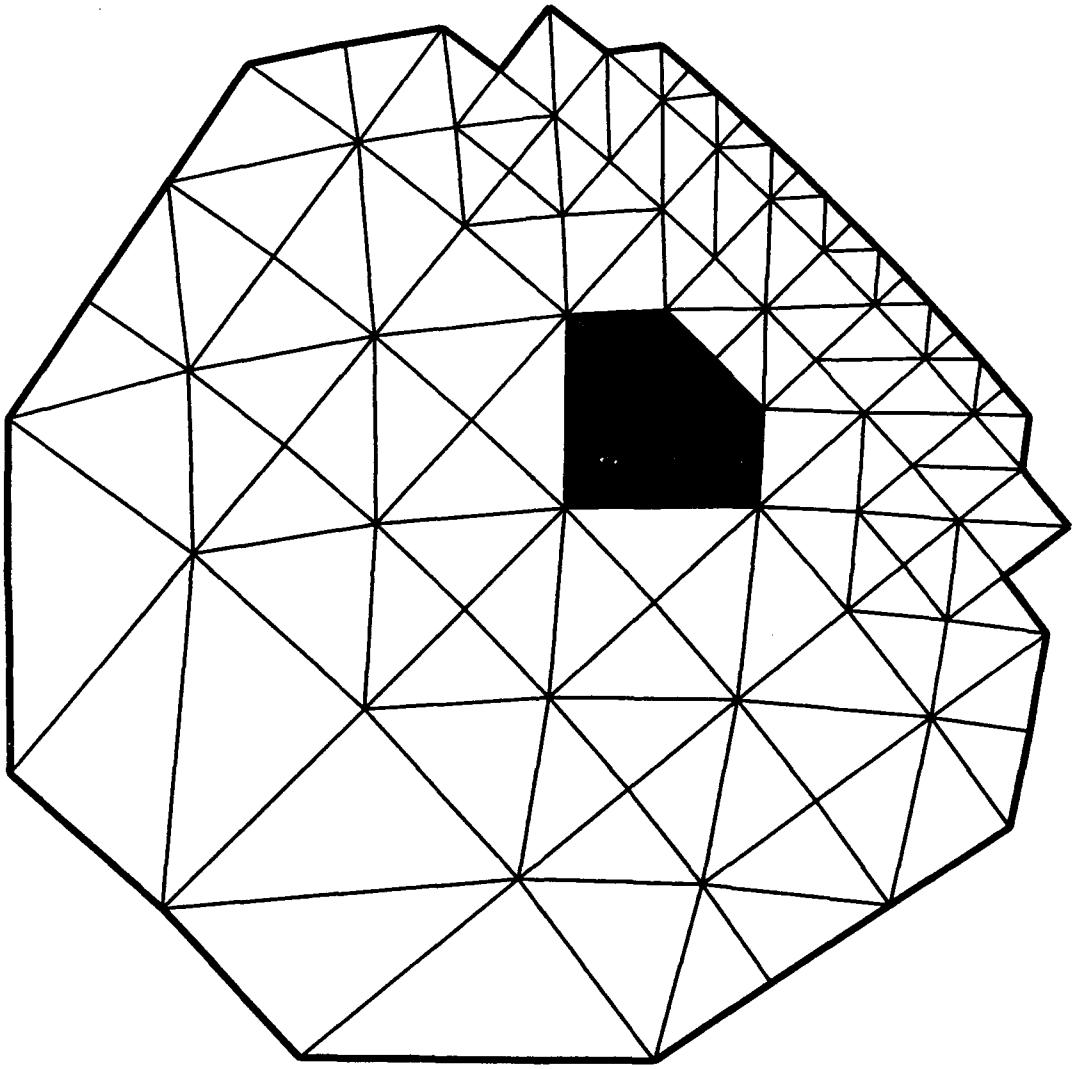

Fig. 9a

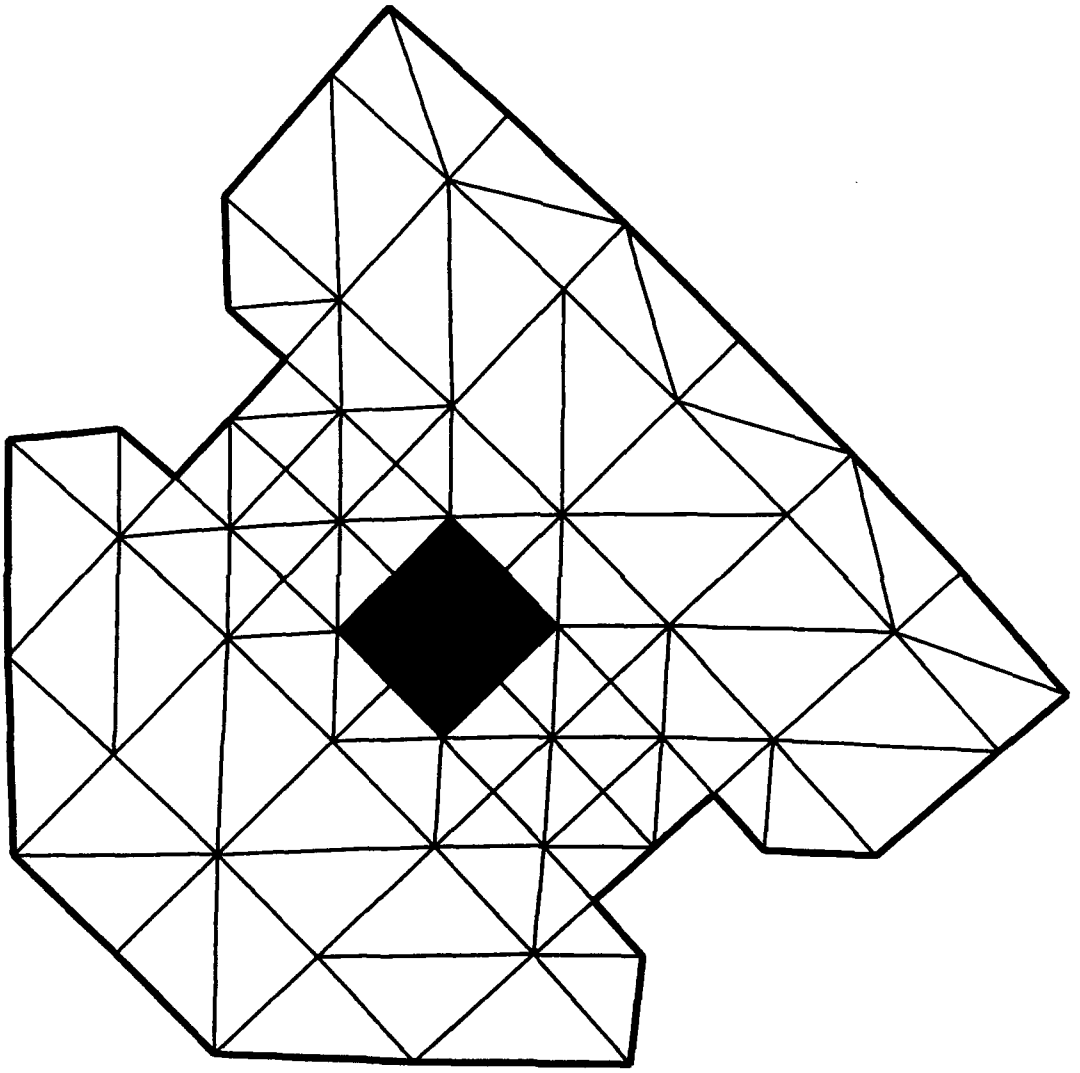

Fig. 9b

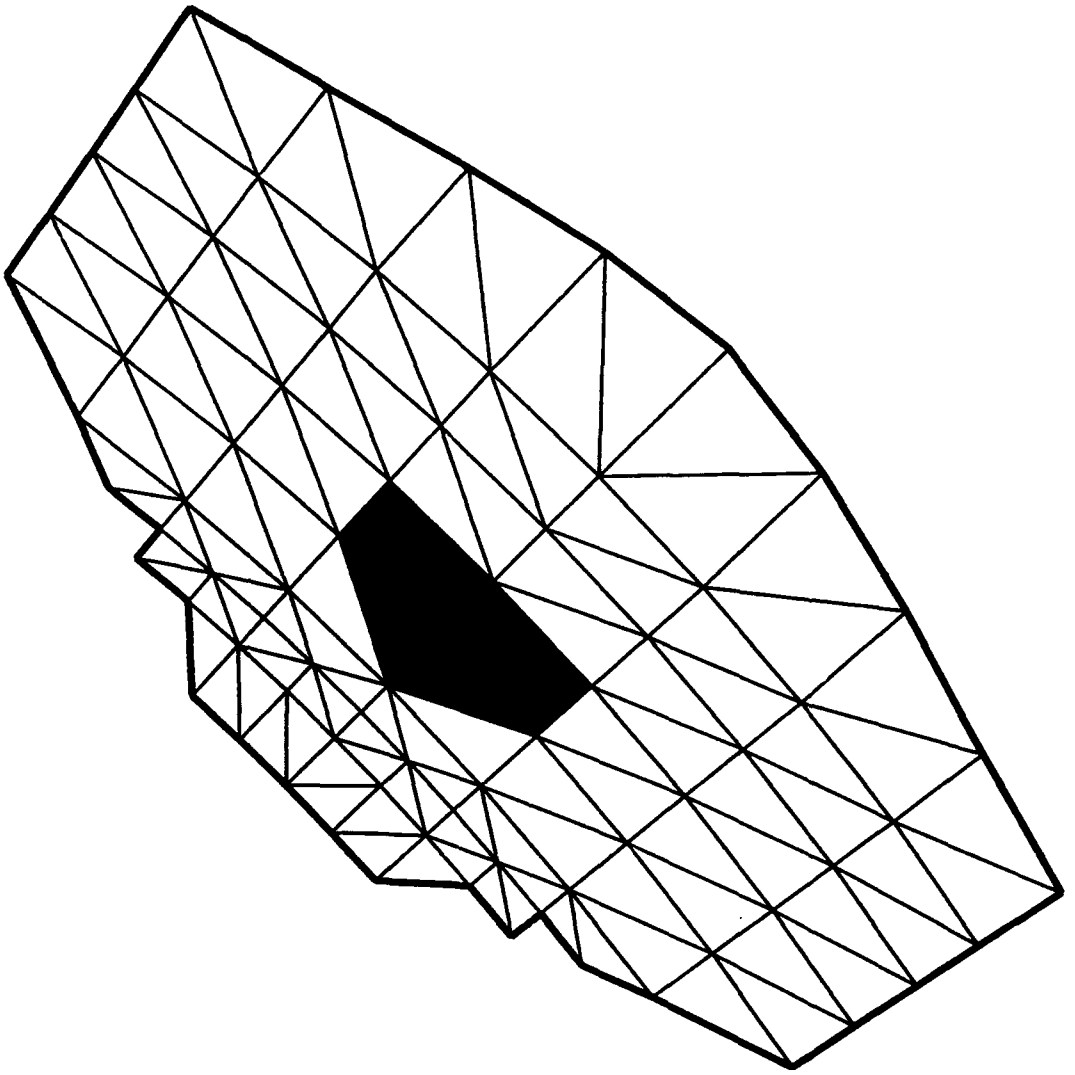

Fig. 9c

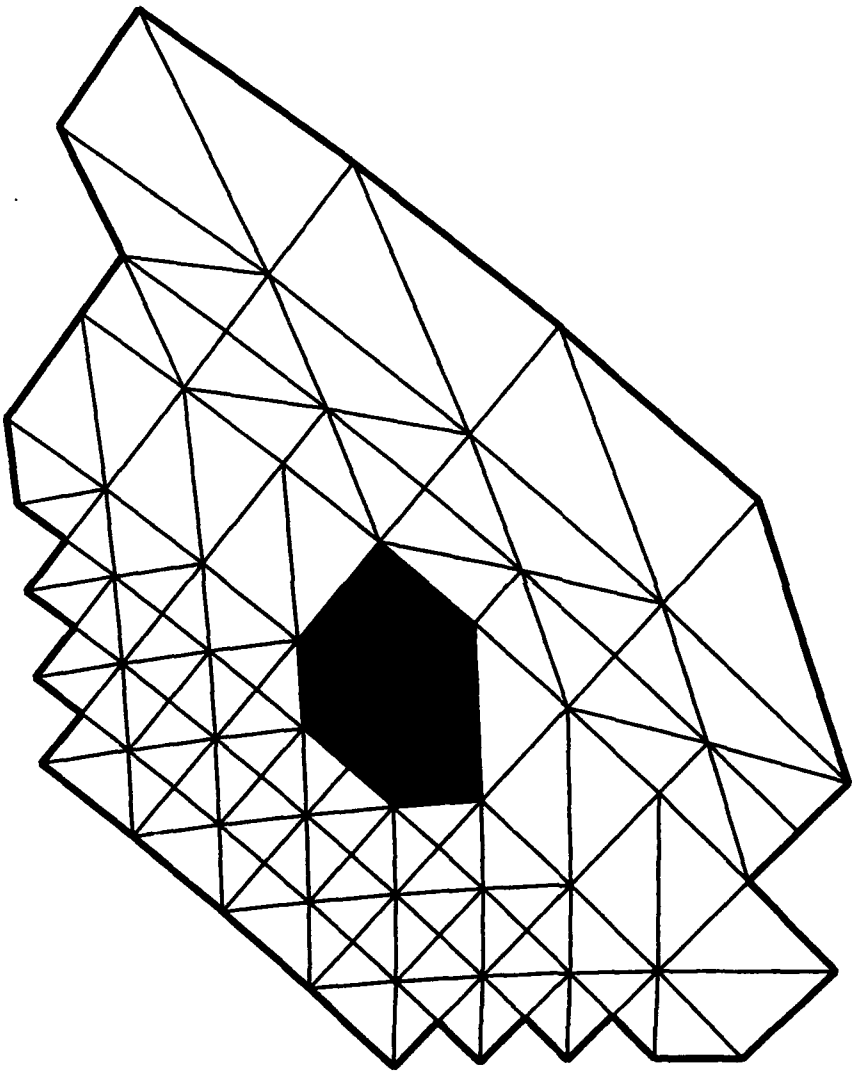

Fig. 9d

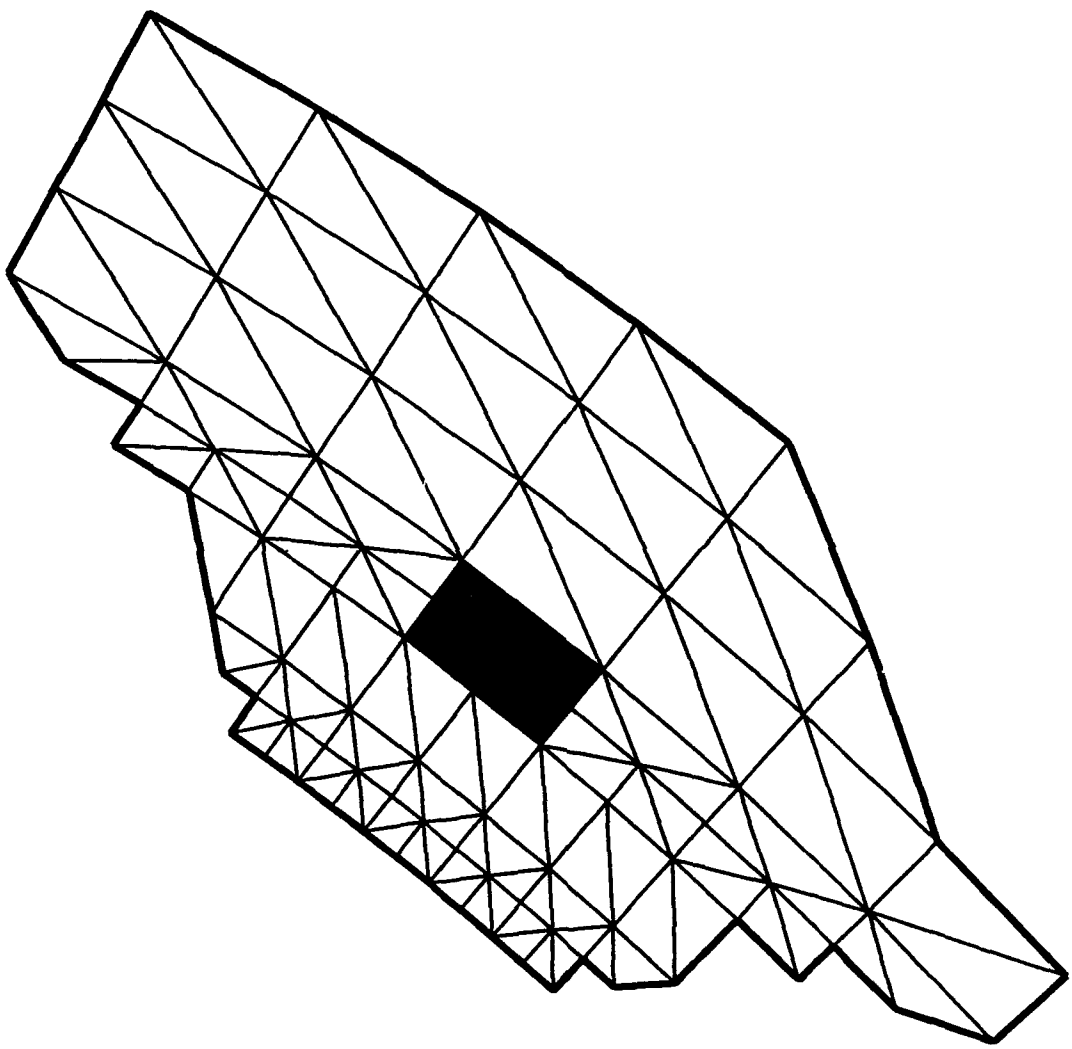

Fig. 9e

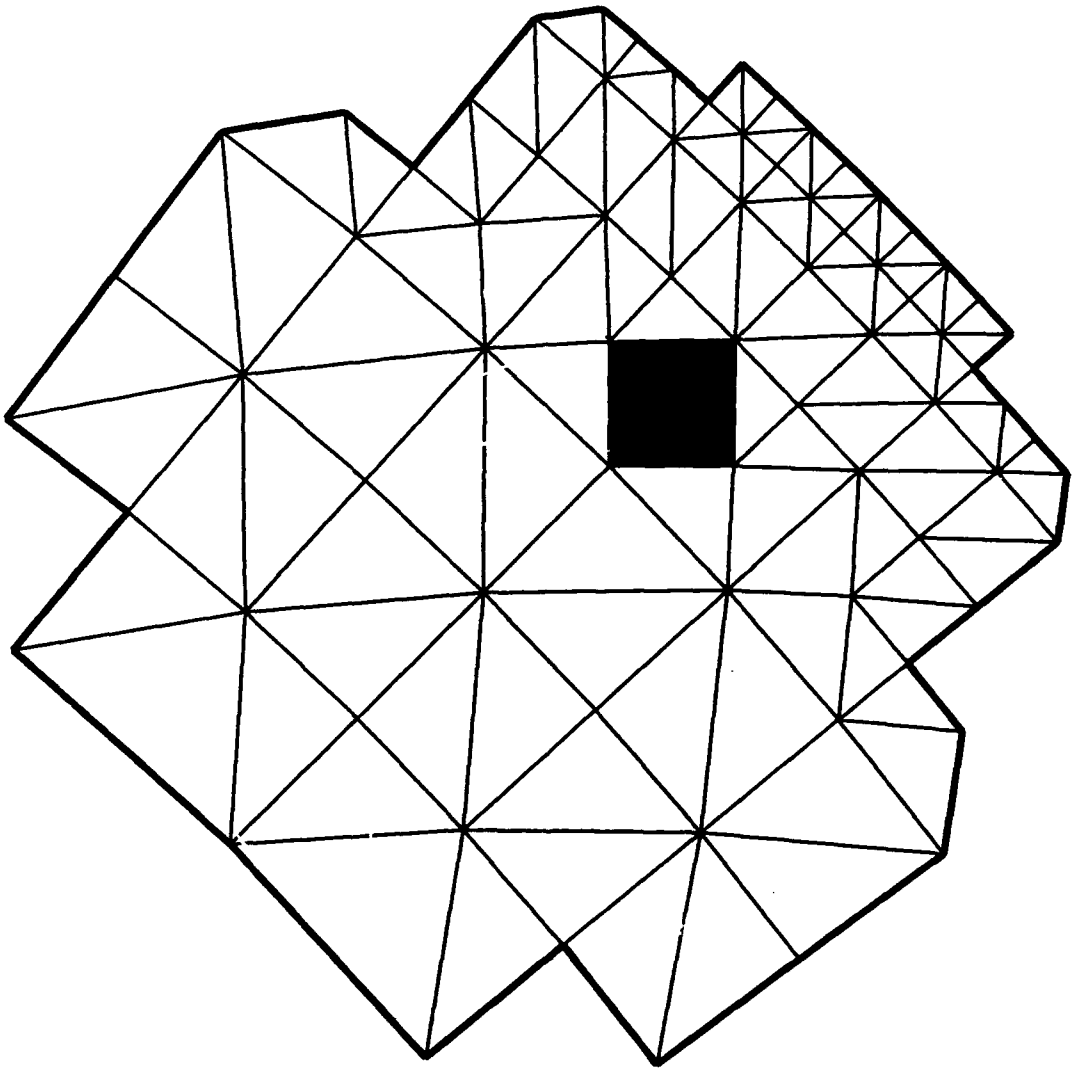

Fig. 9f

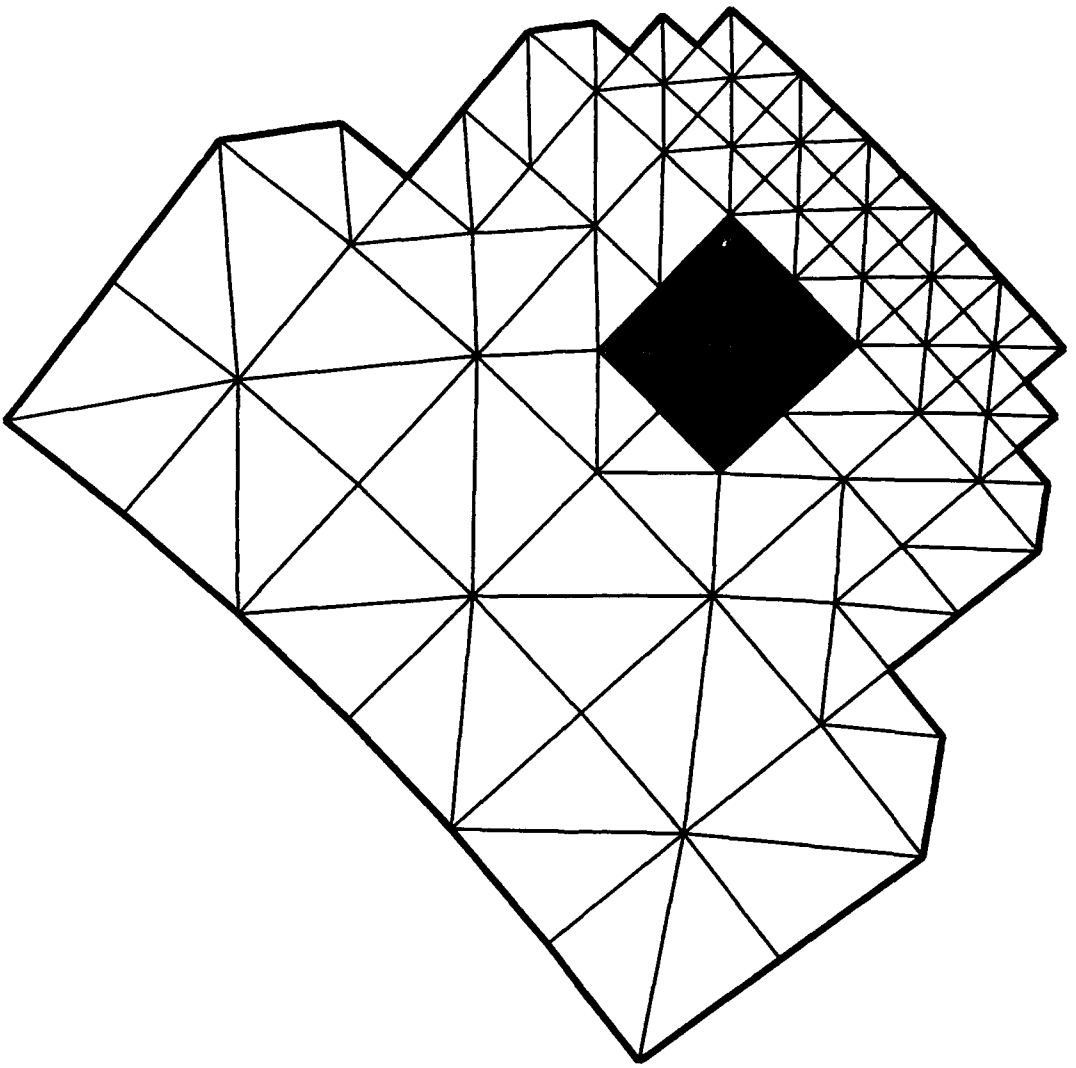

Fig. 9g

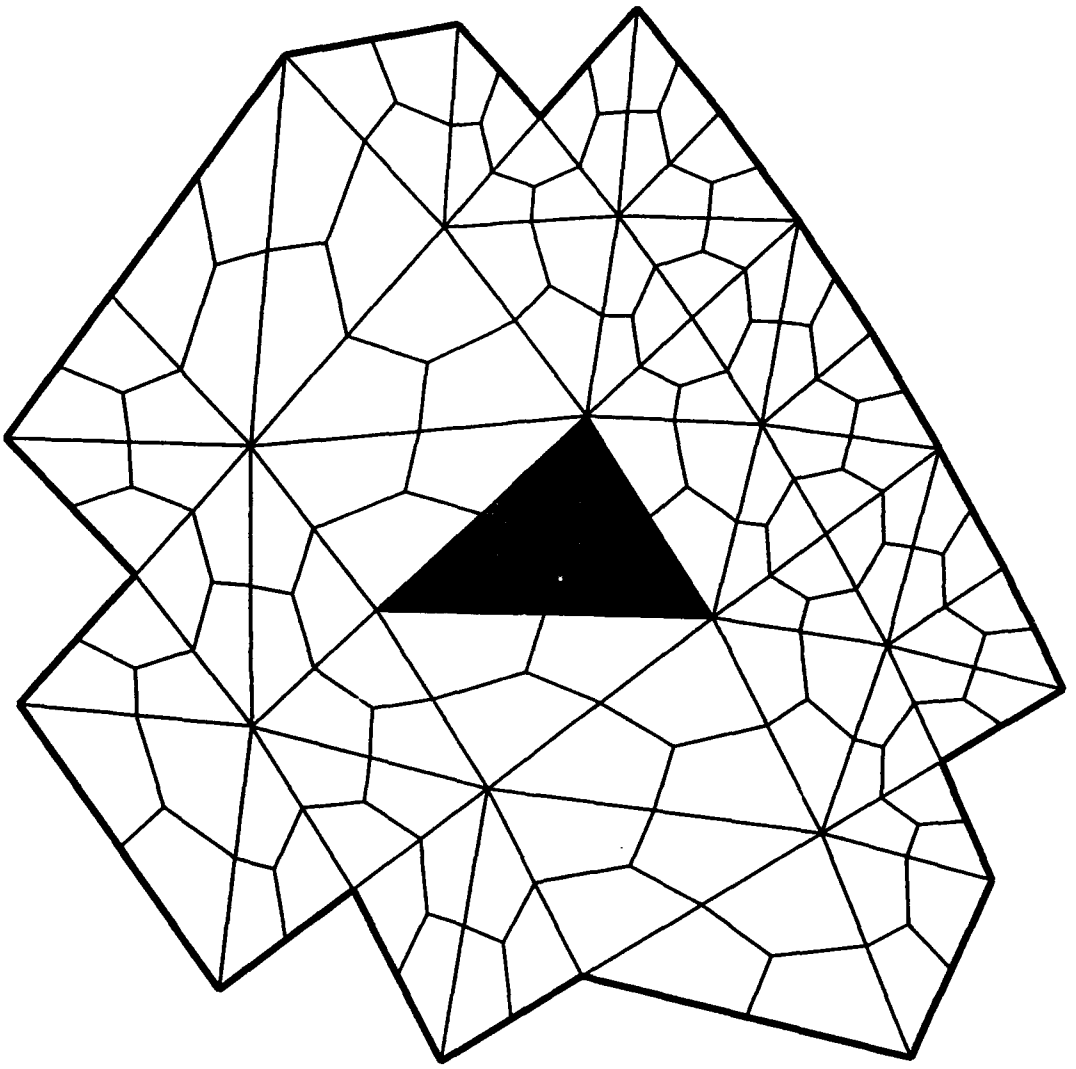

Fig. 10a

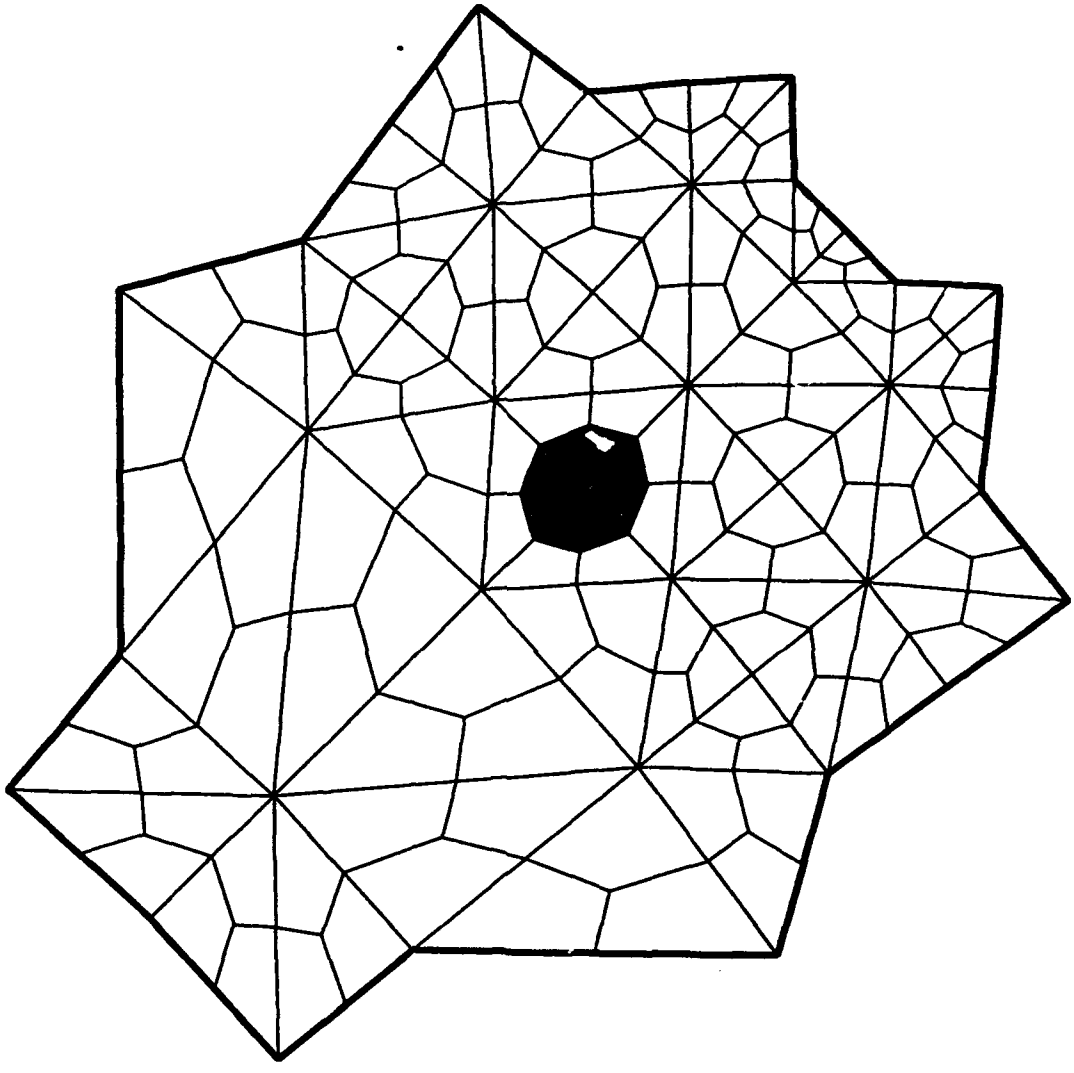

Fig. 10b

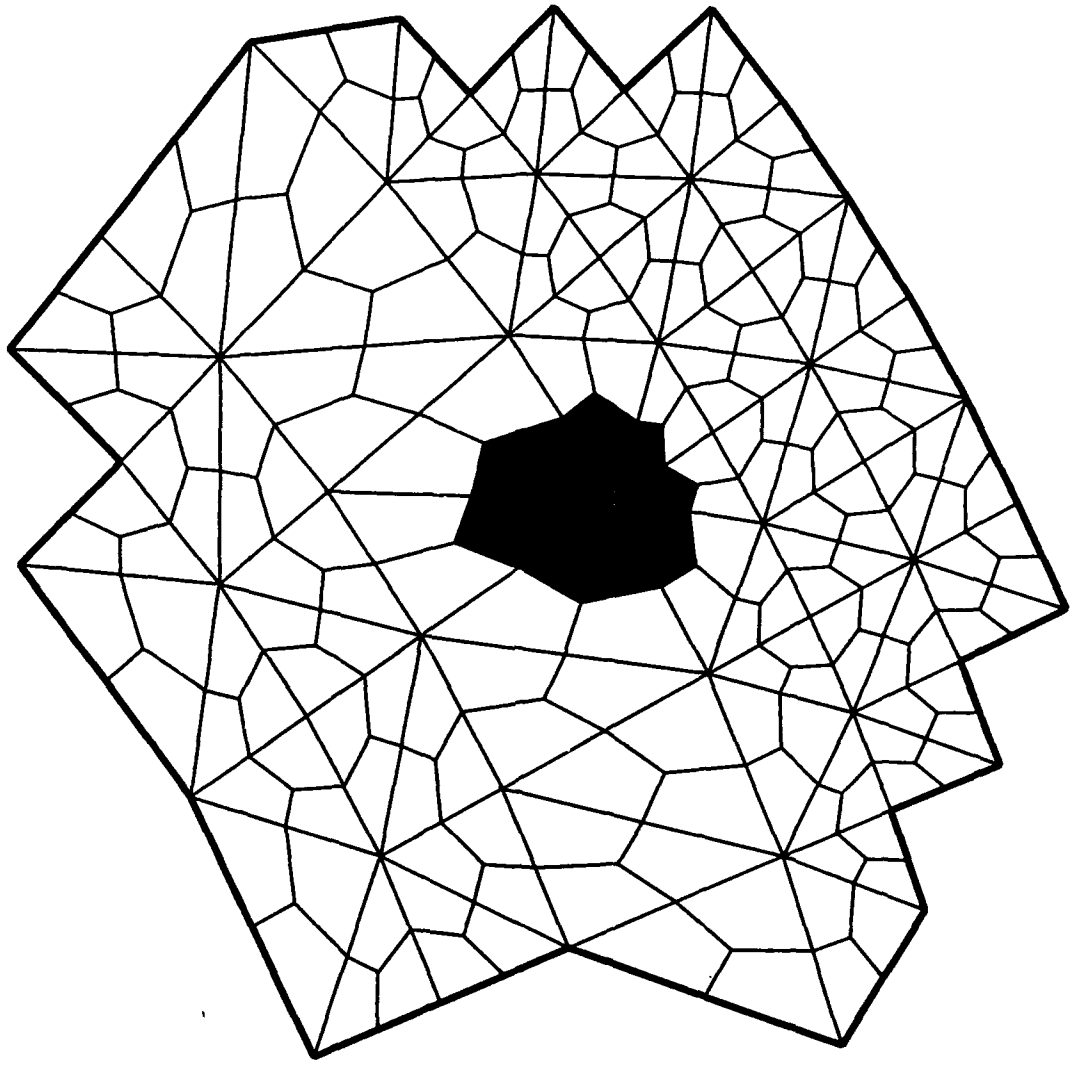

Fig. 10c

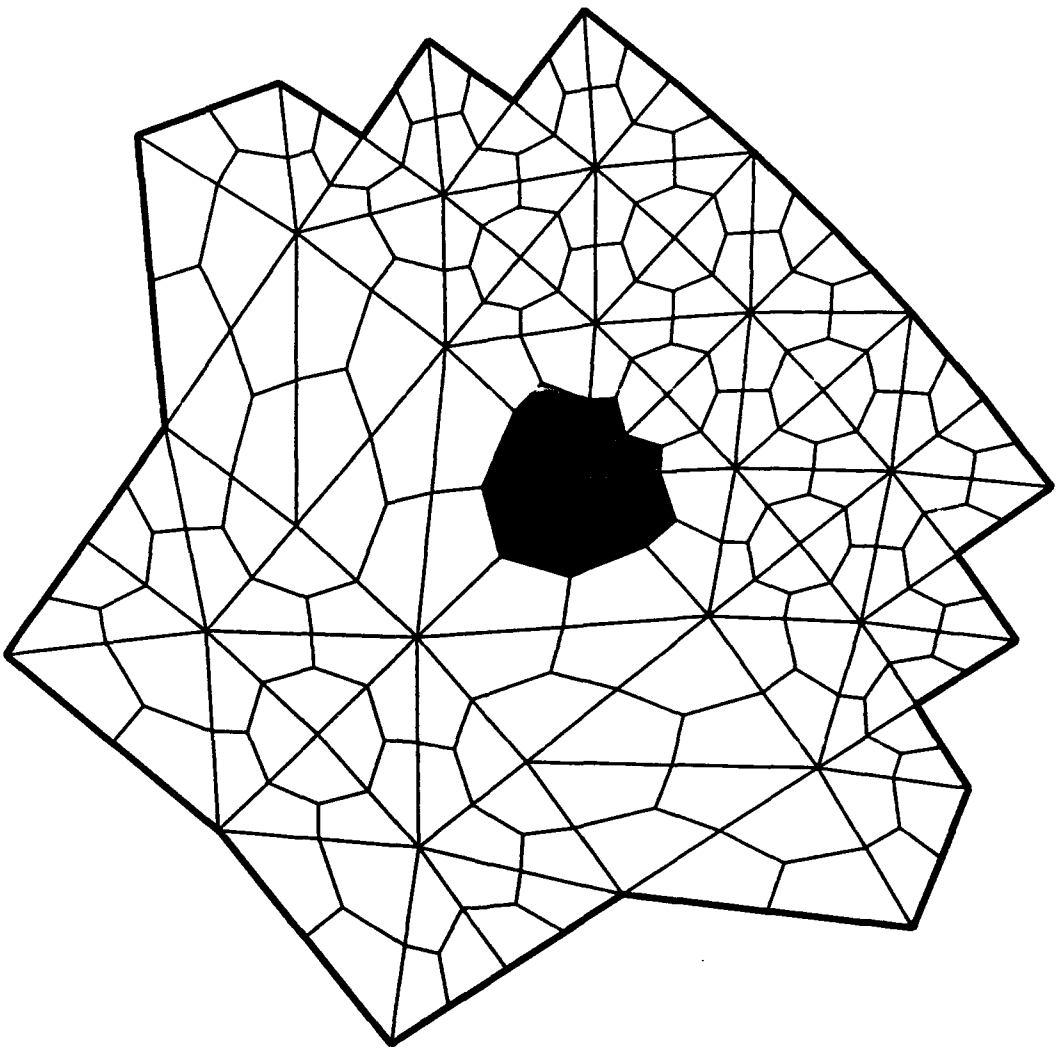

Fig. 10d

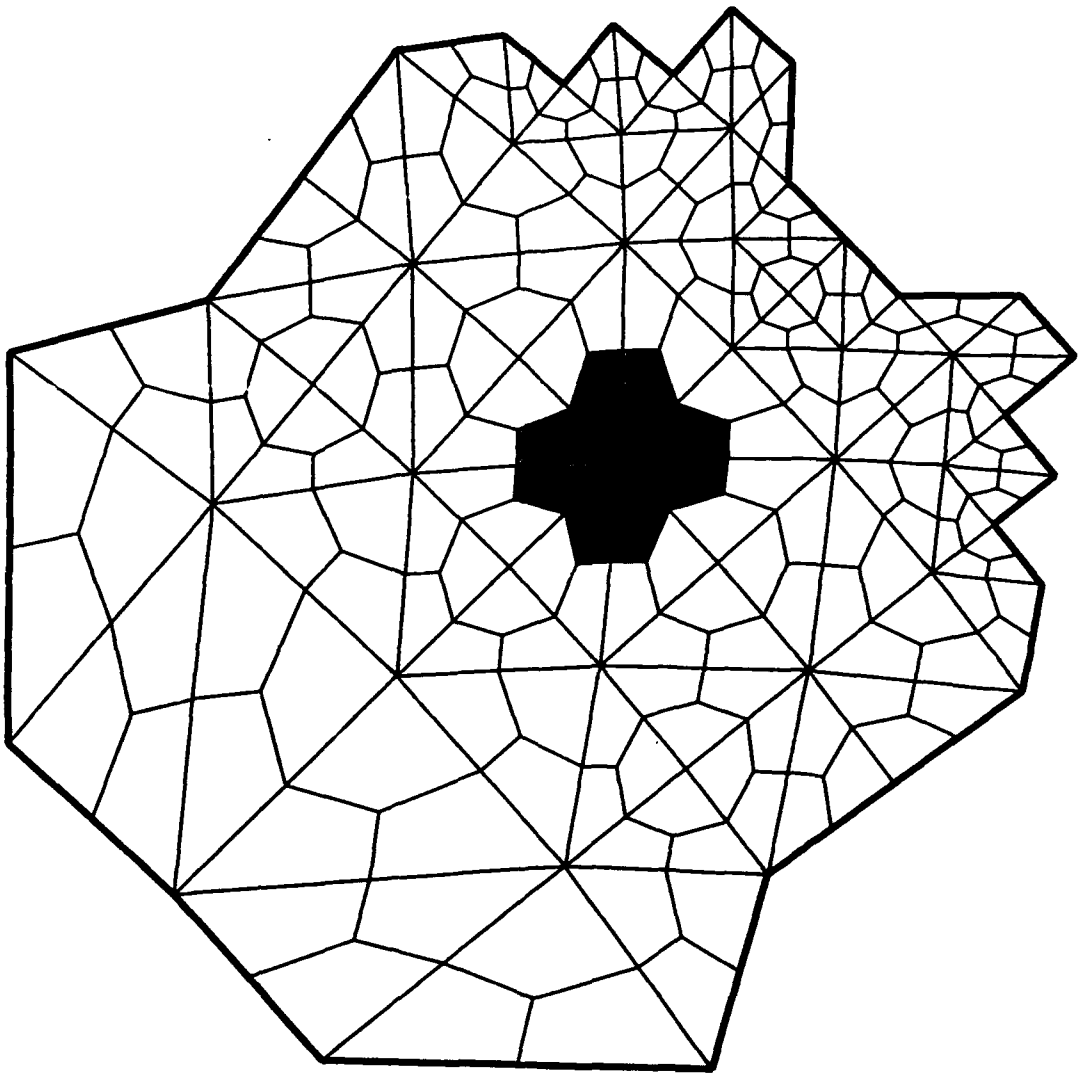

Fig. 10e

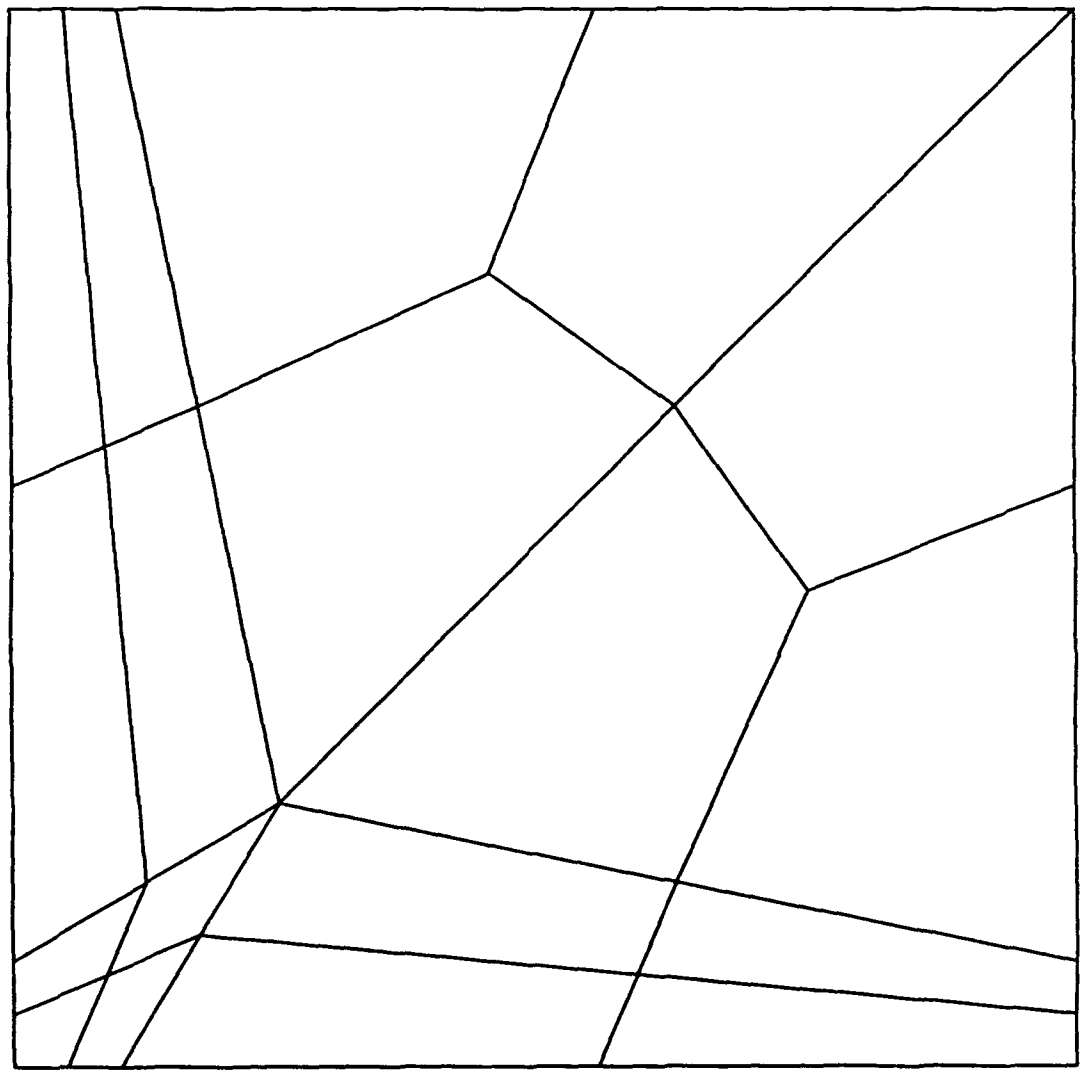

Fig. 11a

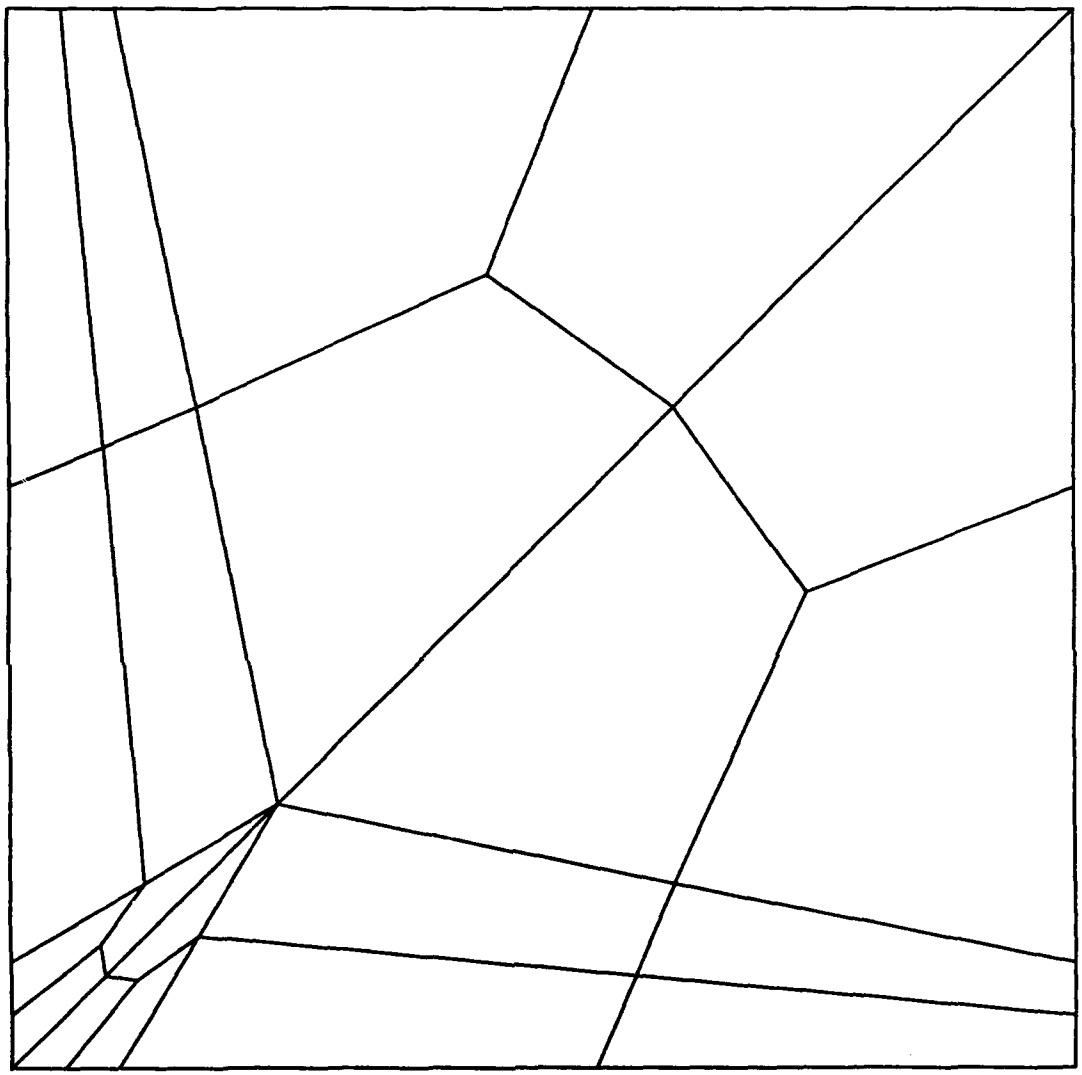

Fig. 11b

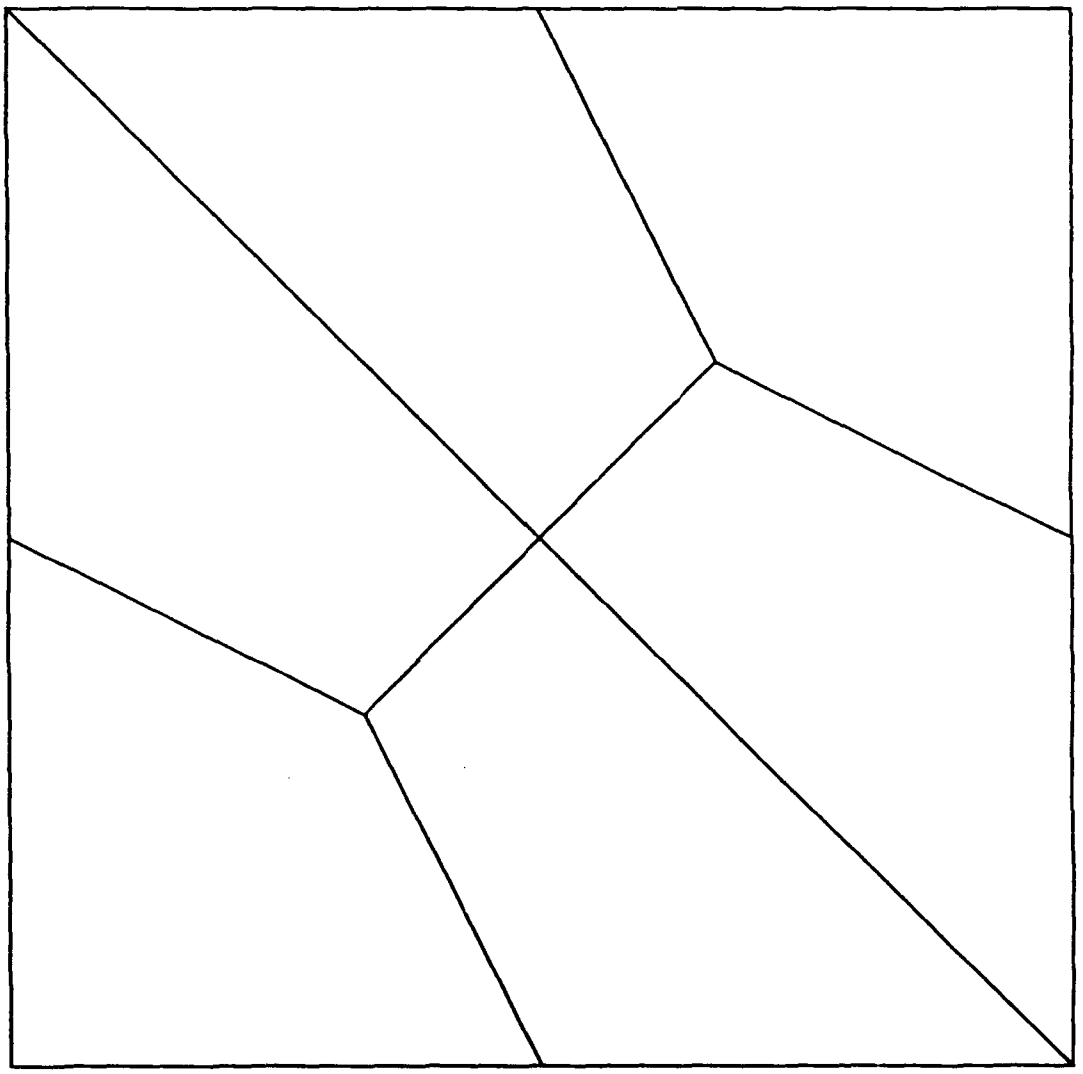

Fig. 11c

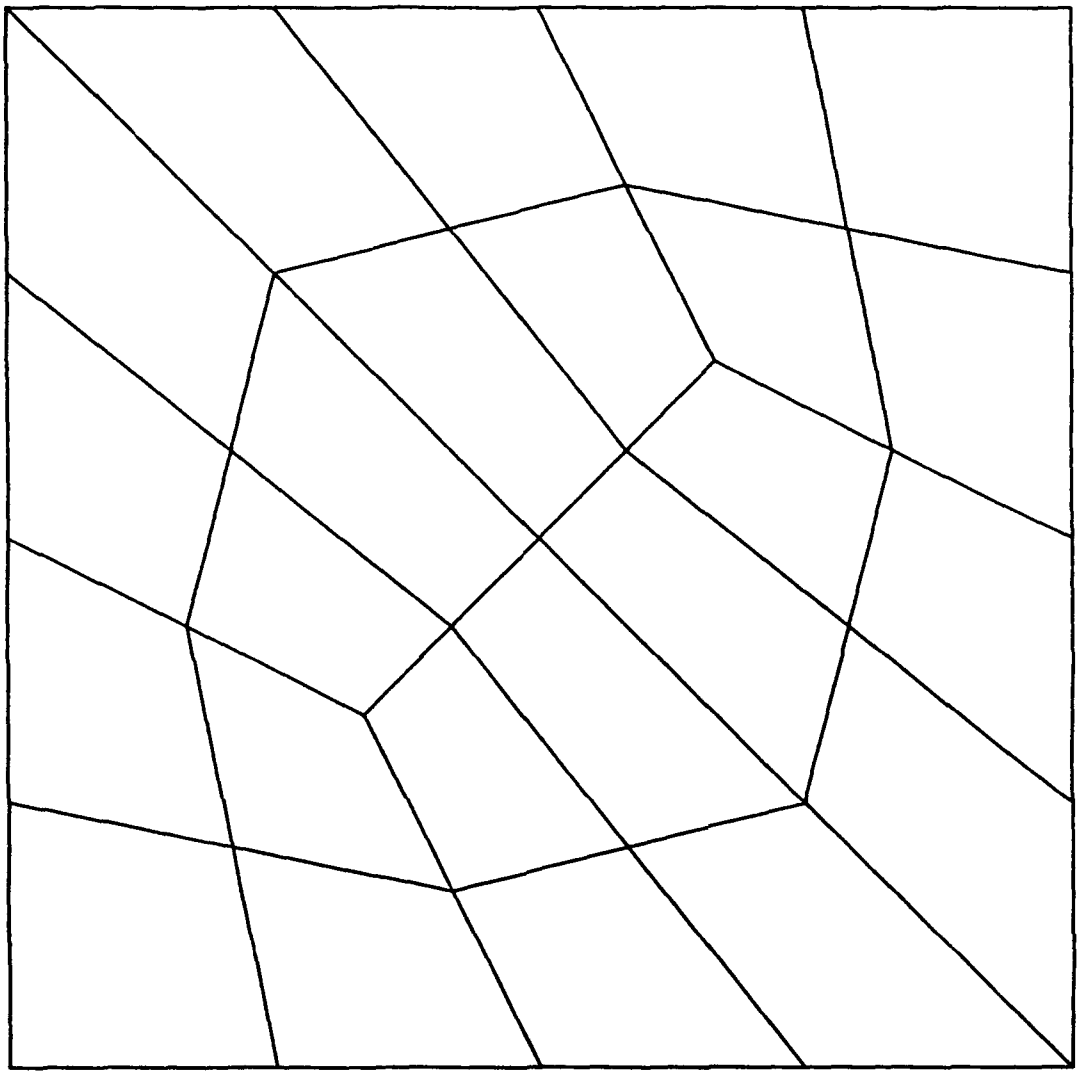

Fig. 11d

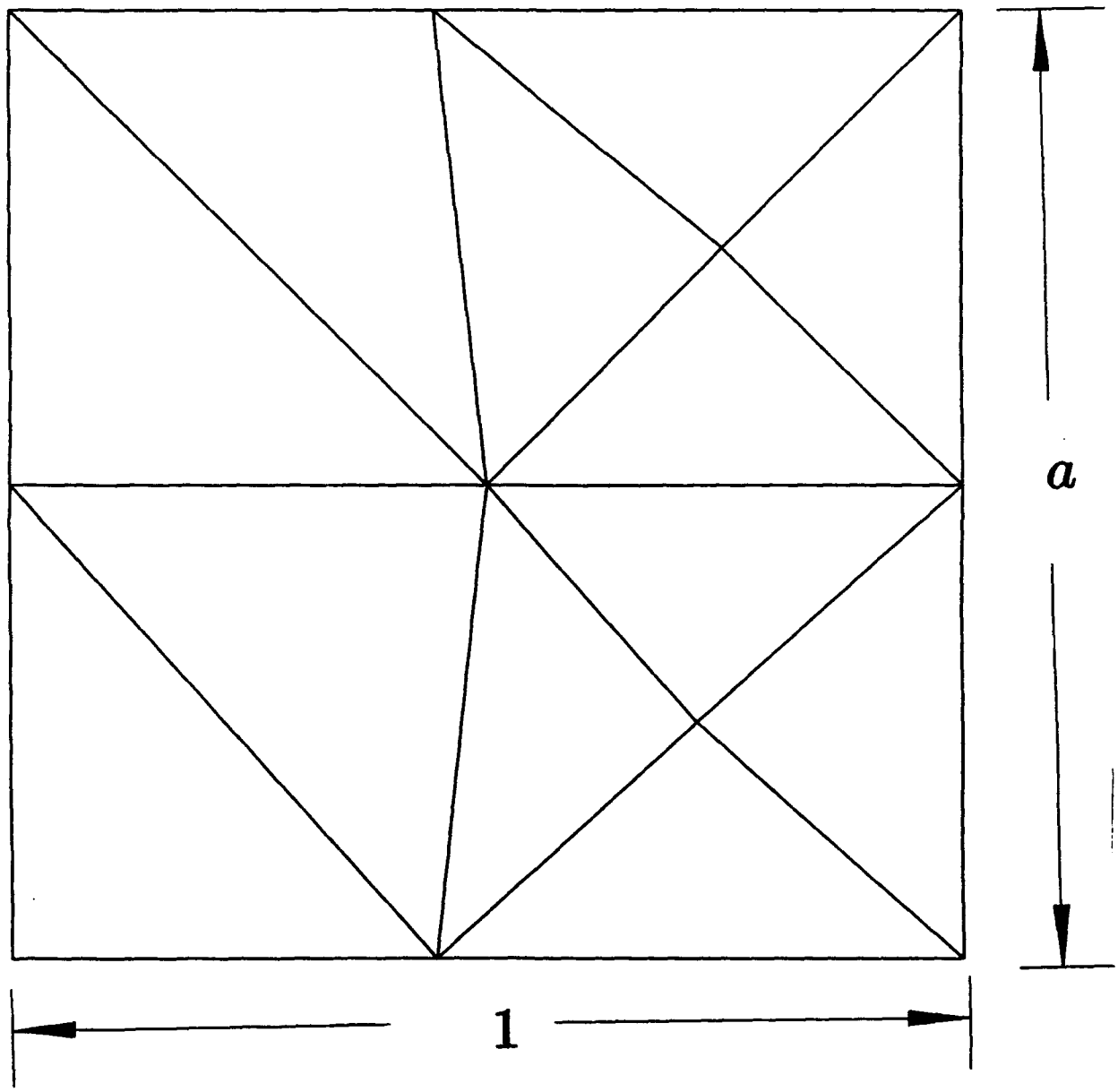

Fig. 12a

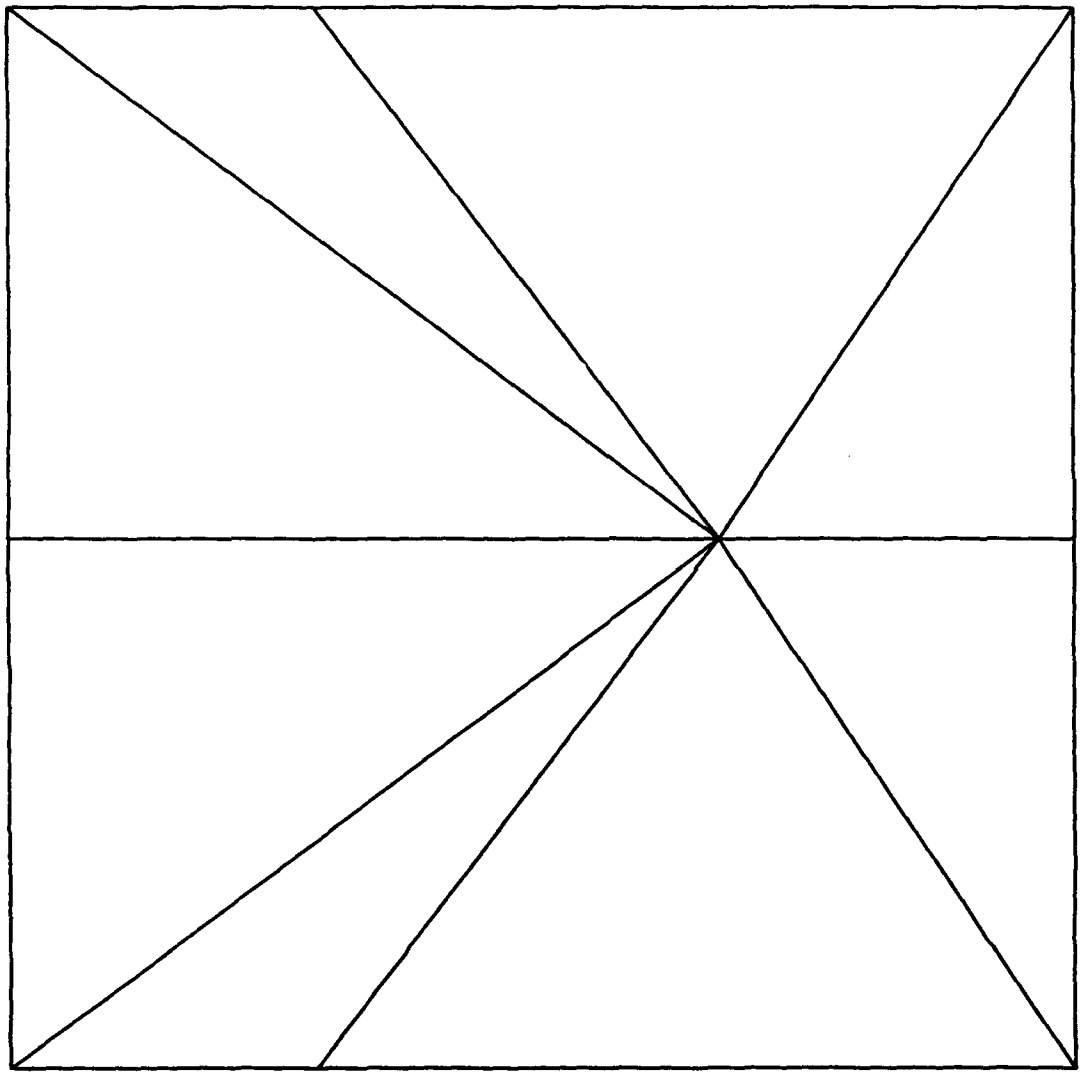

Fig. 12b

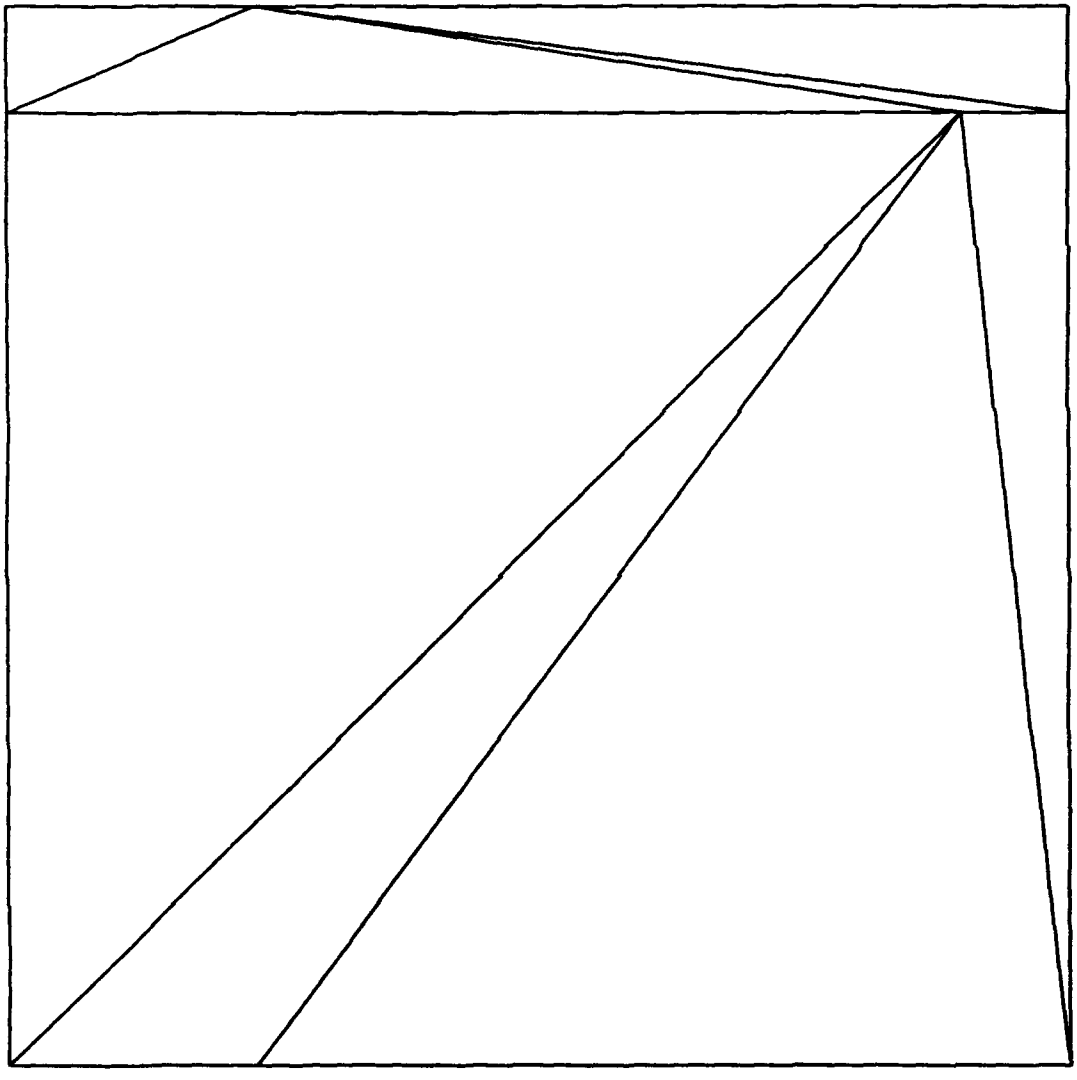

Fig. 12c

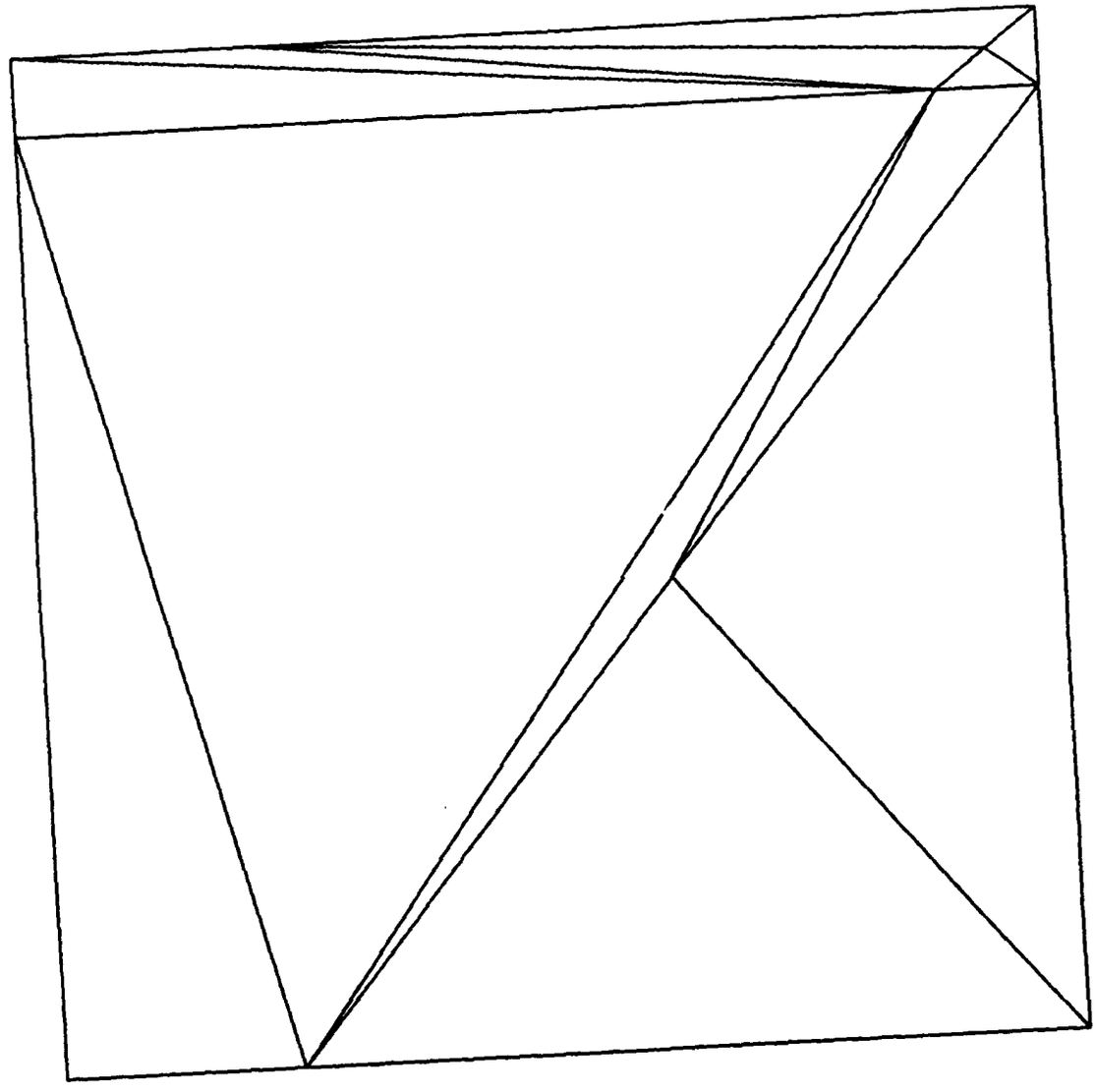

Fig. 12d

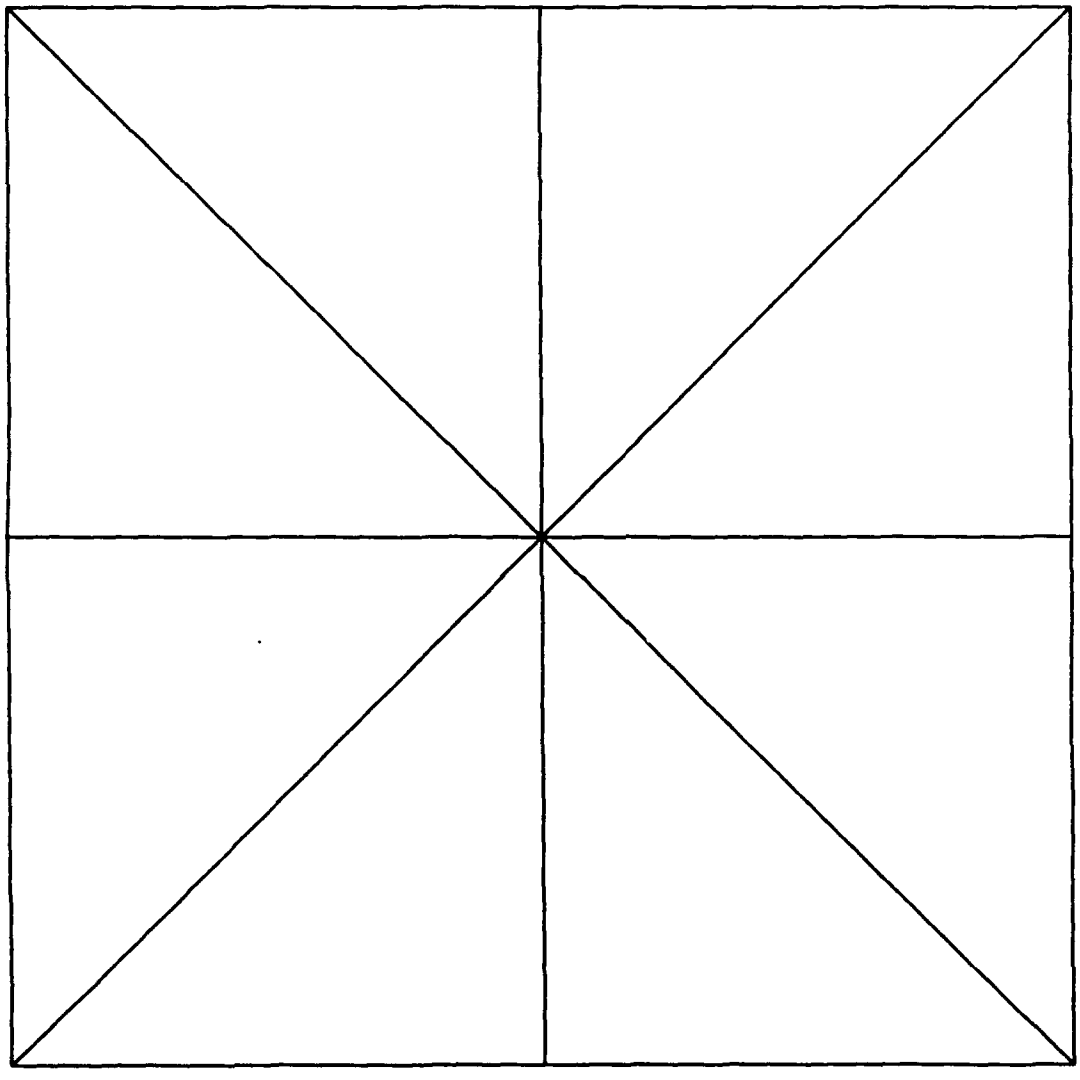

Fig. 12e

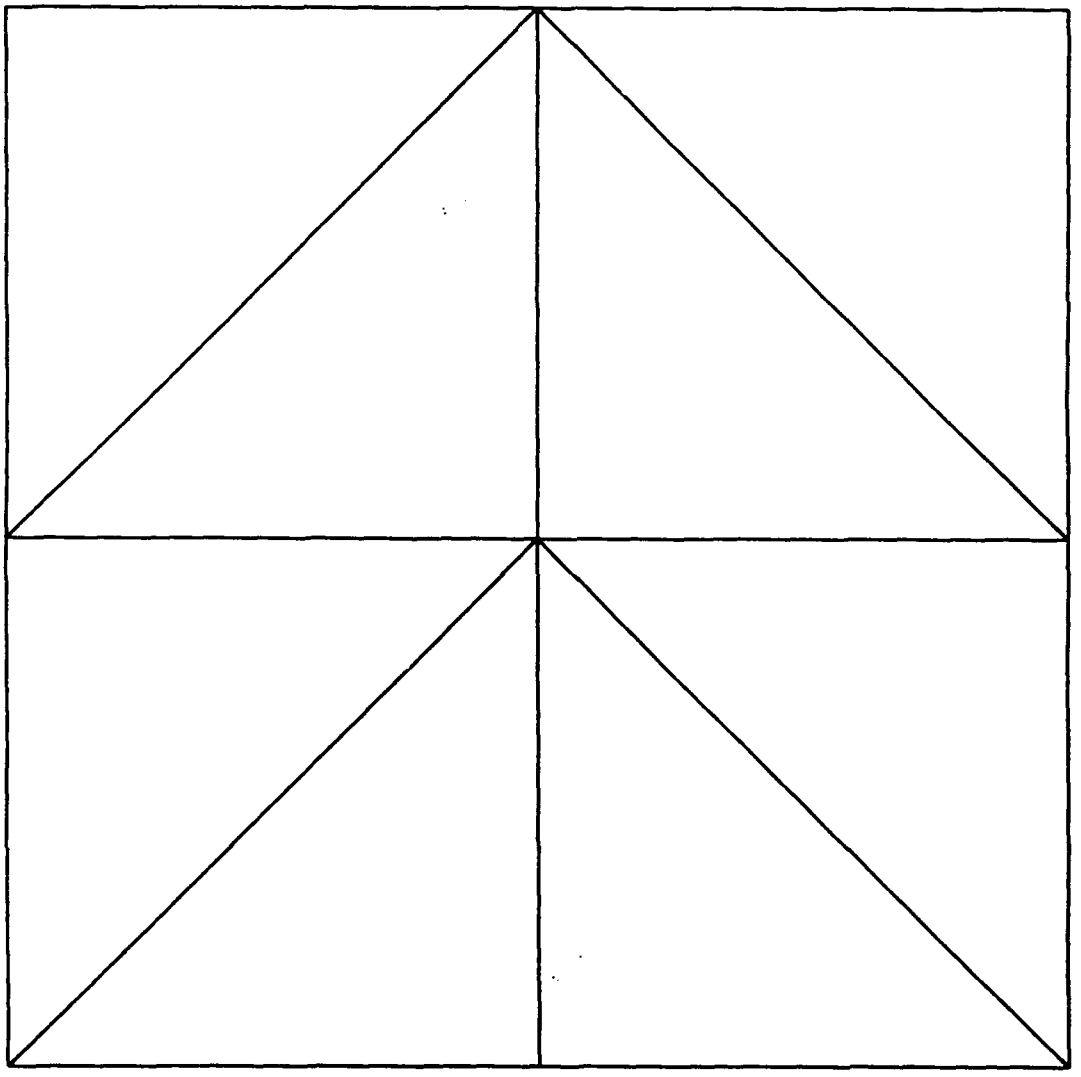

Fig. 12f